NOTE TO USERS

Design and Implementation of 2400 MHz - 144 MHz Downconverter

By

Semih Gürkan, B.S.

A Thesis
in
The Department
of
Electrical and Computer Engineering

Presented in Partial Fulfillment of the Requirements
for the Degree of Master of Applied Science (Electrical Engineering) at
Concordia University
Montreal, Quebec, Canada

May 2005

Your file Votre référence
ISBN: 0-494-04372-5
Our file Notre référence
ISBN: 0-494-04372-5

ABSTRACT

Design and Implementation of 2400 MHz - 144 MHz Downconverter

Semih Gürkan, B.S.

In this thesis, the theory, design and the implementation of a 2400 - 2404 MHz input, 144 -148 MHz output downconverter is presented. The theory of coupling structures between folded resonators is discussed and the coupling coefficients are calculated. The full theoretical approach to the hairpin filter, rat race coupler mixer, amplifier and frequency multiplier were discussed. The design and the full wave microwave simulations of the coupling structures, hairpin filters and the rat race coupler mixer were carried out using the Agilent Advanced Design System (ADS). Several simulations (conversion loss, gain, S-parameter, harmonic balance) were carried out in order to analyze the behavior of the hairpin filters, rat race hybrid mixer, harmonic generator and the RF amplifier. The full wave simulation results were compared with the RF simulation mode of ADS; the differences between the results were discussed.

The implementation of the designed and simulated components was accomplished. The creation of Gerber files, drill files, buying the parts and having the board manufactured were completed and the each step explained in detail. The differences between the theoretical design, the ADS simulations and the experiments presented and the possible reasons were discussed.

ACKNOWLEDGMENTS

First and foremost, I am grateful to my parents and my sister for their continual encouragement and support. If it wasn't for them, I wouldn't write this thesis.

I would like to express my sincerest appreciation to my thesis supervisor Dr. Robert Paknys, for his instruction, guidance and experience. His profound knowledge and passion for research have greatly enhanced my enjoyment of this research and made this endeavor a successful experience.

I also would like to recognize my dearest friend Mr. Alper Kürşat Öztürk, I am thankful to the valuable discussions we held during this research.

List of Acronyms

ADS	Agilent Advanced Design System
Fund	Fundamental Frequency
HG	Harmonics Generator
RF AMP	Radio Frequency Amplifier
Spur	Spurious
TL	Transmission Line

Table of Contents

List of Figures

Chapter 2:

Chapter 3:

Chapter 4:

Chapter 5:

Chapter 6:

List of Tables

Chapter 1:

Chapter 3:

Chapter 4:

Chapter 6:

1 Introduction

With the development of microwave technology, computer-aided design techniques, designing microwave circuits has become less complicated. Moreover with the help of computer aided simulation programs for predicting the effect of small changes in the design in a short time is possible. More importantly, the cost of designing a microwave circuit is not as expensive as it was. Due to these reasons, many radio amateurs are interested in and able to easily build microwave systems for amateur radio.

The goal of this thesis is to design and implement a downconverter, which has 2400 - 2404 MHz input, 144 – 148 MHz output. The band between 2350 MHz and 2450 MHz are reserved for amateur radio applications so the downconverter will work in a fraction (2400-2404 MHz) of the amateur radio band of 2300 – 2450 MHz. The frequency range we are interested is the satellite band of 2400 MHz - 2410 MHz. The downconverter designed and implemented would be capable of downconverting the 2400 - 2404 MHz to 144 - 148 MHz.

The 144-148 MHz signal, which is the output of the downconverter, is intended as the input to a commercially manufactured amateur radio. It has been noted that at the present time, there are no commercially available amateur band radios capable of receiving signals beyond 1.3 GHz. Hence, a downconverter for 2400 – 2404 MHz is essential.

The satellite in the band of 2400 – 2410 was provided by The Amateur Radio Satellite Corporation (AMSAT). AMSAT's goal is to promote Amateur Radio's participation in space research and communication. For over 36 years AMSAT groups have played a key

role in significantly advancing the state of the art in space science, space education, and space technology [3].

AMSAT has three operational satellites, which work at the frequency of interest and one more is planed to be launched. One particular satellite, AO-51 which has downlink at 2401.200 MHz 38,400 bps, AX.25 and UO-11 satellite has a downlink of 2401.500 MHz. The AO-40, which became non-operational around January 2004 had a downlink of 2400.225 -2400.475 MHz. As seen, the 2400 – 2404 MHz range is very popular among amateur radio users.

In the market there are some designs to fulfill the assignment of receiving amateur radio signals. For instance Down East Microwave Inc. has designs for 2304 MHz, 2400 MHz, 3456 MHz, 5760 MHz, 10368 MHz [1]. Moreover, there are many design books in the market today for amateur radio applications. The publications of the ARRL [3] show some designs for amateur radio users, who are interested in implementing their own design. These designs can be modified for new situations and specifications. One aspect of these publications is that they are far from being scientific because few insights of the application are given, using mathematical modeling based on physical facts.

The "No-Tune Transverter for 3456 MHz" by Jim Davey [2] is one of them. In [2], the circuit schematics, layout and the parts used are given. A straightforward explanation of the components of the design is given, but there is little information on the theory, the design process and the simulation.

The design presented in this thesis is inspired from, the article entitled "No-Tune Transverter for 3456 MHz" by Jim Davey [2]. In order to reach the goal of designing a

downconverter for 2400 MHz, first the design of Jim Davey had to be understood in detail. Secondly, every individual component of the design such as the rat race hybrid mixer, harmonics generator, hairpin filters, bias and amplification circuits were analyzed. The mathematical and physical explanations of the models were understood. Thirdly, the circuits were redesigned for the desired 2400 MHz application, and simulated by using a computer aided design tool (CAD) named ADS (Agilent Advanced Design System). The necessary optimizations were done at this stage in order to improve the performance. In the fourth step, the fabrication of the design was accomplished and as the fifth step the tests on the physical design were carried out. In the end, some conclusions were reached and discussed.

The contributions of this thesis consist of three parts. Firstly, we started with a well-known design by Davey [2]. His design, however, was for 3456 MHz. We rescaled the design for use in our 2400 MHz application. Second, detailed simulations of the harmonics generator, RF amplifier and mixer were done using the Agilent Advanced Design System (ADS) [15]. Third, ADS was used to write Gerber files, which were then sent to a circuit board manufacturing company, APCircuits in Alberta [16]. Hence, we have gained experience in these three areas.

The work done was presented in this thesis as follows. Chapter 2 gives a brief insight about the design of the receiver, and its topology.

Chapter 3 discusses the physical and mathematical models behind the circuit components. The ideas of hairpin filter, mixer, rat race coupler are discussed with reference to. Each sub section of Chapter 2 discusses the different components in great detail.

Chapter 4 is "ADS Simulation Results" and describes the computer simulation used to model the design as well as the results. The simulation models use ADS, the difference between such models and the reliability are explained in this chapter.

In Chapter 5, the fabrication process of the circuitry is discussed in great detail. The software used, the difficulties encountered and effects of the physical limitations on to the design are discussed.

Chapter 6 "Testing and Results" discusses the experimental results obtained and how the experiments were accomplished as well as the test setups. The validity of the theoretical approach and the simulations were also discussed

Chapter 7 is the conclusion and the overall results of the project and the developments introduced are described.

2 The Design

2.1 The Basic Principle of the Downconverter

When an antenna is pointed towards the sky, it receives many signals at different frequencies and with various amplitudes. In order to get the data in a signal of any given source, filtering the signal of interest and splitting the information carrying signal from carrier signal is required. This is accomplished by using a device called downconverter and it is the stage between the antenna and the radio. The downconverter in this thesis was designed specifically to receive 2400 MHz and downconvert the information to a signal of 144 MHz. The output of the downconverter is the input of the 144 MHz radio. The performance of the downconverter dramatically affects the performance of the overall system.

In order for a downconverter to accomplish its job of receiving, it has to have some design blocks in it. These design blocks can be divided into three parts named as: Receiver front end (named RF AMP), harmonics generator (named HG) and mixer. Each of them is responsible for different tasks. The purpose of the RF AMP is to extract the signal band of interest (2400 -2404 MHz) from the other signals picked up by the antenna and get the signal ready for mixing. The HG is responsible for generating the necessary mixing signal, which is used to split up the information carrying signal and carrier signal. The final block is the mixer, which mixes the two incoming signals (splits up) and outputs the information carrying signal of 144 MHz.

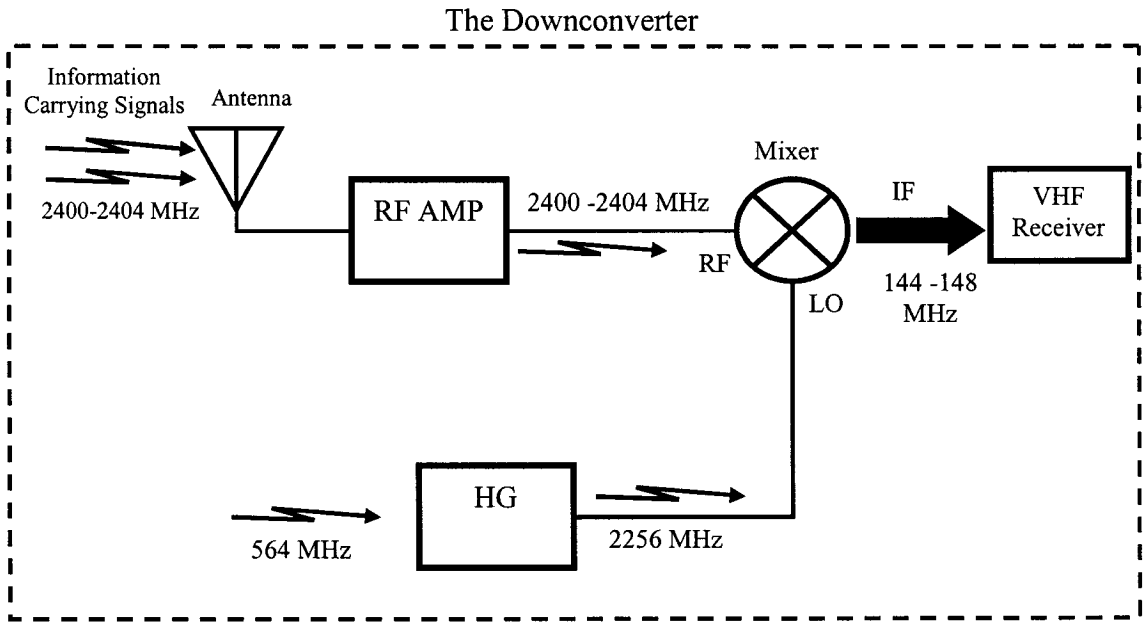

Figure 2.1: The downconverter box topology.

In this process, there are some critical points in the design. First of all, the RF AMP part has to filter out the signal of interest with minimum loss and noise and supply the necessary gain. Moreover, it has to reject the spurious frequency with a great performance. The idea of spurious frequency is given in Chapter 3 in great detail. Similarly, the HG part has to give a clear LO signal to the mixer because the mixer mixes any given two signals so if the signals at the input ports of the mixer are not clean, in the output there will be many unwanted signals, which will degrade the performance of the radio. Indeed, even though there applied clean signals, there will be harmonics, which are generated by the nonlinear nature of the mixer. The theories behind the working principles of the design blocks will be discussed in Chapter 3 in great detail.

In the design a harmonic generator used in order to supply the local oscillator signal to the mixer. Basically, the harmonics generator multiplies the externally applied signal at

564 MHz to give 2256 MHz. The harmonics generator used to multiply the signal instead of directly applying the 2256 MHz from outside because, in the future, work it is anticipated so that a crystal controlled oscillator for 564 MHz will be designed and built. It is relatively difficult to design and build an oscillator for 2256 MHz. Hence, a harmonics generator is used.

2.2 How Does It Work?

The input signal comes in to the RF AMP part of the circuit. The schematic block diagram is shown in Figure 2.2. The signal is filtered by using a 5-pole hairpin filter and amplified using an Agilent MGA 86576 GaAs FET amplifier and reaches the mixer. The other signal for the mixer is supplied from the HG. With a similar approach, a 564 MHz signal is applied from an outside source to the input of the HG. The block diagram is shown in Figure 2.3. In the HG, the harmonics of the incoming signal are generated, the fourth harmonic of 564 MHz, 2256 MHz is filtered out and amplified by using the Agilent MGA 86576. In the mixer, the two signals (2400 MHz and 2256 MHz) are mixed to give 144 MHz output.

RF Amplifier

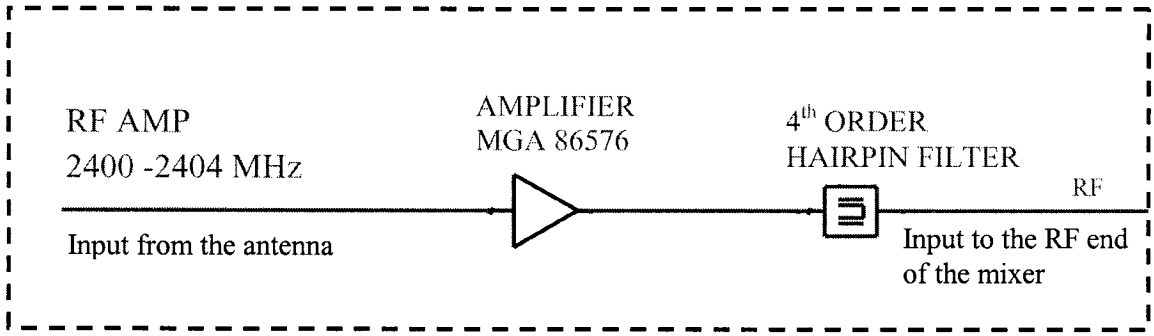

Figure 2.2: System schematic of the RF amplifier.

The RF amplifier consists of an Agilent MGA 86576 amplifier and a 5-pole hairpin filter.

Harmonics Generator

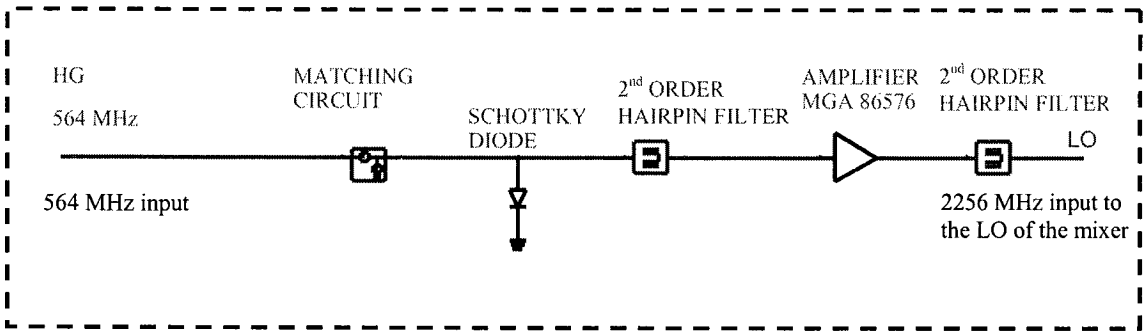

Figure 2.3: System schematic of the harmonics generator.

The harmonics generator consists of a glass Schottky diode, an Agilent MGA 86576 amplifier and two 3-pole hairpin filters.

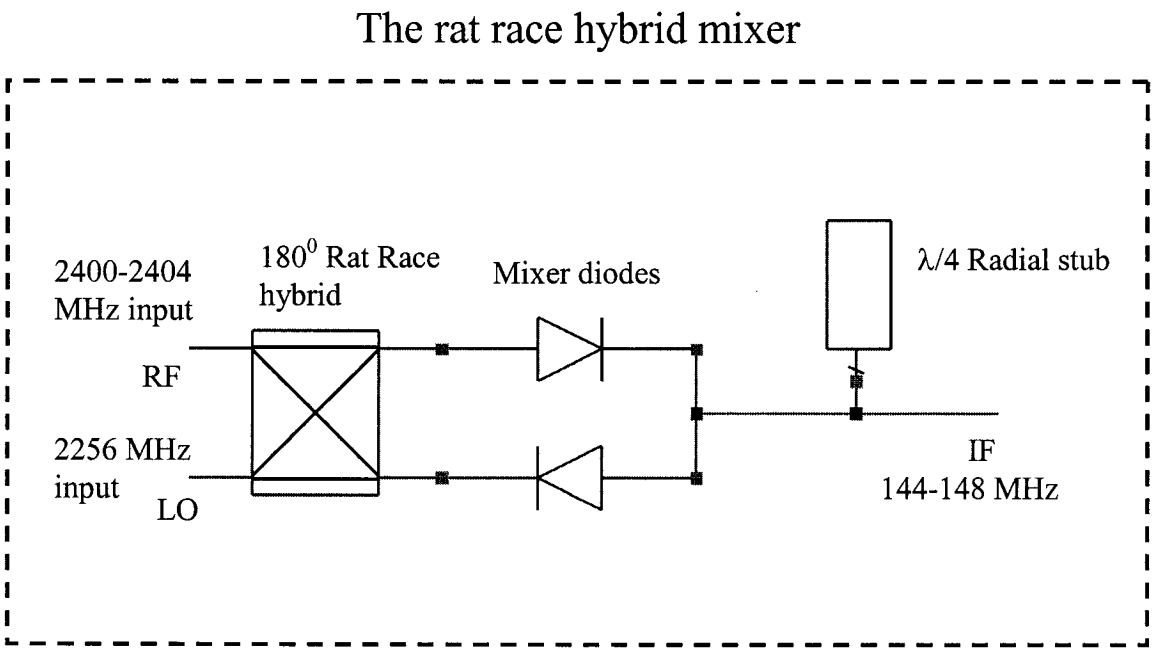

Figure 2.4: System schematic of the rat race hybrid mixer.

The rat race hybrid coupler consists of a rat race 180^0 degree coupler, two MA4E2054B-287T mixer diodes and a quarter wave radial stub.

During this operation, hairpin filters are used for filtering purposes, a rat race mixer is used for mixing, and the nonlinearity of HG was achieved by using a Schottky glass diode. In the design, maximum spurious response (spur) rejection and efficiency was the goal.

3 The Analysis and the Theory

3.1 Introduction

In this chapter, the theory behind the design is investigated. The theoretical approach to coupling structures, hairpin filter, rat-race coupler mixer and harmonics generator are discussed in detail.

3.2 Hairpin Filter

3.2.1 Background

Today, wireless communication is rapidly growing. The extensive usage of cell phones and satellite systems require modern microwave communication systems. These modern microwave communication systems require high-performance, narrow-band bandpass filters with low insertion loss. One solution to this necessity is the hairpin bandpass filter.

The hairpin filters are commonly used in many microwave applications due to its small size, weight, cost and easy reproducibility. First, hairpin line filters were introduced by Cristal and Frankel in 1972 [4] in order to fulfill the demand in the market and reached to success shortly after introduced. The developments are summarized in the book by Hong and Lancaster [5] Microstrip Filters for RF/Microwave Applications, in which the coupling structures and hairpin design issues discussed in detail. Wong, [8] introduced microstrip tapped-line filter design which made realizing the input and output ports easier. Not a long time ago, Hong and Lancaster developed mathematical models to analyze the coupling of microstrip square open-loop resonators for a cross-coupled planar

microwave filter [7], which discusses the effects of magnetic and electric coupling between hairpin resonators.

3.2.2 Theory and Design of Hairpin Filters

The hairpin filter structure is a compact structure but basically it is the "U" shape folded versions of the coupled edge resonators. The discussion for coupled-edge lines are also valid for hairpin filters however, since the resonators are folded, the coupling between two arms of the resonators plays an important role. The idea of the hairpin filter is to change the physical orientation of the resonators to reduce the size of the filter, while keeping the same performance as a coupled line filter. Nevertheless the coupling between the resonator arms and the parasitic effects at the bends make the design of the hairpin filter more challenging [6]. The filter prototype is shown in Figure 3.1.

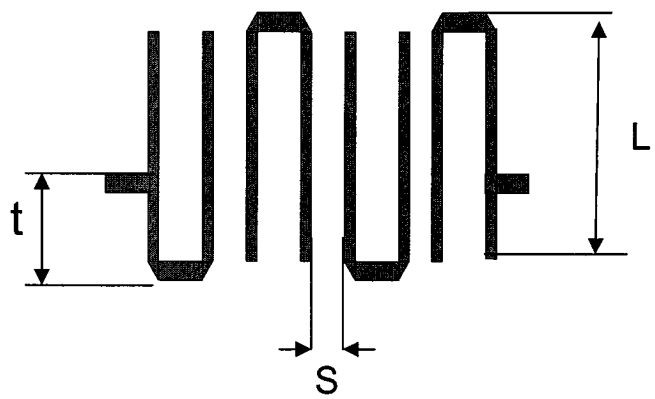

Figure 3.1: Four resonator hairpin filter tapered line feed.

The basic theory of hairpin filters is based on the idea of the half-wavelength parallel-coupled (edge-coupled) microstrip transmission lines. Following the design procedure for the coupled line filter then converting it to a hairpin filter is possible.

In this thesis two hairpin filters are designed with the specifications described in Table 1. Besides, the substrate has a dielectric constant of 3.48, loss tangent of 0.0031 at 2.5 GHz and thickness of 0.020 inch. In both filters, 0.5 dB Chebyshev equal-ripple prototype values are used and the width of the transmission line is specified by the requirement of a 50 ohms impedance.

	The 5-pole filter	The 3-pole filter
Center frequency	2400 MHz	2256 MHz
Fractional Bandwidth $\left(\frac{\Delta f}{f_0}\right)$	4.4%	5.1%
Bandwidth	105 MHz	115 MHz
The rejection	More than 30 dB at 2112 MHz	More than 30 dB at 1692 MHz and 2820 MHz

Table 1.1: The design goals for the hairpin filters.

A bandwidth of around 100 MHz is preferred for both filters because it is very possible that there will be errors in the manufacturing and the errors will affect the response of the

filter. After manufacturing it is possible to have a shift in the response. So, in order to compensate the possibility of error, a wide bandwidth is preferred.

So, first the lumped element versions of the filters specified above are designed using the design approach in [8].

3.2.2.1 The Lumped Element Filter

Thee pole means three resonators, N = 3 so, the prototype values are

$$g_1 = g_3 = 1.5963 \qquad g_2 = 1.0967 \tag{3.1}$$

where the fractional bandwidth is

$$\Delta = \frac{\omega_2 - \omega_1}{\omega_o} \quad \Rightarrow \quad \Delta = \frac{150}{2256} = 0.07. \tag{3.2}$$

So, the lumped element values are for the circuit shown in Figure 3.2

$$L_1' = \frac{g_0 Z_0}{\Delta \omega_o}, C_1' = \frac{\Delta}{g_0 \omega_0 Z_0}, L_2' = \frac{g_1 Z_0}{\Delta \omega_o}, C_2' = \frac{\Delta}{g_1 \omega_0 Z_0}. \tag{3.3}$$

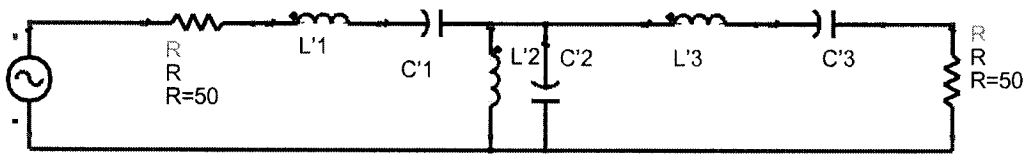

Figure 3.2: Lowpass 0.5 dB equal-ripple filter prototype. Reprinted from [8].

Hence, according to the prototypes given in (3.1) the values of the lumped elements become

$$L_1' = L_3' = 80nH, \quad C_1' = C_3' = 0.062\text{pF}, \quad L_2' = 0.46\text{nH}, \quad C_2' = 10.8\text{pF}. \tag{3.4}$$

The response of the circuit in Figure 3.2 is given in Figure 3.3

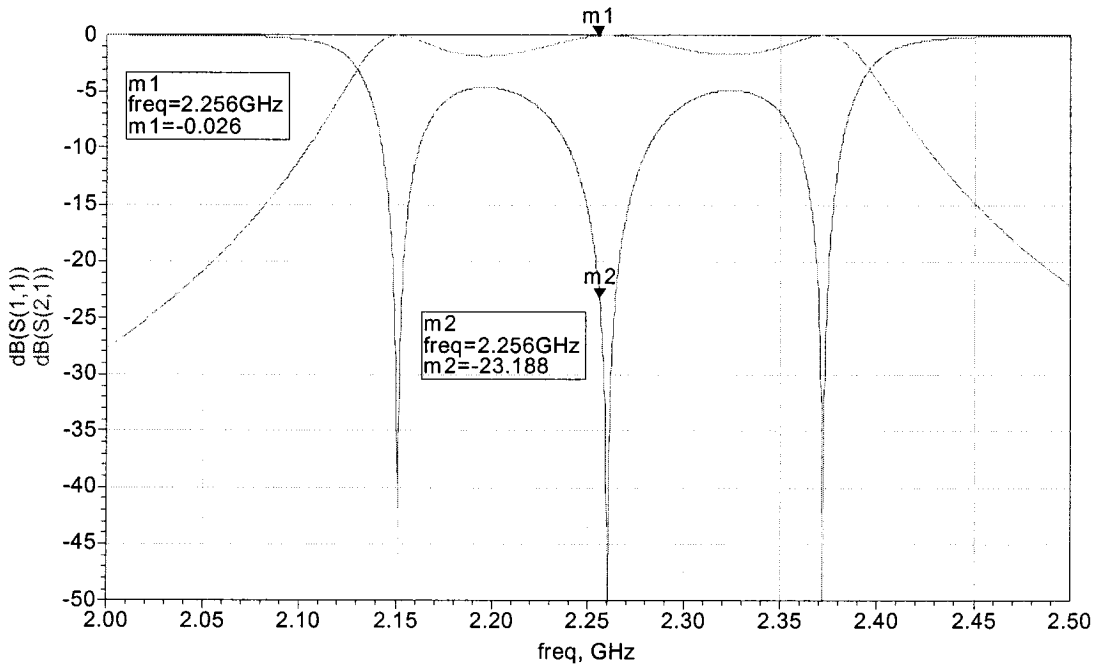

Figure 3.3: The response of the three pole lumped circuit filter.

By using the same procedure, with the prototype values given in (3.5) the 5-pole filter is produced (not shown), using

$$g_1 = g_5 = 1.7058 \qquad g_2 = g_4 = 1.2296 \quad g_3 = 2.5408\ . \tag{3.5}$$

Before going from lumped element filter prototype to the hairpin filter, there are some issues, which need to be discussed such as the coupling between transmission lines, tapping location of the input and output ports, the effect of discontinuities in the hairpin structure.

3.2.3 Couplings of Microstrip Square Open-loop Resonators

The next discussion is the coupling between the microstrip square open-loop resonators and their filter applications, which will lead us to the coupling theory of the hairpin filter [7].

3.2.3.1 Coupling Structures

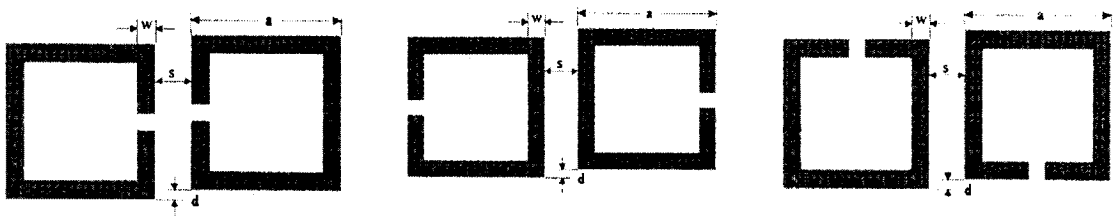

Electric Coupling (a) **Magnetic Coupling (b)** **Mixed Coupling (c)**

Figure 3.4: Coupling structures. (Reprinted from [7]).

As shown in Figure 3.4 there are three basic coupling structures encountered in cross-coupled filters. These different coupling structures arise from the different orientations of open-loop square resonators separated by a distance of *s*. The couplings form in those structures due to the fringe fields yet, the nature and the strength of the fields determine the type of the coupling. It is known that the maximum electric coupling in a single resonator occurs at the side of the open-gap whereas, the maximum magnetic coupling occurs at the opposite side at the maximum electric field. This is because the electric fringe field is stronger at the side, where electric field distribution is strong, similarly the magnetic fringe fields are stronger, where the magnetic field distribution is strong. So, maximum electric coupling is obtained if the open ended sides of the resonators placed

side by side as shown in Figure 3.4 b, similarly, maximum magnetic coupling is obtained if the sides of the resonators placed side by side. Finally, if the resonators are placed as shown in Figure 3.4 c both strong magnetic and strong electric couplings are obtained, which is referred as mixed coupling.

3.2.3.2 Formulation of Coupling Coefficients and Equivalent Circuit Models

3.2.3.2.1 Electric Coupling

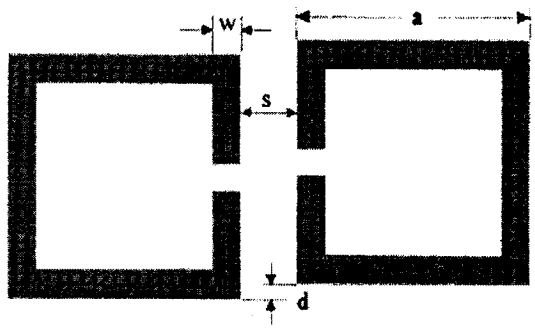

Figure 3.5: Electric coupling structure of open-loop resonator. (Reprinted from [7]).

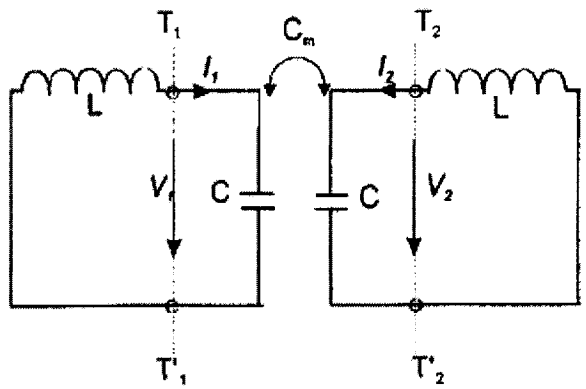

Figure 3.6: The equivalent circuit for the electrically coupled structure. (Reprinted from [7]).

The electric coupling of Figure 3.5 between the two resonators is represented by an admittance inverter $J = \omega C_m$. Where, L and C corresponds self-impedance and self-capacitance and the $(LC)^{-1/2}$ equals to angular frequency of uncoupled resonators and C_m represents the mutual capacitance between resonators. The resonant frequency of the resultant circuit is

$$f_e = \frac{1}{2\pi\sqrt{L(C + C_m)}}. \tag{3.6}$$

The, resonant frequency is lower than of the uncoupled single resonator, which can physically be explained by the coupling effect which enhances the charge storing capacity of the resonator when the electric wall is inserted. Expectedly, inserting a magnetic wall (open circuit) increases the resonant frequency

$$f_m = \frac{1}{2\pi\sqrt{L(C - C_m)}}. \tag{3.7}$$

The equations above can be used to obtain the electric coupling coefficient

$$k_e = \frac{f_m^2 - f_e^2}{f_m^2 + f_e^2} = \frac{C_m}{C}. \tag{3.8}$$

It is also important to mention that k_e is identical to the ratio of coupled electric energy to the stored energy of the uncoupled single resonator.

3.2.3.2.2 Magnetic Coupling

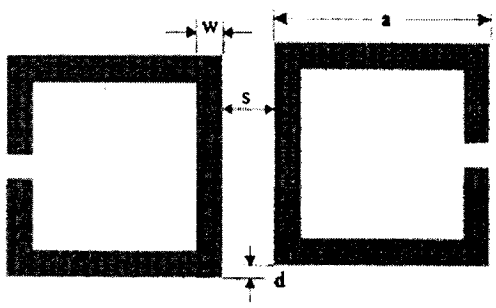

Figure 3.7: Magnetic coupling structure of open-loop resonator (Reprinted from [7]).

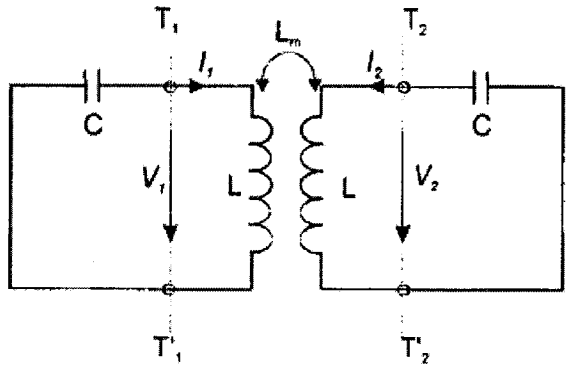

Figure 3.8: Equivalent circuit for magnetically coupled structure (Reprinted from [7]).

In a similar manner, it is possible to calculate the magnetic coupling coefficient. The L and C correspond to self-impedance and self-capacitance, the $(LC)^{-1/2}$ equals the angular frequency of uncoupled resonators and L_m represents the mutual capacitance between resonators in Figure 3.7.

$$f_e = \frac{1}{2\pi\sqrt{C(L - L_m)}}. \tag{3.9}$$

$$f_m = \frac{1}{2\pi\sqrt{C(L + L_m)}}. \tag{3.10}$$

The equations above can be used to obtain the magnetic coupling coefficient

$$k_m = \frac{f_e^2 - f_m^2}{f_m^2 + f_e^2} = \frac{L_m}{L}. \tag{3.11}$$

It is also important to mention that k_m is identical to the ratio of coupled magnetic energy to the stored energy of uncoupled single resonator. Most importantly, k_m and k_e are in reverse phases, which is the crucial property of the cross-coupled filters.

3.2.3.2.3 Mixed Coupling

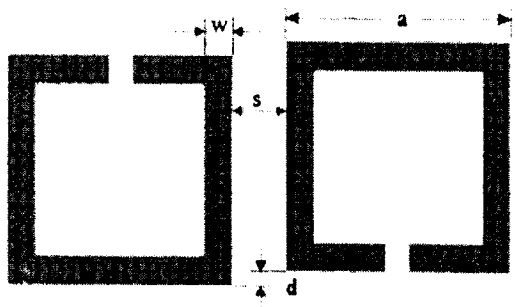

Figure 3.9: Mixed coupling structure. (Reprinted from [7]).

In the mixed coupling structure, both the magnetic and electric coupling are strong and comparable to each other so that neither of them could be ignored. The coupling structure of this situation is called *mixed coupling*. The resonant frequencies can be found as

$$f_e = \frac{1}{2\pi\sqrt{(C - C'_m)(L - L'_m)}} \tag{3.12}$$

$$f_m = \frac{1}{2\pi\sqrt{(C + C'_m)(L + L'_m)}}. \tag{3.13}$$

Here, L and C correspond to self-impedance and self-capacitance. C_m and L_m represent the mutual capacitance and mutual inductance between resonators. Using (3.12) and (3.13), the mixed coupling coefficients become,

$$k_B = \frac{f_e^2 - f_m^2}{f_m^2 + f_e^2} = \frac{CL'_m + LC'_m}{LC + L'_m C'_m}. \tag{3.14}$$

It is reasonable to assume $L'_m C'_m << LC$ so that

$$k_B \approx \frac{L'_m}{L,} + \frac{C'_m,}{C,} = k'_M + k'_E. \tag{3.15}$$

So, as seen from above, mixed coupling is the superposition of the electric and the magnetic couplings in phase, which is the result that been expected. The ratios of k'_M/k_M and k'_E/k_E depends on to the structure and calculated either using a CAD or experimentally [5].

In here it is important to mention that in all the derivations above, it has been assumed that both resonators are identical. When both resonators are identical, this is called *Synchronous Coupling*. In this case the resonant frequencies of both resonators are the same. However, in the asynchronous mode, the resonators are not identical and the resonant frequencies are different. The approach to find the equivalent circuit for asynchronous mode is not very different than the method given in the discussion above. If interested, the reader can find the detailed approach in [5].

3.2.3.3 Numerical Examples

To demonstrate the theory presented above, some experiments were done in [5]. Some coupling structures were formed from half wave folded resonators and tested. The detailed theory is very involved; the reader is referred to [5] for the details.

In order to design the hairpin filter, the coupling coefficient versus distance information is required. As mentioned earlier in Chapter 3, this information can only be obtained experimentally or by a full wave computer simulation. So, in order to obtain the information, a full wave simulation was done by using the ADS.

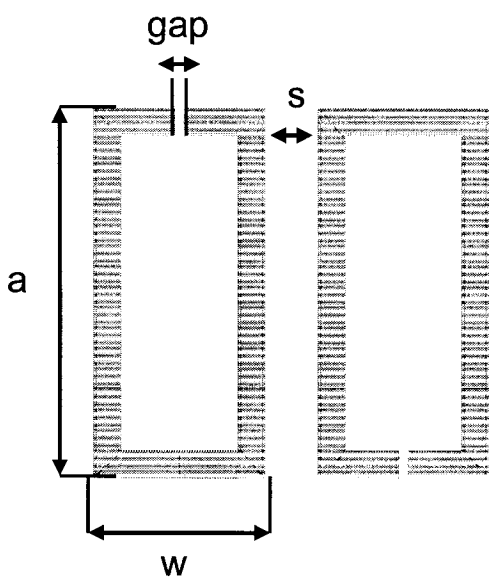

Figure 3.10: The coupled line structure.

The resonators shown in Figure 3.10 were uniquely designed in order to extract information about the coupling coefficients that are needed for designing the hairpin filters. The substrate with a dielectric constant of 3.48 with loss tangent of 0.0031 and

thickness of 0.020 inch was used and the resonators were synchronously tuned, which have a length, *a*, of 13 mm for 2400 MHz and 14.2 mm for 2256 MHz and width, *w*, of 1.154 mm. The simulations, will be discussed in Chapter 4, were done using a gap distance of 2 mm and changing coupling distance *s*. Hence, the responses in Figure 3.11 were achieved and the mixed coupling coefficient versus coupling distance graph was obtained as shown in Figure 3.12.

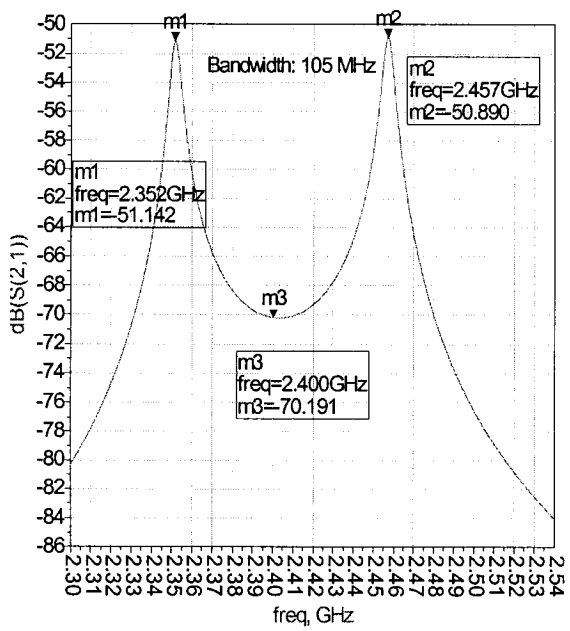

Response for the 5-pole filter at 2400 MHz.

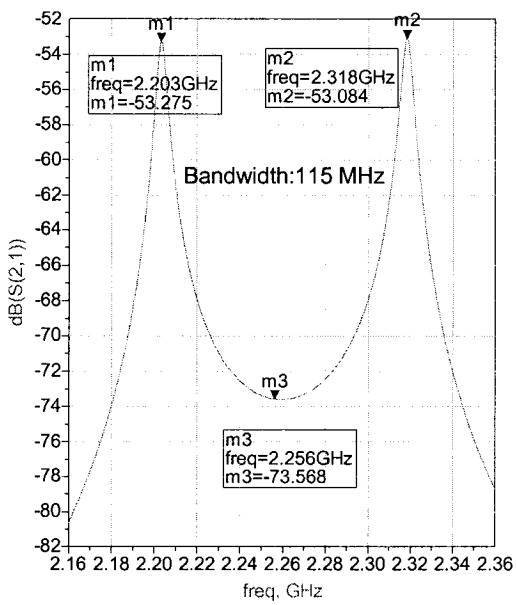

Response for the 3-pole filter at 2256 MHz.

Figure 3.11: Responses of the mixed coupled resonators for two center frequencies of 2400 MHz and 2256 MHz.

The coupling distances of the resonators shown in Figure 3.11 are S = 0.8 mm and S = 0.75 mm respectively. The markers indicate the two poles and the frequency of the

interest for each filter. Note that, since two resonators used, there are only two poles. The frequency shift between the two responses is due to the difference in the length of the coupled lines. The length of the coupling lines were chosen to obtain the center frequencies indicated in Figure 3.11. The future discussions about the coupled resonators are done in Chapter 4. Also, from the same coupled resonators used above, the response in Figure 3.12 was obtained. How Figure 3.12 is obtained is shown in (3.16).

$$k_B = \frac{f_1^2 - f_2^2}{f_1^2 + f_2^2} = \frac{(2457)^2 - (2352)^2}{(2457)^2 + (2352)^2} = 0.044\,. \tag{3.16}$$

As seen from (3.16), the coupling distance, S, of 0.8 mm corresponds a coupling coefficient of 0.044. So, by calculating the coupling coefficient for varying coupling distance, Figure 3.12 is obtained.

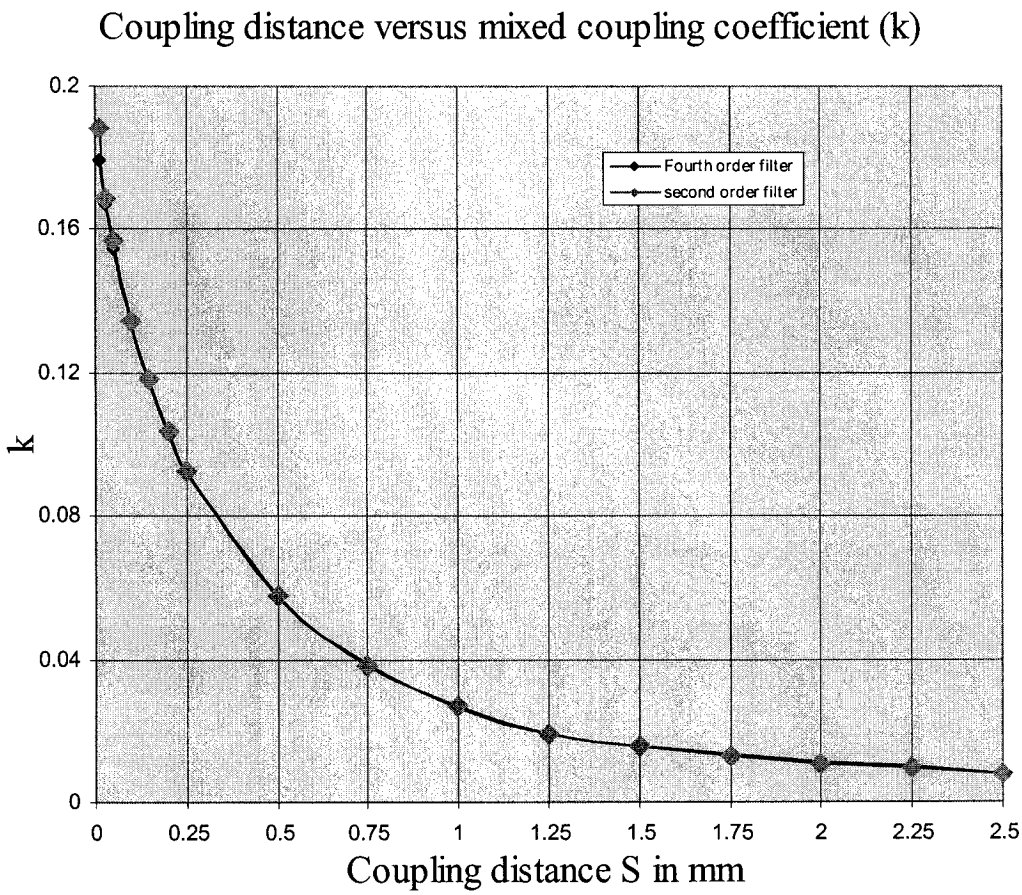

Figure 3.12: Mixed coupling coefficient k_B versus distance S.

Figure 3.12 shows the change in the value coupling coefficient versus the coupling distance S. The two lines correspond to the two different structures designed for two different center frequencies. The "5-pole filter" indicates the resonators designed for the center frequency at 2400 MHz, similarly, "3-pole filter" indicates a center frequency of 2256 MHz. The reason why these two responses are almost same is that the coupling structures are not very different from each other, only the length of the coupling lines is different and this difference is 1.2 mm.

Importantly, the full wave simulation result of the ADS shown in Figure 3.12 is consistent with the outcomes of [7] and [5].

So, the discussion in this section concludes the discussion of the couplings between the hairpin resonators. The following section discusses how to introduce a port to a hairpin resonator.

3.2.4 Formulation for Extracting External Quality Factor Qe

In order to excite the resonators, the power transfer between the feed line and the resonator should be accomplished. In order to obtain maximum power transfer, the feed line should be matched to the resonator. There are various coupling structures but only two types are discussed in here due to the matter of practical interest. [6]

The quality factor, Q of a resonator is one of its important features. Q is a measure of the loss of a resonant circuit. Q is inversely proportional with the loss so, the higher the Q value, better for the resonator. The quality factor is defined as [6]

$$Q = \omega \frac{Average \text{ Energy Stored}}{\text{Energy loss/second}}. \tag{3.17}$$

For the analysis of the coupling structures, defining of ports is required or in other words, exciting the resonators is necessary. There are two possible ways to define the ports. One is using tapped lines and the other is to use coupled line structures, both are shown in the Figure 3.13.

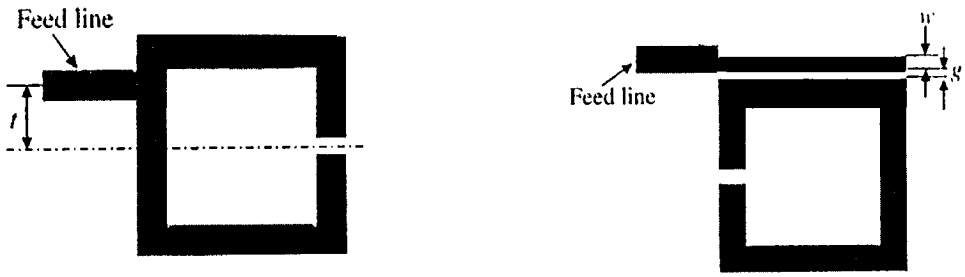

Tapped-line feed. (Reprinted from [5]). Coupled line feed. (Reprinted from [5]).

Figure 3.13: Possible feeding methods.

In the tapped line case, generally a 50 ohm (or in any other impedance) feed line is tapped directly onto the I/O resonator and the external quality factor Q_e is defined according to the tapping position *t*. For instance, if the tapping distance gets smaller, the tapped line gets closer to the virtual ground of the resonator and this causes weaker coupling, which means higher external quality factor. The other way to introduce the I/O port is to use coupled-line coupling. In that case, a smaller gap and a narrower line results in strong coupling or smaller external quality factor [5].

3.2.4.1 Tapped Microstrip Hairpin Resonator

The realization of the tapped hairpin resonator structure and its equivalent circuit is given in Figure 3.14 [8].

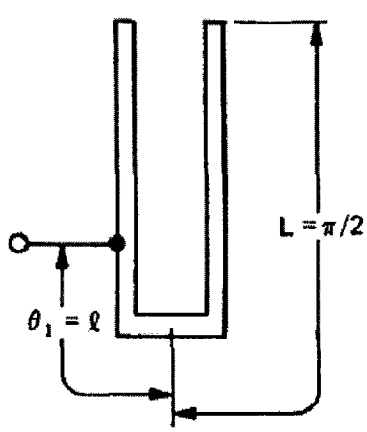

Tapped hairpin resonator. (Reprinted from [8]).

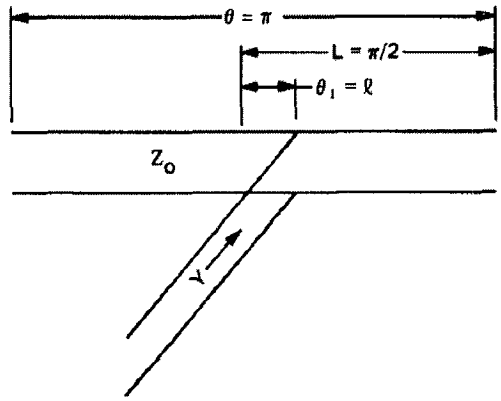

Equivalent circuit for tapped hairpin resonator. (Reprinted from [8]).

Figure 3.14: Tapped hairpin resonator.

It is crucial to mention that the equivalent circuit for a tapped hairpin resonator is valid when the coupling between two arms of the resonators is minimum and negligible. For the calculation of the tap point, the singly loaded Q values (calculated from the prototype values) of the first and the last resonators are required as well as the coupling coefficient, k, between the adjacent resonators. The tapping distance is given as [8]

$$l = \frac{2L}{\pi}\sin^{-1}\left(\sqrt{\frac{\pi}{2}\frac{Z_0/Z_r}{Q_e}}\right). \tag{3.18}$$

In the calculation of the tapping distance, the effect of the neighboring resonator ignored in order to simplify the formula. However, the experimental results show that the tapping

distance calculated the using (3.18) gives a good approximation. Zr stands for the characteristic impedance of the tapping line.

However, both [5] and [8] indicate that running a full wave simulation would give a slightly different result. In the end, both writers point out that (3.18) is a good approximation.

3.2.5 Equivalent Circuit Approach to Hairpin Line

The equivalent circuit approach for a hairpin line was presented in [9] in 1971 by S. Frankel, and since then that model is used. The equivalent circuit model is based on the assumption that the coupling beyond the neighboring resonators is negligible.

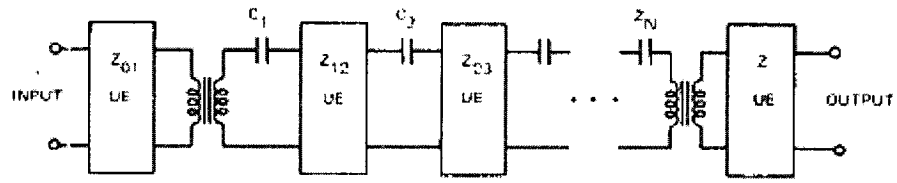

Figure 3.15: Equivalent circuit of hairpin line. (Reprinted from [4]).

C_i represents the open-circuited transmission line of characteristic impedance of C_i, and U.E. represents the unit element characteristic impedance $Z_{i,\,i+1}$ [4].

As seen from Figure 3.15, the equivalent circuit models for coupled line filters and hairpin filters are very similar, which is what was expected. The only difference is that for the hairpin filter extra coupling between adjacent arms of a single resonator is introduced. This is modeled using a capacitor, spaced between two unit elements. The effect of coupling is given in the following section.

3.2.6 The Effect of Unwanted Couplings in Hairpin Filters and Ways to Avoid It

The modeling by using a capacitor was introduced by E. Cristal and S. Frankel in [4] as the reduction in the fractional bandwidth due to the coupling between the arms of the resonators and named *cp*.

In [4], the reduction in the fractional bandwidth due to the coupling between the arms of the resonators (cp) is discussed. The cp is formulated as follows

$$cp = -20\log_{10}\left(L_{ij}\Big/\sqrt{L_{ii}L_{jj}}\right) \text{ for } j = i + 1 \tag{3.19}$$

where $L_{ij}\Big/\sqrt{L_{ii}L_{jj}}$ is the mixed coupling coefficient, which was defined earlier in Chapter 3.

Going from inductance to capacitance is given as

$$[C] = [L]^{-1} . \tag{3.20}$$

The coupling between the arms of a single resonator and its effect on the bandwidth contraction is given in Figure 3.16.

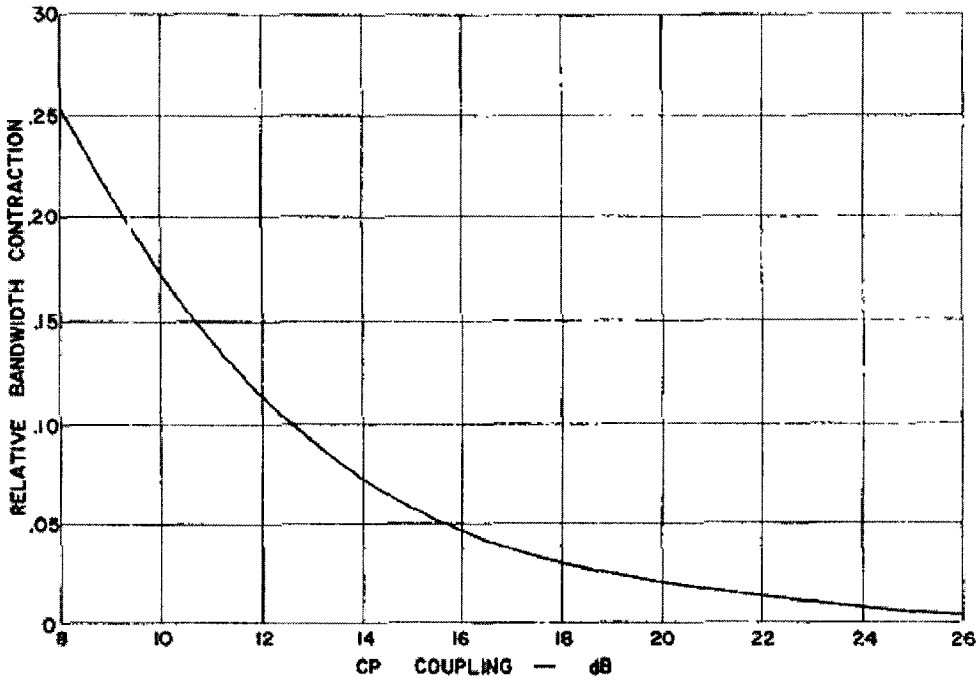

Figure 3.16: Relative bandwidth contraction versus coupling. (Reprinted from [4]).

Fractional Bw. Obtained = Fractional Bw. proposed X (1-Relative Bw. Contraction)

As seen in Figure 3.16, with increasing cp (coupling between the arms of a single resonator), the effect of bandwidth reduction reduces and $cp = \infty$ indicates the case of coupled line filter that no coupling between the arms of the hairpin resonator happens. The percentage bandwidth contraction was found to be virtually independent of the proposed fractional bandwidth of the design and the number of resonators, N.

It is important to mention that the *cp* value must be defined in the very beginning of the hairpin filter design by the designer, and [4] proposes defining a coupling greater than 24 dB is a good approximation for hairpin filter so that ignoring the effect of the coupling between the adjacent arms of the single resonator can be possible [4].

If (3.19) used as well as Figure 3.16, it will be seen that 24 dB indicates that the distance between the resonators should be chosen 2.5 times larger than the coupling distance between the resonators. This is shown in Figure 3.17.

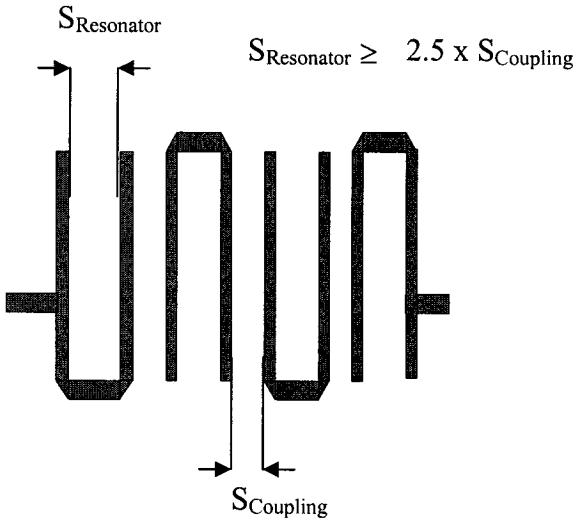

Figure 3.17: Coupling distances in a hairpin filter.

So to sum up, if the distance between the arms of the resonator is chosen 2.5 times larger than the coupling distance between the hairpin resonators, the capacitance between the adjacent arms of the hairpin resonator, which was introduced in the equivalent circuit can be ignored. If that capacitance is ignored, the equivalent circuit of the hairpin filter simplifies to the coupled line filter case. However, the parasitic effects at the bends of the hairpin filter must be discussed in order to truly simplify the case.

If the spacing between the arms of the resonator is not well designed, the filter can suffer from reduced bandwidth and increased insertion loss [11].

So, in the design of the hairpin filters for the harmonics generator and the RF amplifier, the distance between the arms of the resonators were taken around three times larger than the distance between the coupling resonators.

3.2.7 Effect of Bend Discontinuities

The microstrip bends are used to change the direction of the microstrip line and are generally 90^0. However, the bends create discontinuities in the field. In a bend of 90^0, the currents are concentrated near the inner corner which causes fringing effects at the outer corner as compared with non-bent homogenous microstrip lines. So, due to this phenomenon, the corner can not be modeled with Z_0, ε_r and a known length. However, it is possible to model the corner with an equivalent circuit, given in Figure 3.18 [19].

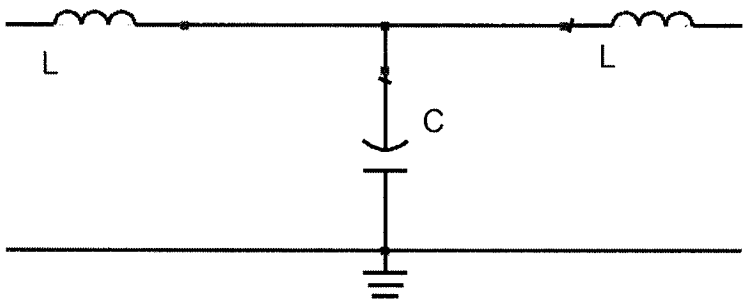

Figure 3.18: The equivalent circuit for the 90^0 degree bend. (Reprinted from [19]).

If the discussion in [19] is followed, the inhomogeneous distribution of currents at the bend causes the characteristic impedance of the outer corner to change. The change in characteristic impedance at the bend causes reflections. Since a reflection free bend is required, compensation is introduced by cutting the corner of the bend at 45^0 as shown in the Figure 3.18. The relative compensation (chamfer) in percent is given as:

$$S^* = 100\,s/d = \left(1 - \frac{b}{d}\right)100 = \left[1 - \frac{b}{w\sqrt{2}}\right]100. \tag{3.21}$$

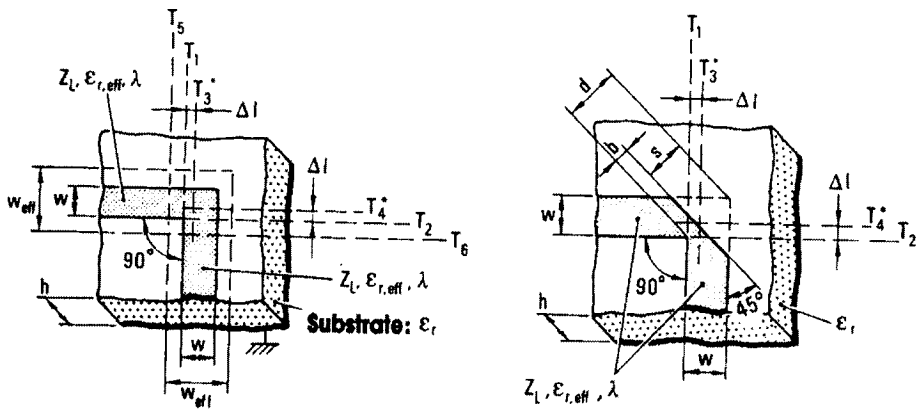

Uncompensated bend. Compensated bend.

Figure 3.19: Bending structures. (Reprinted from [19]).

The chamfered bend can also be called a partially compensated bend. If S^* increases, the C_1 in the equivalent circuit reduces, which means the parasitic capacitance reduces. Similarly, the value of L_1 reduces with the increasing chamfer. The ideal case is to have no parasitic capacitance ($C_1 = 0$), which is called as optimal compensation denoted as S_{opt} and when it happens, a reflection free response achieved. For cases $S^* > S_{opt}$, $C_1 < 0$ is called an overcompensation and causes a reduction in the electric field strength [19].

Hence, an optimally compensated bend is the very goal of designing a reflection free bend, which reduces the effect of discontinuities. For detailed discussion about the effect of bend discontinuities, please refer to [19].

3.2.8 Design Formulas for Microstrip Lines

In the design, transmission lines with two different characteristic impedances (50 Ohm and 70 Ohm) were required for various components. According to the substrate properties, (3.22), (3.23) and (3.24) were used to obtain the necessary transmission line widths.

$$\varepsilon_e = \frac{\varepsilon_r + 1}{2} + \frac{\varepsilon_r - 1}{2} \frac{1}{\sqrt{1 + 12d/W}} \tag{3.22}$$

$$A = \frac{Z_o}{60}\sqrt{\frac{\varepsilon_r + 1}{2}} + \frac{\varepsilon_r - 1}{\varepsilon_r + 1}\left(0.23 + \frac{0.11}{\varepsilon_r}\right) \tag{3.23}$$

$$\frac{W}{d} = \frac{8e^A}{e^{2A} - 2} \tag{3.24}$$

So, the following results obtained:

$$\varepsilon_r = 3.48,\ \mathrm{Tan}\delta = 0.0031, \mathrm{d} = 0.020\,\mathrm{inch} \tag{3.25}$$

$$\begin{aligned} Z_0 = 50\Omega &\Rightarrow \mathrm{Width} = 1.154\,\mathrm{mm} \\ Z_0 = 70\Omega &\Rightarrow \mathrm{Width} = 0.629\,\mathrm{mm}. \end{aligned} \tag{3.26}$$

Moreover, the dielectric constant has an influence on the physical size of the hairpin filters. It is possible to reduce the size by using a high-dielectric substrate or a thin substrate. However, increasing the dielectric constant increases the dielectric loss. In amateur radio applications in order to keep the physical dimensions small, a thick

substrate can be used. However, with a thick substrate, the power consumption of the circuitry dramatically increases. On the other hand, a lower dielectric constant and thin substrate increases the physical dimensions as well as causes an increase in the board radiation [14].

3.2.9 Finalization of the Design of Hairpin Filters

The design procedure of the hairpin filter is not very different than the conventional filter design proposed in [6, Ch. 8]. Initially, the decision about the pass-band behavior of the filter has to be made (maximally flat bandwidth, 0.5 dB equal-ripple, 3 dB equal-ripple, etc.) as well as the order of the filter *N*. Then, the desired attenuation (insertion loss) and bandwidth of the filter are determined. The tables and the charts in [6] can be used to get the filter prototype values (g_n) of the filters. Furthermore, the fractional bandwidth of the filter has to be determined and the cutoff frequency ω_1'. It is important to mention that the design procedure explained so far is for the low-pass filter prototype of the actual filter. After designing the prototype low-pass filter, the desired band-pass filter can be designed using filter transformation techniques explained in [5] and [6]. After transforming the low-pass prototype to the band-pass filter the filter design procedure is complete. For illustration, the example in [5 Ch. 5] can be investigated.

If we continue to design the filters for the downconverter, the prototype values and the specifications of the filters as well as the lumped element models are known and discussed earlier in Chapter 3.

From the given prototype values, the bandpass parameters values obtained as follows

$$Q_{e1} = \frac{g_o g_1}{FBW} \Leftrightarrow Q_{en} = \frac{g_n g_{n+1}}{FBW} \tag{3.27}$$

$$M_{i,i+1} = \frac{FBW}{\sqrt{g_i g_{i+1}}}, \text{ for i = 1 to n.} \tag{3.28}$$

Where Q_{e1} and Q_{en} are external quality factors of the resonators, explained earlier in Chapter 3, at the input and the output and $M_{i,j+1}$ are the coupling coefficients between the adjacent resonators. The g_n values are the prototype values of the lowpass filter and FBW corresponds to the fractional bandwidth. For a 100 MHz bandwidth and center frequency of 2400 MHz, fractional bandwidth become 4.43%.

For the 3-pole filter at 2256 MHz, since the prototype values are given in (3.1), the Q_{en} and $M_{i,j+1}$ values become

$$Q_{e1} = Q_{e5} = 34.51 \tag{3.29}$$

$$M_{1,2} = M_{2,3} = 0.034. \tag{3.30}$$

From Figure 3.11, a coupling coefficient of 0.034 corresponds to a coupling distance between 0.75 to 0.90 mm. Besides, from (3.18) Q_{e1} of 34.51 corresponds to 2 mm. The meaning of 2 mm is shown in Figure 3.20.

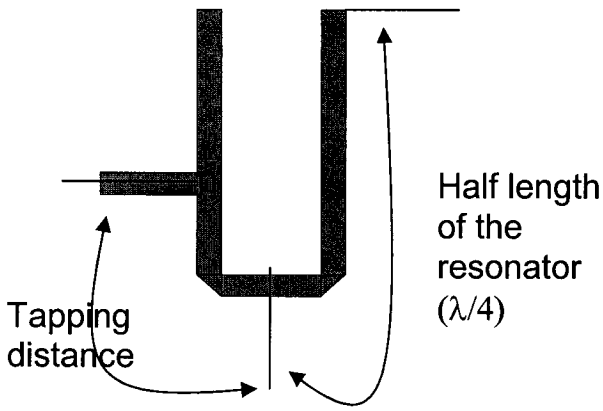

Figure 3.20: The tapping location on the resonator. (Reprinted from 5).

In [5] it is recommended to use a full wave simulation for determining the spacing between the adjacent resonators and the arms of the single hairpin resonator. However as discussed above, 2 to 2.5 times of the coupling resonator distance is enough to get rid of the unwanted coupling between arms of the single hairpin resonator. It is important to keep in mind that if the spacing is not well designed, the filter can suffer from reduced bandwidth and increased insertion loss.

So, the distance between the arms of the resonators was taken as 3 mm which is around 3 times of the coupling distance between the resonators. So the filter in Figure 3.21 is obtained.

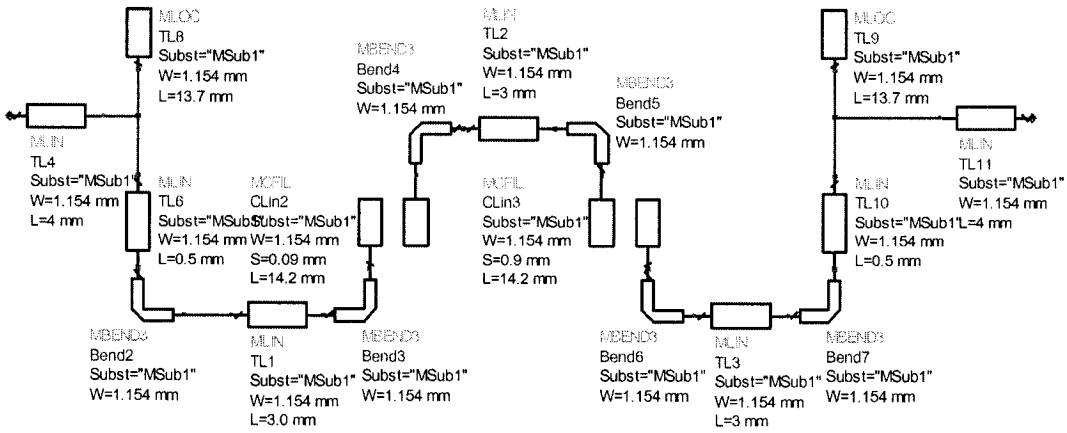

Figure 3.21: The 3-pole filter for harmonics generator centered at 2256 MHz designed by the Hong-Lancaster method [5].

With a similar approach, the filter for the RF amplifier at 2400 MHz was designed. The prototype values are shown in (3.31)

$$g_1 = g_5 = 1.7058 \qquad g_2 = g_4 = 1.2296 \;\; g_3 = 2.5458. \tag{3.31}$$

The FBW for 100 MHz bandwidth is 0.0443,

$$Q_{e1} = Q_{e5} = 47.85 \tag{3.32}$$

$$M_{1,2} = M_{4,5} = 0.03 \;\; M_{2,3} = M_{3,4} = 0.025. \tag{3.33}$$

The coupling coefficients of 0.003 and 0.025 correspond around 1 mm and 1.25 mm respectively. Q_{e1} of 47.85 corresponds around 1.8 mm. The distance between the arms of the resonator is chosen as 4.2 mm. So the resulting filter is shown in Figure 3.22

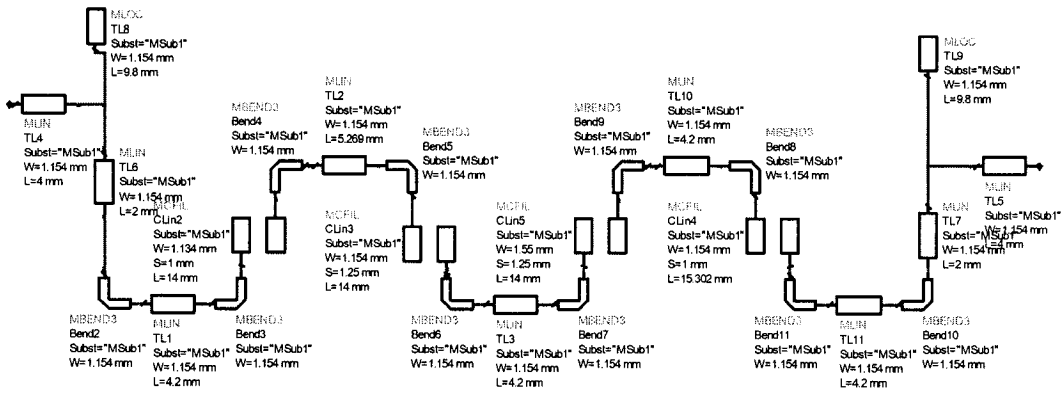

Figure 3.22: The 5-pole filter for RF amplifier centered at 2400 MHz designed by Hong-Lancaster method [5].

3.3 The Mixer

As recalled from Figure 2.4, for the downconverter, a 180^0 hybrid coupler mixer is preferred.

3.3.1 Theory of the Mixer

A mixer is a nonlinear device used to achieve frequency conversion of an input signal. Microwave diodes are the most commonly used nonlinear elements, indeed the nonlinear voltage-current characteristics of a diode causes the desired conversion. The conversion is based on to the diode equation of $I(V) = I_s\left(e^{\alpha V} - 1\right)$, where, $\alpha = q/nkT$, q is the charge of an electron, k is the Boltzmann's constant, T is the temperature, n is the ideality factor and I_s is the saturation current. Typically Is is between 10^{-6} and 10^{-15} A and $\alpha = q/nkT$ is approximately 1/(25 mV) for T = 290^0 K. The value of ideality factor, n, depends on the structure of the diode itself and about 1.2 for Schottky barrier diodes [6].

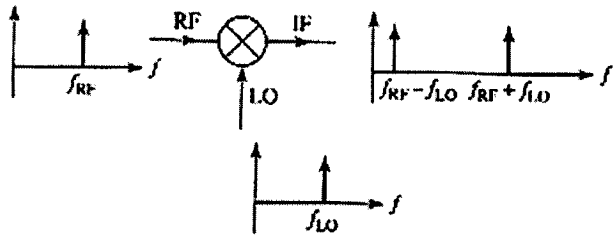

Figure 3.23: Theory of the mixer. (Reprinted from [6]).

3.3.1.1 Single-Ended Mixer

A mixer uses the nonlinearity of a diode to generate an output spectrum consisting of the sum and the difference of the two input signals. In a receiver application, a low level RF signal and a local oscillator (LO) are mixed together to produce an intermediate frequency (IF), $f_{IF} = f_{RF} - f_{LO}$ and a much higher frequency $f_{IF} = f_{RF} + f_{LO}$.

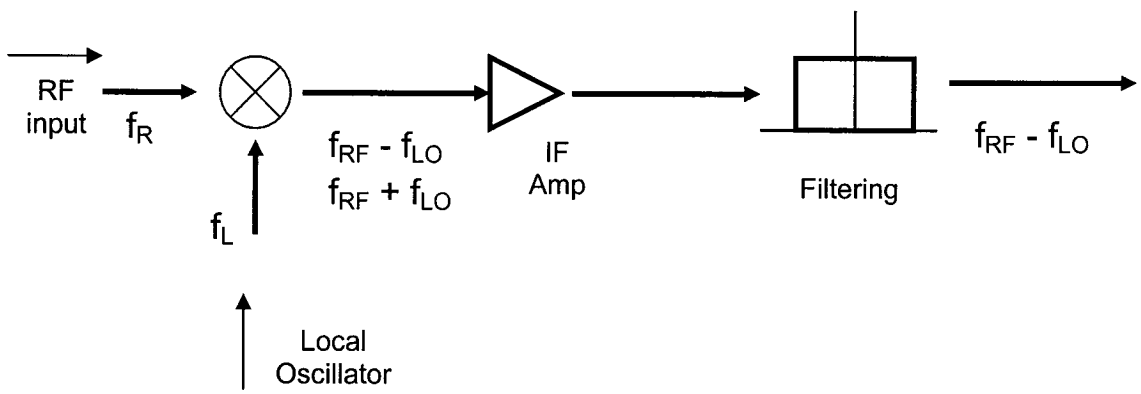

Figure 3.24: Down conversion receiver. (Reprinted from [6]).

3.3.1.2 Balanced Mixer

A balanced mixer combines two or more identical single ended mixers with a 3 dB hybrid junction (90^0 or 180^0) to give better RF input standing wave ratio (SWR) for better RF/LO isolation. The circuit below consists of two single-ended mixers with matched characteristics, driven with a 3 dB hybrid coupler.

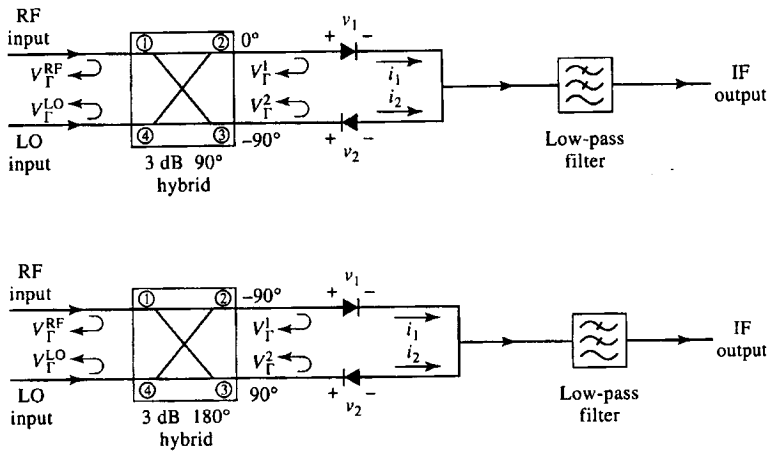

Figure 3.25: Balanced mixer circuits for 90^0 and 180^0 hybrid. (Reprinted from [13]).

In the calculations below, it will be proved that the 90^0 hybrid gives good RF input matching, while 180^0 hybrid gives better RF-LO isolation.

In order to see the improvement introduced by balanced mixer, consider a small signal random noise voltage, $v_n(t)$ applied to LO. Then the RF and LO voltages at the input of the hybrid can be expressed as

$$V_{RF}(t) = v_r \cos \omega_r t \tag{3.34}$$

$$V_{LO}(t) = [v_o + v_n(t)]\cos\omega_0 t\,. \tag{3.35}$$

Where, $v_r << v_0$ and $v_n(t) << v_0$. If the hybrid coupler is 90^0 degrees, the two reflections will arrive and combine back at RF and LO input ports with following amplitudes

$$V_\Gamma^{RF} = \frac{V_{\Gamma 1}}{\sqrt{2}} - j\frac{V_{\Gamma 2}}{\sqrt{2}} = \frac{1}{2}\Gamma V_r - \frac{1}{2}\Gamma V_r = 0 \tag{3.36}$$

$$V_\Gamma^{LO} = \frac{V_{\Gamma 2}}{\sqrt{2}} - j\frac{V_{\Gamma 1}}{\sqrt{2}} = \frac{j}{2}\Gamma V_r - \frac{j}{2}\Gamma V_r = -j\Gamma V_r\,. \tag{3.37}$$

Γ is the reflection coefficient of each diode and V_r is the phasor RF input voltage. So, the RF port is matched but the reflected wave appears in LO port. Similarly, when LO port is driven, the reflected wave appears in RF port. So, using a 90^0 degree coupler gives good SWR characteristics but poor isolation between LO and RF ports.

Instead, if a 180^0 degree hybrid coupler is used with RF applied to sum port and LO applied to difference port, the RF waves reflected from the diodes become.

$$V_\Gamma^\Sigma = \frac{V_{\Gamma 1}}{\sqrt{2}} + \frac{V_{\Gamma 2}}{\sqrt{2}} = \Gamma V_r \tag{3.38}$$

$$V_\Gamma^\Delta = \frac{V_{\Gamma 1}}{\sqrt{2}} - \frac{V_{\Gamma 2}}{\sqrt{2}} = 0\,. \tag{3.39}$$

The LO waves reflected from the diodes will be

$$V_{\Gamma 1} = -V_{\Gamma 2} = \frac{\Gamma V_r}{\sqrt{2}} \tag{3.40}$$

So the reflection back at the sum and difference ports will be

$$V_{\Gamma}^{\Sigma} = \frac{V_{\Gamma 1}}{\sqrt{2}} + \frac{V_{\Gamma 2}}{\sqrt{2}} = 0 \tag{3.41}$$

$$V_{\Gamma}^{\Delta} = \frac{V_{\Gamma 1}}{\sqrt{2}} - \frac{V_{\Gamma 2}}{\sqrt{2}} = \Gamma V_{r}. \tag{3.42}$$

Thus, in both cases, the mismatch appears at the corresponding input port, while RF and LO ports are well isolated. The advantages and the disadvantages of using single-ended mixer, balanced 90^0 and 180^0 mixers were summarized.

Mixer Type	**Number of Diodes**	**RF Input Match**	**RF-LO Isolation**	**Conversion Loss**
Single-ended	1	Poor	Fair	Good
Balanced (90^0)	2	Good	Poor	Good
Balanced (180^0)	2	Fair	Excellent	Good

Table 3.1: The comparison of the mixers. (Reprinted from [13]).

There are some important points in the design procedure of the mixer. The conversion loss, the noise figure and the spur response of a mixer are important.

3.3.1.3 Conversion Loss

In the mixer design procedure, the conversion loss is an important factor, which is defined as

$$L_c = 10\log\frac{\text{Avaliable RF Input Power}}{\text{Avaliable IF Output Power}} \geq 0dB\,. \tag{3.43}$$

This loss occurs due to the resistive elements in the mixer, such as the diode, and the loss in the microstrip and the matching introduced. The matching at both ports is critical because the mixer generates unwanted harmonics and they have to be reduced as much as possible. Good matching can help to reduce the influence of the unwanted harmonics at the output but it contributes to the conversion loss. The matching is accomplished by using a radial stub or a quarter wave length transmission line. Moreover, the RF-IF isolation of the mixer is also important, a poor isolation can cause the mixer to suffer from higher conversion loss.

The typical conversion losses are between 4 to 7 dB in 1 GHz - 10 GHz range. In order to minimize the conversion loss we keep LO value in between 0 to 10 dBm [13].

3.3.1.4 Noise Figure

The noise figure of a mixer is also an important characteristic of the mixer. The noise is unavoidable due to the loss in the diode and the other resistive elements. Besides, noise can come from outside sources like a nearby electromagnetic interference source such as a cell phone or a base station. For detailed discussion of noise in mixers please refer to [13].

3.3.1.5 Image (Spur) Frequency

Since the mixer mixes any given two signals, the frequencies and the amplitudes of the signals applied to the mixer are important. If two signals named f_1 and f_2 are mixed the outputs will be $|f_1 \pm f_2|$. This is shown in Figure 3.26.

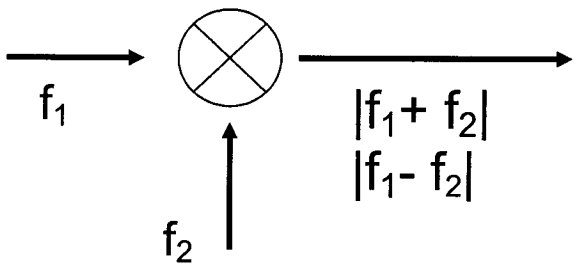

Figure 3.26: Mixer and its spurious response.

This is important because for any given LO signal, there will be two frequencies that will give the same output. In the case of designing a 2400 MHz- 144 MHz downconverter, 2400 MHz is mixed with 2256 MHz gives 144 MHz, likewise, 2112 MHz mixed with 2256 MHz gives the same output of 144 MHz, which makes 2112 MHz the image (spur) frequency of 2400 MHz. In designing both the filters and the mixers, maximum spurious rejection is aimed for enhanced performance.

3.3.2 The Rat Race Hybrid Mixer

The 180^0 hybrid rat-race couplers were introduced long time ago but using them as mixers for microwave applications started in the 1970s. In many amateur radio

applications, designers preferred using 180^0 hybrid rat-race couplers due to its compact size and satisfactory performance. More importantly, its low cost, easy to build nature attracted many designers [12].

The important reason why a 180^0 hybrid coupler was chosen is that a high isolation between RF and LO can be achieved. The rat-race coupler provides a 3 dB power split and 180^0 degree of phase difference. In most cases, couplers are used in balanced mixers but the limiting factor is the isolation between RF and LO over broad bandwidths [8].

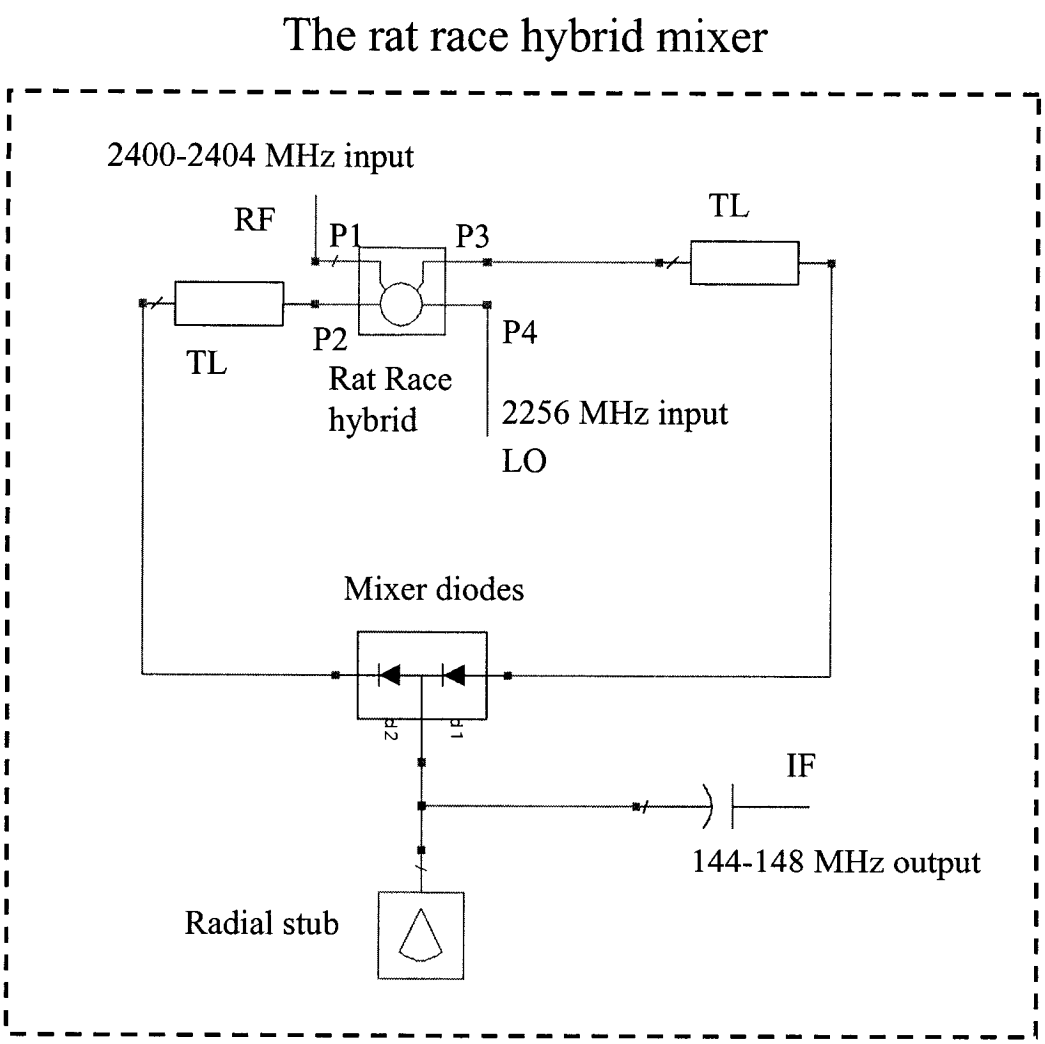

Figure 3.27: The mixer, schematic view.

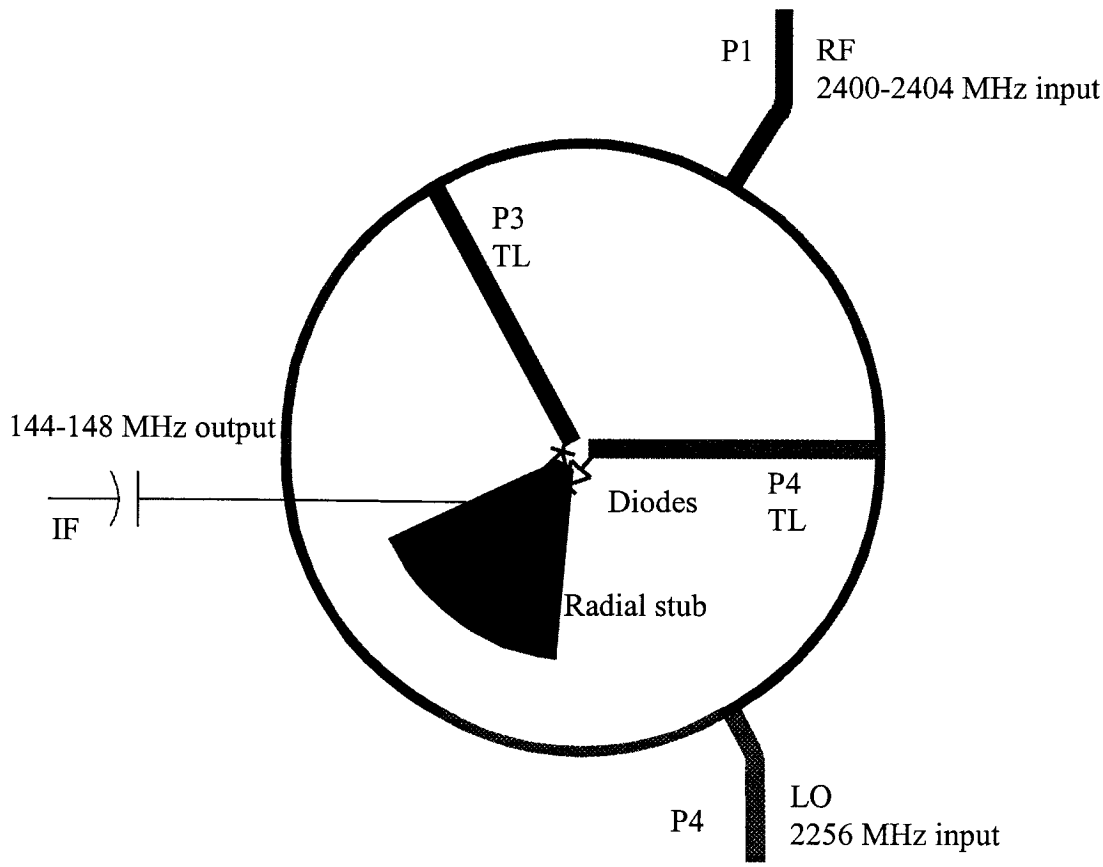

Figure 3.28: The mixer, layout view.

The design parameters for the mixers shown in Figure 3.27 and Figure 3.28 are given in Section 3.4.1 after the theory of 180^0 hybrid and the radial stub are presented.

3.3.3 Rat Race Hybrid

The 180^0 hybrid junction is a four-port network with 180^0 phase shift between the two output ports. It can also be operated so that the outputs are in phase [6].

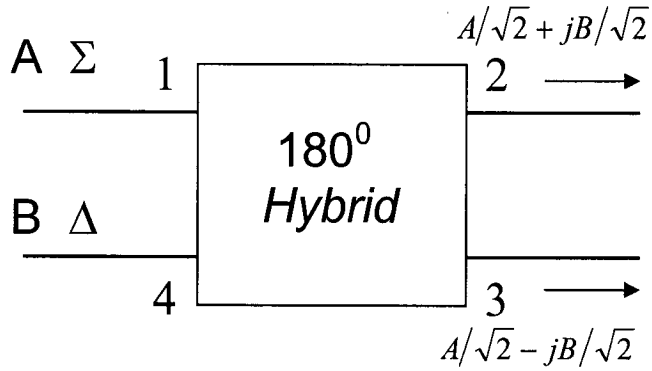

Figure 3.29: Symbol for an 180^0 hybrid junction. (Reprinted from [6]).

As seen from Figure 3.29, a signal applied to port 1 will be evenly split into two in-phase components at ports 2 and 3, while port 4 will be isolated. Similarly, if the signal is applied to port 4, it will be split into ports 2 and 3 with 180^0 degree phase difference while port 1 will be isolated. Also, it is possible to use 180^0 degree hybrid coupler as a combiner. When input signals are applied at ports 2 and 3, the sum of the inputs will be formed at port 1, while difference will be formed at port 4. So, the ports 1 and 4 referred as sum and difference ports respectively. The scattering matrix for 3 dB 180^0 degree hybrid coupler is given as follows [6]

$$[S] = \frac{-j}{2}\begin{bmatrix} 0 & 1 & 1 & 0 \\ 1 & 0 & 0 & -1 \\ 1 & 0 & 0 & 1 \\ 0 & -1 & 1 & 0 \end{bmatrix}. \tag{3.44}$$

As seen, the matrix is unitary and symmetric.

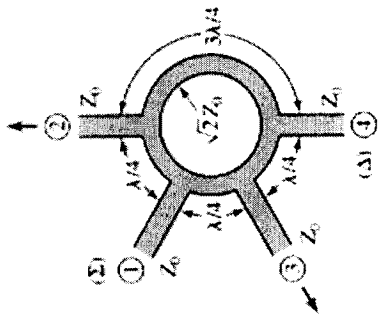

Figure 3.30: Rat race coupler. (Reprinted from [6]).

Figure 3.30 shows the layout of the hybrid coupler. If the coupler is designed for a characteristic impedance of Z_0, the lines along the circumference of the coupler should be $\sqrt{2}Z_0$. The distance between the ports is shown in wavelengths.

3.4 Radial Stub Matching

A quarter wavelength ($\lambda/4$) stub is used to provide a ground for the diodes at 2400 MHz. A radial stub has a better bandwidth than a straight $\lambda/4$ transmission line stub.

Traditionally, open ended quarter wave stubs were used for creating a ground at a certain frequency. However, the performance of a $\lambda/4$ transmission line stub is very sensitive with frequency, and suffers from bandwidth restrictions. In the later designs, a radial stub replaced the $\lambda/4$ transmission line stub, due to the radial stub is superior performance over a wider bandwidth [17].

The purpose of matching is to get rid of possible reflections at the IF port. The matching is designed to give a better RF-IF and LO-IF isolation and the radial stub in the mixer works as follows: the RF and LO signals appear in the IF as harmonics. In order to get rid of them, an open ended radial stub designed at either frequency or two open ended quarter wave transmission lines designed in each frequency is introduced to the very end of the diodes. The signals at RF and LO frequencies go through these quarter wave transmission lines and come back at the reverse phase so a cancellation occurs at these two frequencies. So at both frequencies the voltage at the output leg of the mixer is zero in theory.

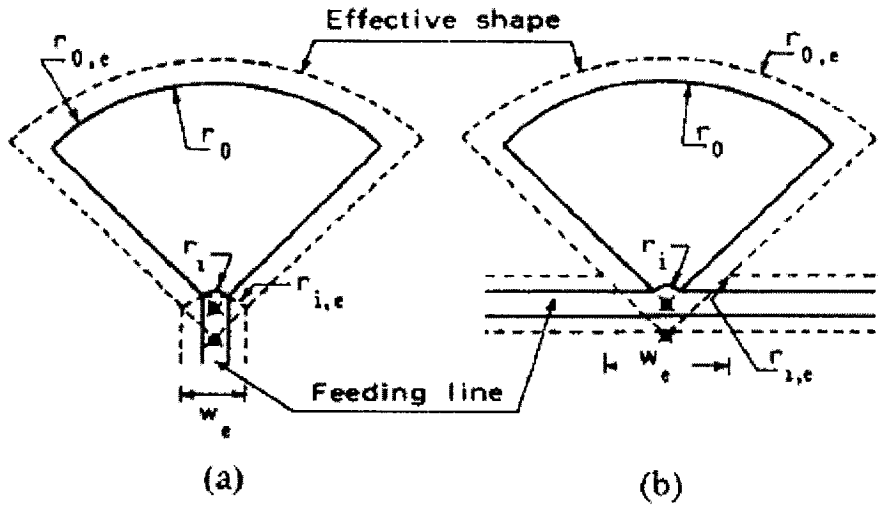

Figure 3.31: Geometries of (a) series, (b) shunt radial stubs. (Reprinted from [18]).

The parameters important in the design of the radial stub are the vertex angle and outer radius provided that the dielectric constant and the thickness of the substrate are known. The pure analysis of radial stub is impossible because, the propagation is not pure TE or

TM mode however; the approximate analysis is a good estimate. The input terminal impedance for a radial stub is given in both [17] and [18]. The equations are very complicated. Due to space limitations only the results will be provided in here but the results of the experiments are introduced.

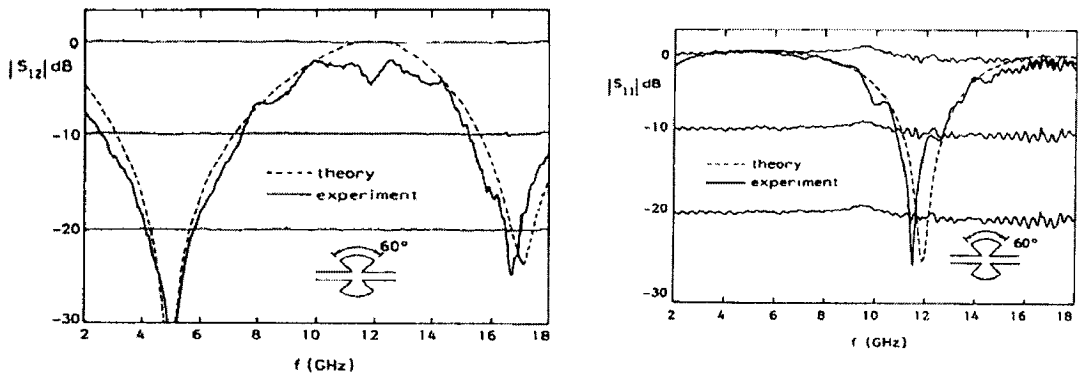

Figure 3.32: The S_{12} and S_{11} results of the radial stub. (Reprinted from [18]).

The experimental results in [18] show that a radial stub with a vertex angle of 60^0 and outer radius of 0.5 cm gives good matching results between frequencies of 8.5 GHz and 13 GHz. So, this broad band matching property of radial stub is important in the design of matching networks for a large frequency bandwidth [18].

The radial stub in the mixer is used to have a good matching at the IF port for the RF and the LO signals. The radial stub designed for the rat race coupler mixer will be presented and simulated in Chapter 4 in great detail.

3.4.1 The Design of the Mixer

The design method of the rat race hybrid mixer based on the theory was presented in this chapter. Since the design frequency is 2400 MHz and dielectric constant is 3.48 the wavelength in the microstrip becomes 6.379 cm. The width of the transmission line for 50 ohm and 70 ohm were also calculated earlier in this chapter as 1.154 mm and 0.629 mm respectively. The radial stub has a vertex angle of 60^0 and the length of 1.15 cm was designed with the help of ADS. So the mixer in Figure 3.27 and Figure 3.28 were obtained.

3.5 Frequency Multiplier (Harmonics Generator)

In the process of frequency multiplication, electron devices are used due to their nonlinear characteristics. An important requirement of such devices is to be fast enough in microwave frequencies that they can cope with the fast varying signals up to high frequencies. There are two kinds of devices that can fulfill the requirements mentioned above: one is a rectifying metal-semiconductor device and the other one is a p-n junction devices. In this thesis, a p-n junction device based frequency multiplication will be discussed [20].

For the frequency multiplication as in the mixer, the non linearity of the diodes is used. The non-linear voltage current characteristic of the diode causes harmonics at the discrete multiples of the input frequency. Then the harmonic of interest is filtered out and amplified.

As the mathematical approach to the frequency multiplication, the nonlinear charge-voltage characteristics can be explained by solving the power series expansion at a bias voltage, V_b with a presence of a small signal V, while Q indicates the total charge in the diode [20].

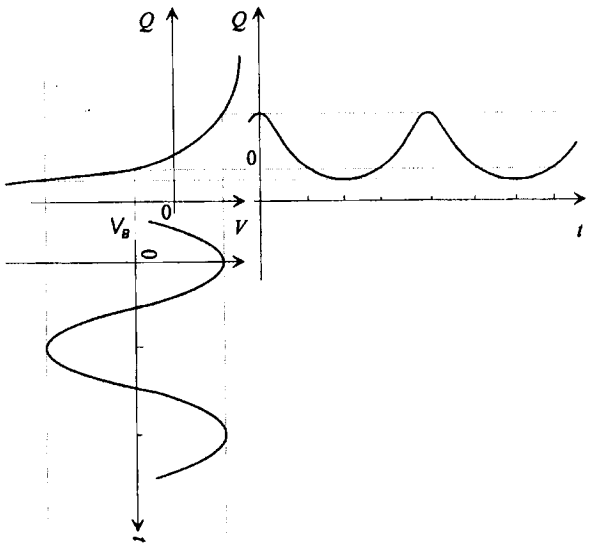

Figure 3.33: The input signal versus output at the presence of a p-n junction diode. (Reprinted from [20]).

$$Q(V_B + \Delta V) = b_0 + b_1 \Delta V + b_2 \Delta V^2 + b_3 \Delta V^3 + \ldots \tag{3.45}$$

$$\Delta V = V_d \cos(\omega_g t). \tag{3.46}$$

If the ΔV is inserted into $Q(V_B + \Delta V)$.

$$Q(t) = Q_0 + Q_1 Cos(\omega_g t) + Q_2 Cos(2\omega_g t) + Q_3 Cos(3\omega_g t) + \ldots . \tag{3.47}$$

After generation the high order harmonics of the applied signal, a filtering circuitry is used to filter out the desired harmonic from the rest [20].

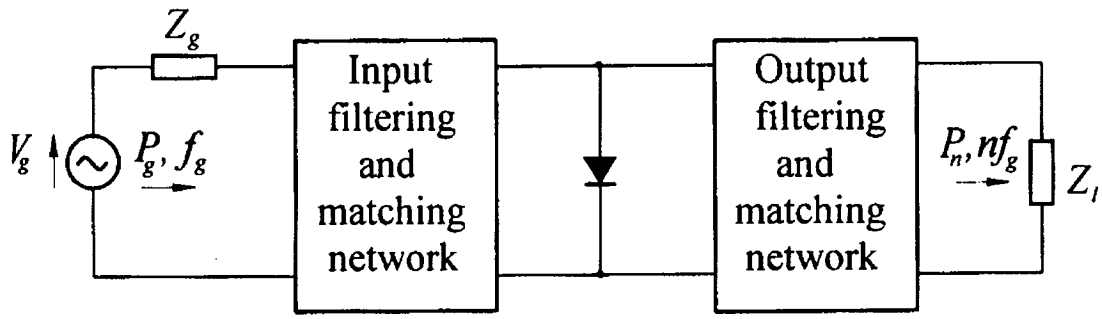

Figure 3.34: A sketch of a harmonics generator. (Reprinted from [6]).

So, as seen from Figure 3.34, the overall principle of harmonics generation is that a sinusoidal signal applied turns into a non-sinusoidal voltage wave, which is rich in harmonics. For more detailed description, please refer to [20].

In the design of the harmonics generator, obtaining an undistorted signal at a single frequency plays a vital role. In a receiver, the filters used in the filtering of the input signal are generally not precise enough just to pass the signal at the desired frequency and reject the rest. Indeed, the filters allow other signals in the pass band to pass, yet obtaining a narrow pass band and sharp cut off are not always possible. In that case, supplying an undistorted LO signal to the mixer is the only way to obtain the desired output. If the supplied LO signal is not undistorted and has harmonics in it, the down conversion of the not well filtered input signals with the LO could give a distorted output.

Getting a clear LO signal can only be achieved by narrow filtering in the HG stage. So, the output filtering and matching network in the HG plays an important role in the performance of the receiver.

3.6 RF Amplifier (RF AMP)

The theory of the RF Amplifier is a big part of the downconverter theory. The downconverter receives the signal power level around -100 dBm and the RF amplifier is the first point that the signal enters. The RF amplifier is supposed to amplify and filter the desired signal and not the rest. In a typical RF amplifier, the first is a major noise consideration. After amplification, the filtering stage comes and according to the type of the application, further amplification or filtering can be introduced. The gain of the amplifier is important since large amplification can make the RF amplification stage unstable or even turn it into an oscillator [13].

The filtering stage is so important that designers have always looked for small bandwidth sharp filters to select the desired signal however, the physical realization of such filters is either costly or unpractical. So, using filters that can reject the spur frequency with a good performance is the essential point of the RF amplification stage provided that the LO signal coming from harmonics generator is clean [13].

3.6.1 Noise Considerations in RF Amplifier

The effect of noise is the biggest limiting factor in the performance and the design of an RF amplifier. The dynamic range of the amplifier is limited at the low end by its noise figure. In order to obtain a better noise figure, the amplification stage must come before

the filtering stage. The reason lies in the noise figure equation of a cascaded system, which is given as

$$F_{System} = F_1 + \frac{F_2 - 1}{G_1} + \frac{F_3 - 1}{G_1 G_2} + \ldots . \tag{3.48}$$

F_1 denotes the noise figure and G_1 denotes the gain of the first stage and the other subscripts denote the properties of the other stages that form the cascaded system respectively. As seen from the (3.48), the noise figure of the first system added directly to the system but the noise contributions of the rest are divided to the gain of the earlier components. Hence, a high gain amplification stage at the input of the RF amplifier dramatically improves the noise performance of the system.

3.7 Conclusion

In this chapter, the theoretical approach to the devices used in the design of 2400 MHz – 144 MHz downconverter was discussed. The design approach of each component was explained in detail by using the literature. All the discussions until this point of the thesis formed the theoretical basis of the design.

4 ADS Simulation Results

4.1 Introduction

The Agilent ADS (Advanced Design System) [15] is a powerful CAD simulator for any kind of circuitry. For this thesis, the microwave simulation part of ADS was used. The microwave simulation engine of ADS is called *Momentum*, which uses the method of moments for its operation. This technique uses Maxwell's equations on planar structures to obtain the currents. In Momentum, there are two simulation modes: RF and Microwave. Both use electromagnetic theory but different approaches to obtain the results. Momentum Microwave Simulation, which is called as *full wave simulation* in the thesis, uses full electromagnetic wave solutions of Maxwell's equations, which includes substrate and space wave equations. Momentum RF simulation, which is called *TL (Transmission Line) simulation* in the thesis, uses quasi-static functions based on low-frequency analysis techniques. This excludes substrate and space wave radiation effects. For detailed information please refer to [15].

In the design and the simulation of the 2400 MHz -144 MHz downconverter, both simulations were used. Even though full wave simulation gives better results, the TL simulation takes much less time. The built in automated design tools of ADS use TL simulation techniques in the design of the components. However, it was observed that there are important differences between the results obtained from TL and full wave modes, due to the approximations in the Methods of Moments and in the TL simulation

mode. Since, the full wave mode is more precise than TL mode, for the design and the fabrication of the filters and the coupler, the full wave mode was used.

4.2 Simulations of Coupled Resonators

In order to test the consistency of the ADS simulations with the theories presented in [5] and [7], some simulations were carried out. The simulations include the design of coupled resonators in order to calculate the mixed coupling coefficient and validate their consistency with [5] and [7]. Since in both references, it has been indicated that a full wave simulation based on Method of Moments was used, the full wave simulation option of ADS was used.

The results of the simulations were introduced in Chapter 3 in the design procedure of the hairpin filters. The simulations showed that the ADS full wave simulations are consistent with the theories introduced in [5] and [7].

4.3 Hairpin Filter Design and Results

In all the hairpin filters the specifications of the substrate was Rogers 4350B, which has a dielectric constant of 3.48, loss tangent of 0.0031 at 2.5 GHz and thickness of 0.020 inch. Fabrication was done by APCircuits [16].

4.3.1 The 5-pole Filter for RF AMP

For the design of the filter in the RF AMP part of the circuitry, a 5-pole (N = 5) filter is preferred, for good spur rejection performance. The 0.5 dB equal-ripple prototype was used with a centre frequency of 2400 MHz and a bandwidth of 105 MHz, using the

substrate material Rogers 4350B. For the coupling coefficient, k, of the filters, the simulation results of Section 4.2 for the mixed coupled resonators were used. Similarly, the formula for the tapped line resonator given in Section 3.2.4 was used for the calculation of the tapping distance. The resulting layout of the filter is given in Figure 4.1 and the frequency response is plotted in Figure 4.2.

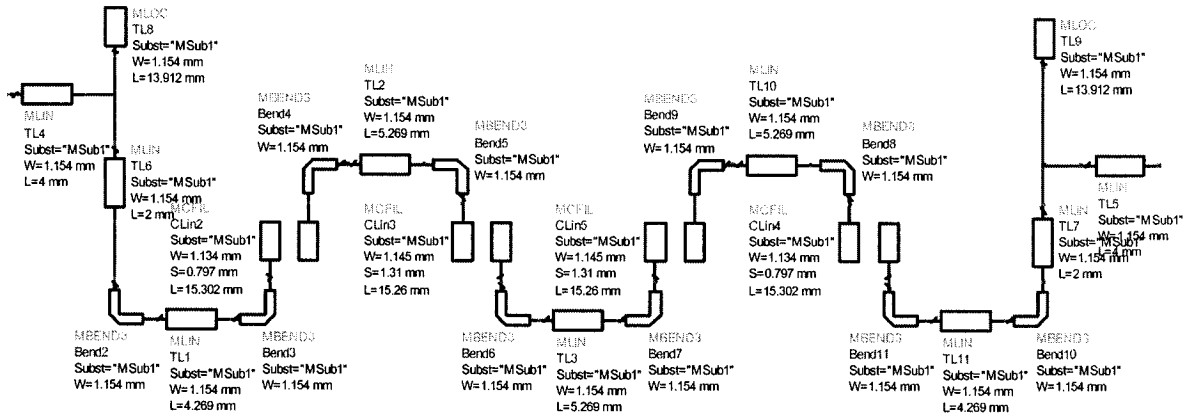

Figure 4.1: The circuit schematic for the five resonator filter.

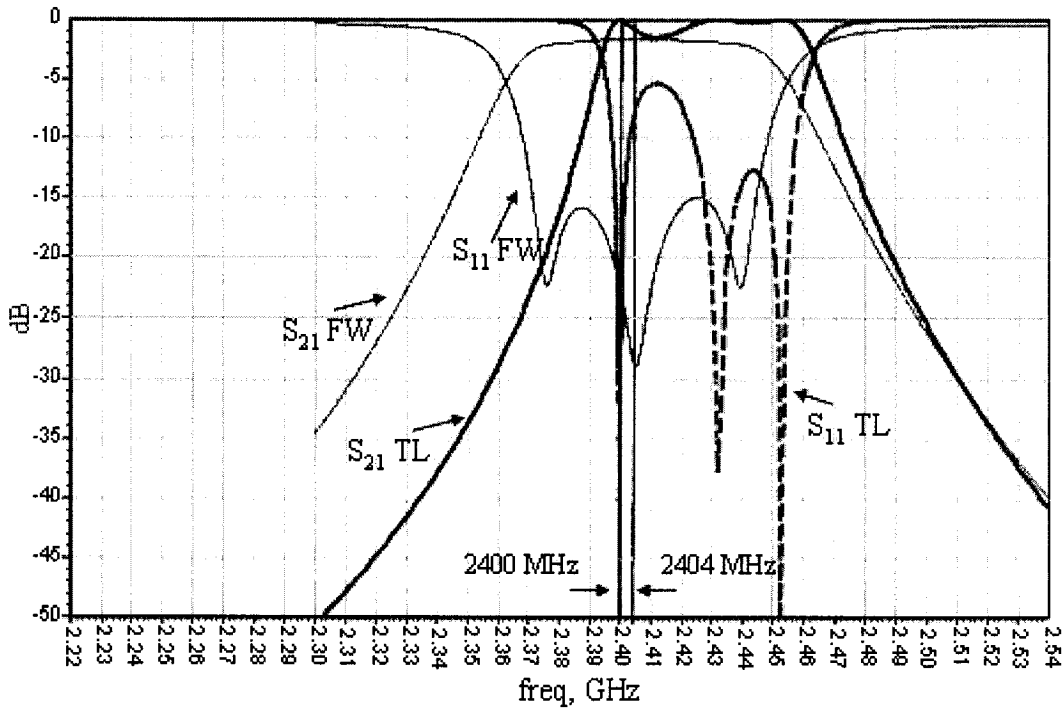

Figure 4.2: Resulting performance, FW correspond to the full wave simulation and TL corresponds to transmission line simulation.

A bandwidth of around 105 MHz is preferred for both filters because it is very possible that there will be errors in the manufacturing and the errors will affect the response of the filter. After manufacturing it is possible to have a shift in the response. So, in order to compensate the possibility of error, a wide bandwidth is preferred.

As marked, in Figure 4.2, the frequency range of interest 2400 – 2404 MHz. The TL and full wave simulation results vary. In the FW simulation, the bandwidth is 100 MHz while in full wave mode it is only 80 MHz, which is narrower than expected. Moreover, both the S_{11} and S_{21} values of the either analyses differ from each other. The S_{11} of FW mode is -22 dBm at 2400 MHz and -25 dBm at 2404, which are good. The TL mode

shows a S_{11} of -40 dBm at 2400 MHz and -8 dBm at 2404 MHz. The value of S_{11} is good at 2400 MHz but not good at 2404 MHz in TL mode. The S_{21} of the filter is almost consistent in both simulations and around -1.5 dB, which should be 0.5 dB because 0.5 dB ripple filter model was assumed. The 1 dB difference could be due to the loss in the filter.

It is expected that the full wave simulation is more precise. The difference between the modes can also be due to the parasitic capacitances at the bends and capacitive coupling between the adjacent arms of the hairpin resonators. The TL simulation simply ignores the existence of the parasitic effects. So, for the actual design, the FW simulation is used.

Since the filter is a five resonator filter expectedly, there should be five poles in the response but both simulations shows only three. The reason of this difference could be some resonators are not very well tuned and not giving the pole as expected. However, the response of the filter is quite satisfactory.

The spurious suppression of the filter, 2112-2116 MHz, (not shown) is found to be below -50 dBm, which is very sufficient.

4.3.2 The 3-pole Filter for the HG

For the HG part of the circuit, two stage filtering was introduced and two 3-pole (N = 3) hairpin filters were used. Each filter was designed at centre frequency of 2256 MHz with a bandwidth of 110 MHz.

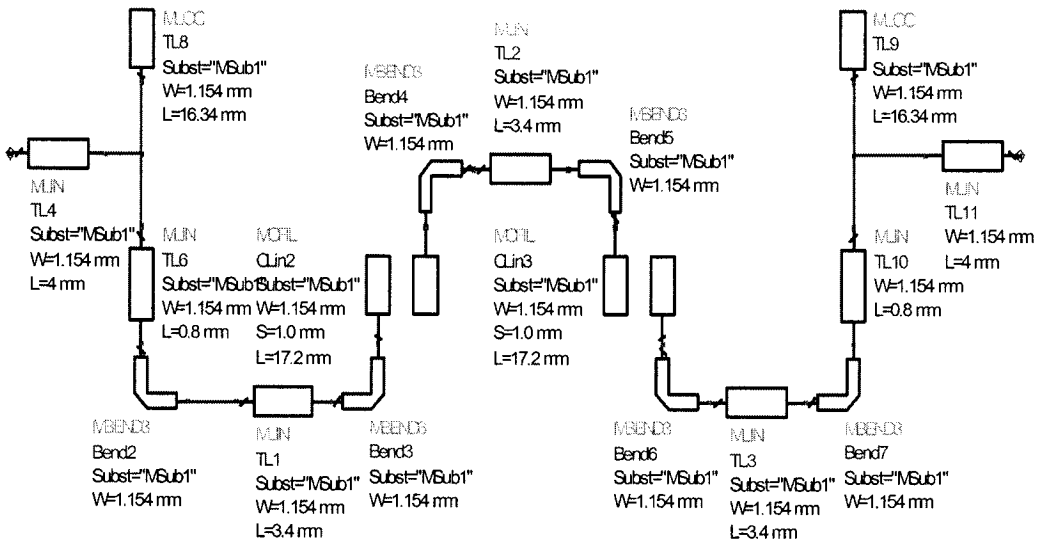

Figure 4.3: The three resonator filter for the HG.

The resulting filter gave two different responses using TL and full wave modes as expected. The graph in Figure 4.4 shows the difference between RF and Microwave modes.

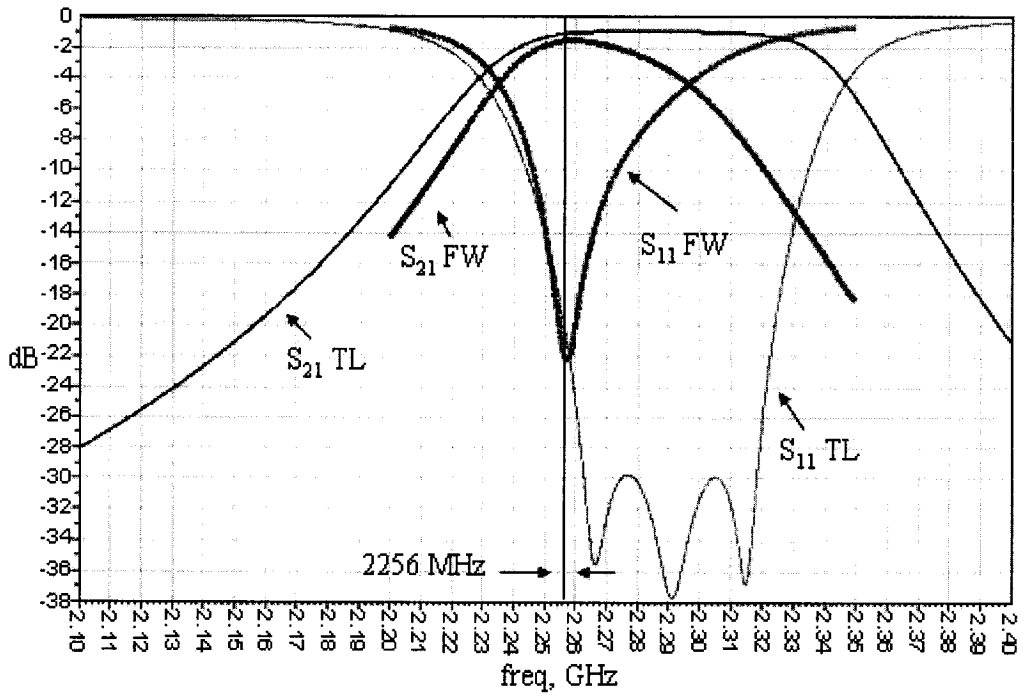

Figure 4.4: The response of the 3-pole filter for the HG. FW corresponds to the full wave simulation; the TL corresponds to transmission line simulation.

From Figure 4.4, in the full wave results of the filter, the centre frequency is at 2256 MHz, the bandwidth is 60 MHz, which is less than the expected value of 115 MHz. The filter is designed by 0.5 dB ripple prototype values but the insertion loss is 0.9 dB. The 0.4 dB difference could be happened due to the loss in the filter. Both the S_{11} and S_{21} of the filter are very satisfactory, yet at the frequency of interest, 2256 MHz, the S_{11} drops -22 dB.

In the result of the TL mode, the S_{11} is -22 dB which is the same as the full wave mode and the S_{21} of the filter is around -0.9 dB, which is also same as the full wave mode.

However, the response of the filter is shifted by 40 MHz in TL mode relative to the full wave mode.

If the TL simulation considered, the frequency of interest (2256 MHz) is not at the middle of the pass band but the FW simulation suggests that 2256 MHz is at the middle of the pass band. For the design, the response of the FW simulation mode was used.

Since the filter is a three pole filter, expectedly, there should be three poles in the result, the TL simulation shows the three poles but they are not seen in the FW mode. This could be because some of the resonators are not very well tuned but the FW response is very satisfactory.

Since the filter under discussion is designed to filter the fourth harmonic of 564 MHz, the two critical frequencies for the filter to suppress are the second and the fifth harmonics of the input frequency, which are 1692 MHz and 2820 MHz respectively. The rejection by the filter of these two frequencies is better than 30 dB (not shown), which is satisfactory because there will be two filters in cascade in order to obtain an undistorted signal at the HG.

Furthermore, the phenomenon observed in the previous section can also be seen here. The TL and full wave simulations gave different results. However, this time the difference is as big as in the five-pole filter case, which can be explained by the difference in the complexity of the two filters. The 5-pole filter had five resonators. The filter introduced here is a 3-pole filter and has only three resonators. Parasitic and crosstalk effects possibly had less influence in the response of the filter, so a better correlation was achieved between TL and full wave simulation modes.

For the HG, two filters were designed. One is a 3-pole filter in the HG section for filtering out 2256 MHz, and the other one is a 5-pole filter for the RF amplifier section and designed to filter out 2400 -2404 MHz signal and reject the spur frequency of 2112 - 2116 MHz.

4.3.3 The Effect of 90^0 Bends

In all the filters designed above, the bends were "optimally mitered" which is a built-in tool in ADS. However, in order to see the effect of the 90^0 bends, the filter used for the HG was part modified. All the "optimally mitered" bends were replaced by 90^0 bends as shown in Figure 4.5. The resulting performance in Figure 4.6 was obtained.

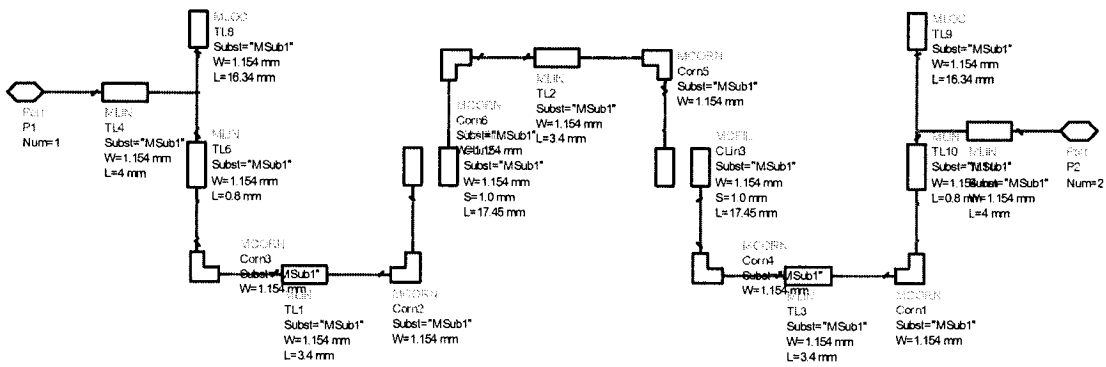

Figure 4.5: The 90^0 bend version of the HG filter.

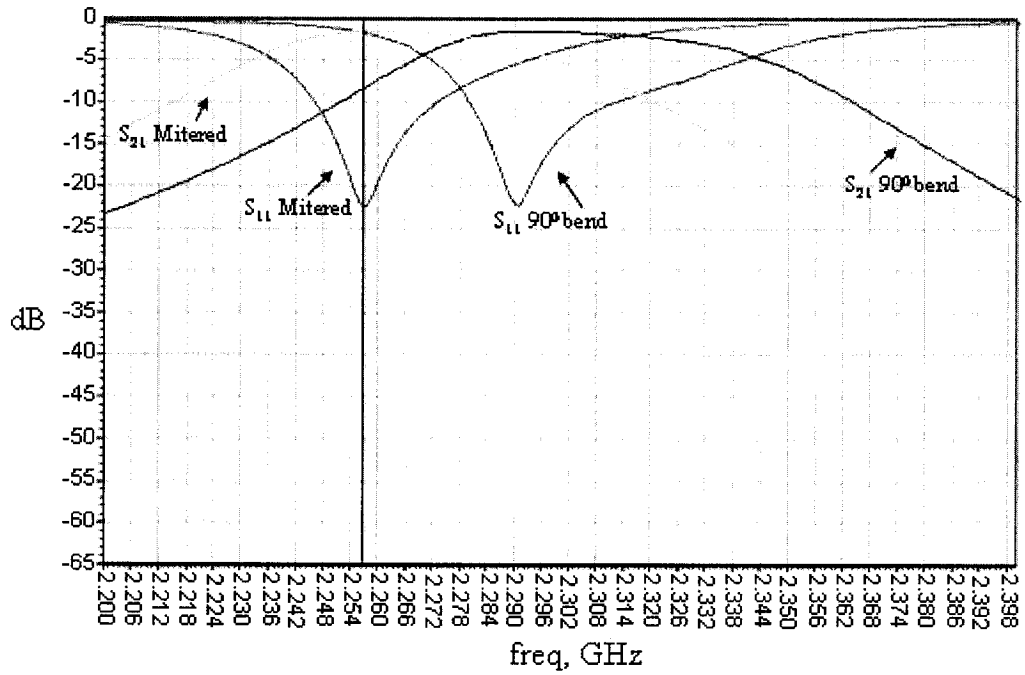

Figure 4.6: The S_{11} and S_{21} characteristics of the filter in Figure 4.5 and Figure 4.3.

In Figure 4.6 a comparison between the 90^0 bend configuration of the filter for HG and the actual filter for HG (schematic shown in Figure 4.3, response shown in Figure 4.4) is done. It is very clear that the response of the 90^0 bend filter in Figure 4.5 shifted up around 35 MHz from the expected center frequency of 2256 MHz. This shift is due to the parasitic effects at the bends. It is cleat that the parasitic effects caused a reduction in the coupling length of the filter, which shifted the response of the filter. Note that only the full wave simulations were compared.

4.3.4 The Difference between ADS Library and Our Filters

It is important to mention that ADS has its built-in filter generation algorithms, which can be reached from the passive circuits menu. When the desired filter type and

specifications are determined, the passive circuit menu can be used for automatic design of the filter based on the TL simulation mode. In order to test the convenience of the passive circuit design engine (ADS library filter), the filters designed for HG and RF AMP were redesigned using the ADS library.

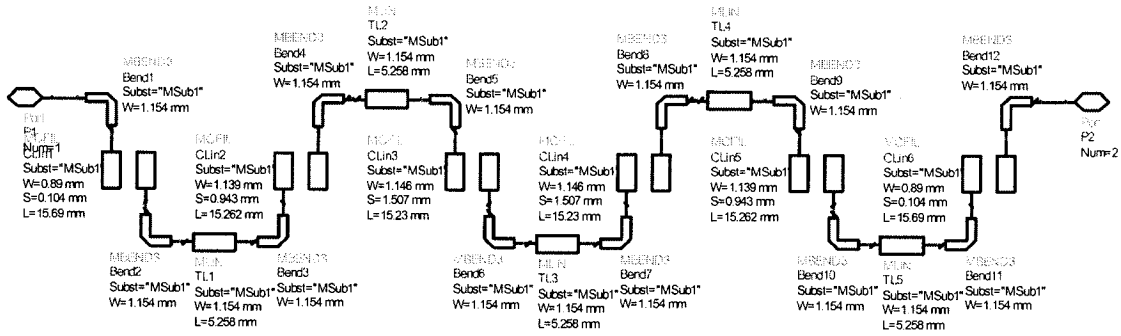

Figure 4.7: The ADS library design for the filter in the RF AMP.

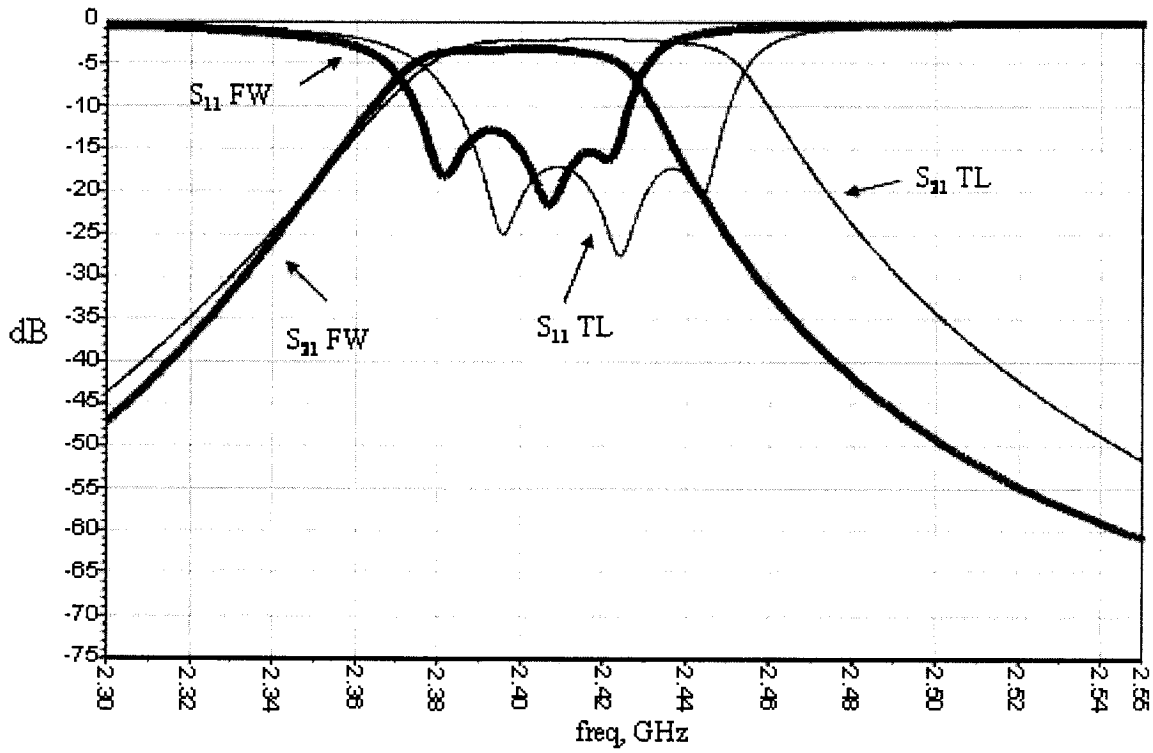

Figure 4.8: The response of the built-in design for the RF AMP hairpin filter. FW corresponds to the full wave simulation; the TL corresponds to transmission line simulation.

The RF AMP filter was designed using the built in algorithm of ADS. The TL and full wave modes were in fair agreement. The filter is centered at 2400 MHz, bandwidth is about 60 MHz and return loss is greater than 9.5 dB.

However, the built in algorithm of ADS could not be used due to the fact that some filters created were physically unrealizable. The design engine uses a gap-coupled structure to excite the filters, (an approach explained in detail in [6]) however, the distance of some gaps were so small (around 5 mil or 0.08 mm) that the construction of the filter with those dimensions would require cutting edge technology machinery. The company that was used to manufacture the circuits needs a minimum clearance of 7 mils. For the design

given in Figure 4.7 the spacing of the gaps was 0.104 mm (4.1 mils), which was smaller than the minimum requirements of the manufacturer. Hence the design could not be used.

The design for the HG that was investigated is shown in Figure 4.9.

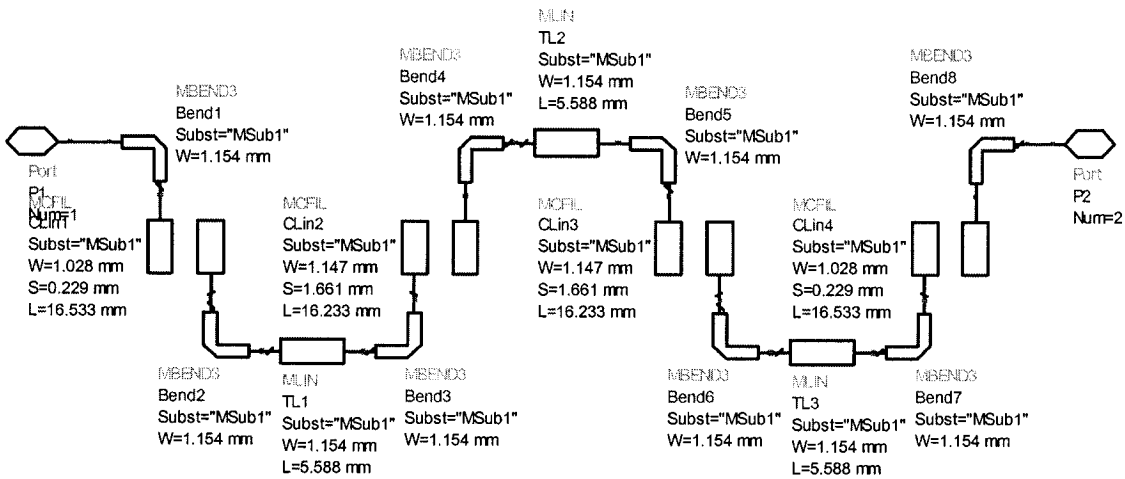

Figure 4.9: The ADS library design for the filter in the HG.

In this case, the clearance of the first coupled lines at the ends is 0.299 mm, which can be seen from the Figure 4.9. This corresponds to 9 mils, which is slightly larger than the minimum clearance required to manufacture the design so this design is usable but 9 mils is so close to 7 mils that in case of any small change in the design could cause the 9 mils to become less than 7 mils. So, in order to stay on the safe side, the design in Figure 4.9 was not used. The response of the filter in Figure 4.9 is shown in Figure 4.10.

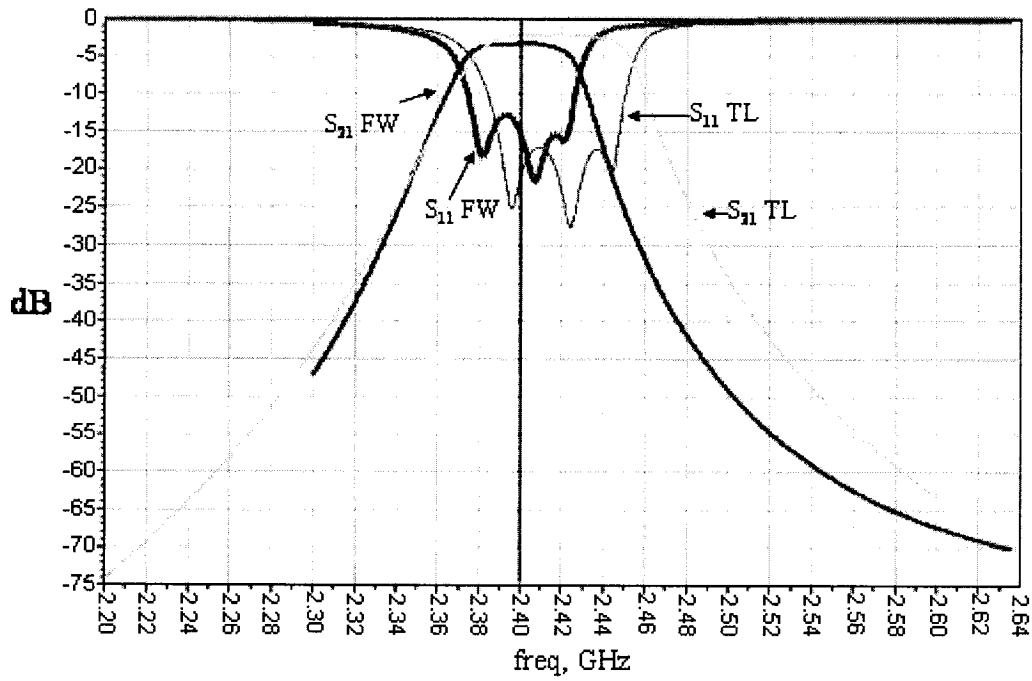

Figure 4.10: The response of the ADS library design for the filter in the HG. FW corresponds to the full wave simulation; the TL corresponds to transmission line simulation.

The TL and full wave simulations were in fair agreement. The filter is centered at 2256 MHz, bandwidth is about 60 MHz and the return loss is greater than 15 dB.

The automatic design utility in ADS led to gap spacing that were very small for the HG filter and too small to manufacture for the RF AMP filter. So, these designs were not used. So, the filters designed by using Hong-Lancaster method [5] were used.

Alternatively, in the filter based on the Hong-Lancaster method [5], the dimensions were specified by the designer initially. So any kind of physical dimension problems were avoided. That is why the Hong-Lancaster method filters were preferred in this thesis and

the simulations showed that our filters work as well as the ADS Library ones indeed, in some situations, ours gave better results.

4.4 Rat Race Hybrid Mixer

The mixer is a nonlinear device; it requires a large-signal analysis. As a preliminary step, we first will analyze a component of the mixer system that can be handled with linear analysis. This is the rat race hybrid.

4.4.1 The Coupler and Its Isolation

The design of a rat-race coupler mixer starts with the design of the rat race coupler. ADS has a built-in coupler designer engine to produce couplers for any given frequency on the specified substrate. It is important to mention again that all the built-in engines in ADS use TL simulations. The designed coupler is shown in Figure 4.11 and it is the same coupler shown in Figure 3.29.

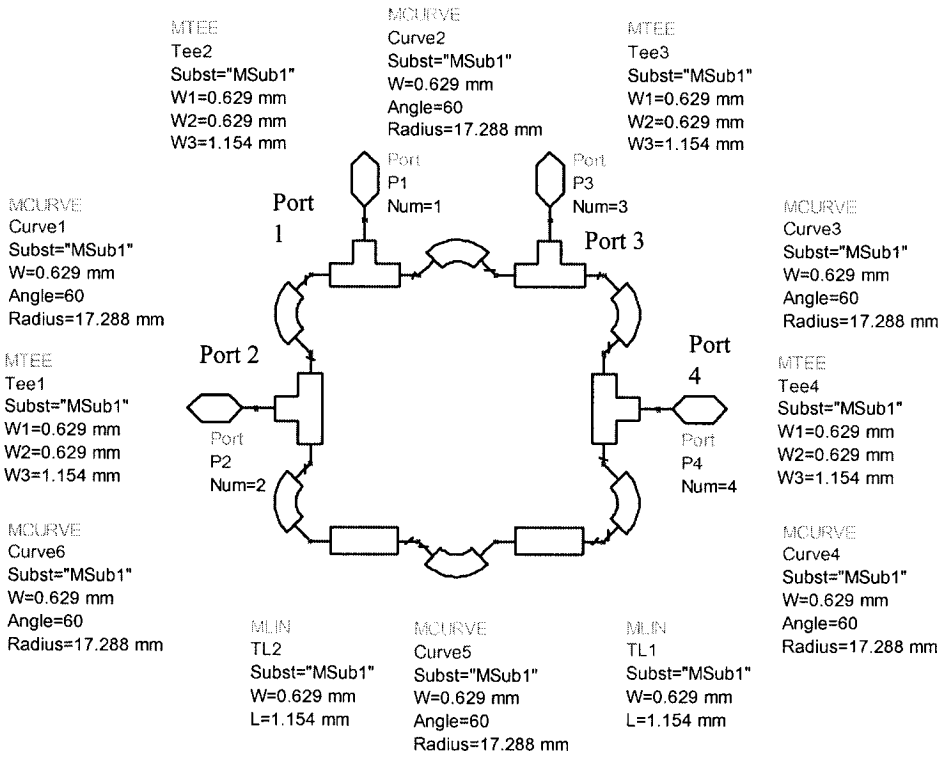

Figure 4.11: The rat-race coupler circuit schematic.

The rat race coupler was designed at 2400 MHz so that minimum loss and maximum isolation are achieved. The isolation of the coupler was an important factor, in theory, it is expected that the applied signal goes only to the intended port, however in reality some of the signal goes to the other ports. This situation is unwanted.

In the design of the downconverter, it is important for the information carrying signal to go to the desired port of the coupler mixer. This was made possible by keeping the isolation as best as it can at the 2400 MHz, that is why 2400 MHz was chosen to be the center frequency for the rat race coupler.

Figure 4.12 shows when 2400 - 2404 MHz comes to the first port and 2256 MHz comes to the third port of the coupler. The output is at the second port. As seen, the RF signal coming from first port goes to the second port with a loss around 4 dB but the coupler isolates the third port (the port which LO applied) from the first, where the RF is applied, with an isolation of 50 dB. This high isolation is a property of balanced mixers that use a 180^0 hybrid. Due to symmetry, the LO signal went to the fourth port with 4 dB loss. Also, the isolation of the LO (at 2256 MHz) was satisfactory and better than 30 dB for 2.3 - 2.5 GHz.

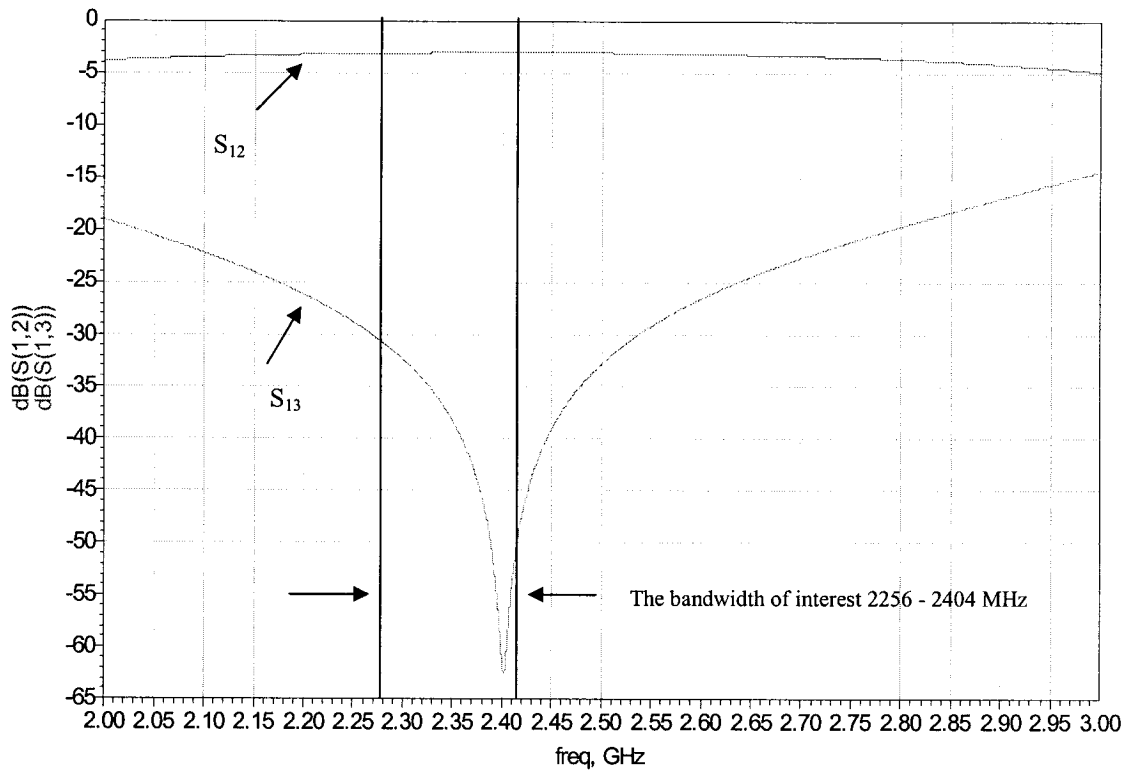

Figure 4.12: The isolation of the rat race coupler.

4.4.2 The Mixer and Its Isolation

The HP HSMS 2822 diode pair was added from component library of ADS, which can be reached from the "Insert" menu then "component" and "component library". The HSMS 2822 pair can be found from the "HF Diodes" menu of the component library. However, in the original design the MA4E2054B-287T diode pair of the AMP Corp. was used. The HSMS 2822 was chosen because its specifications are very similar to the AMP Corp.'s diode.

Moreover, a radial stub was designed by using the built-in design engine of ADS for matching purposes. Finally, by adding a 10 μF capacitor to the output end, the design was complete. The schematic view of the rat race hybrid mixer is shown in the Figure 4.13 and layout in Figure 4.14.

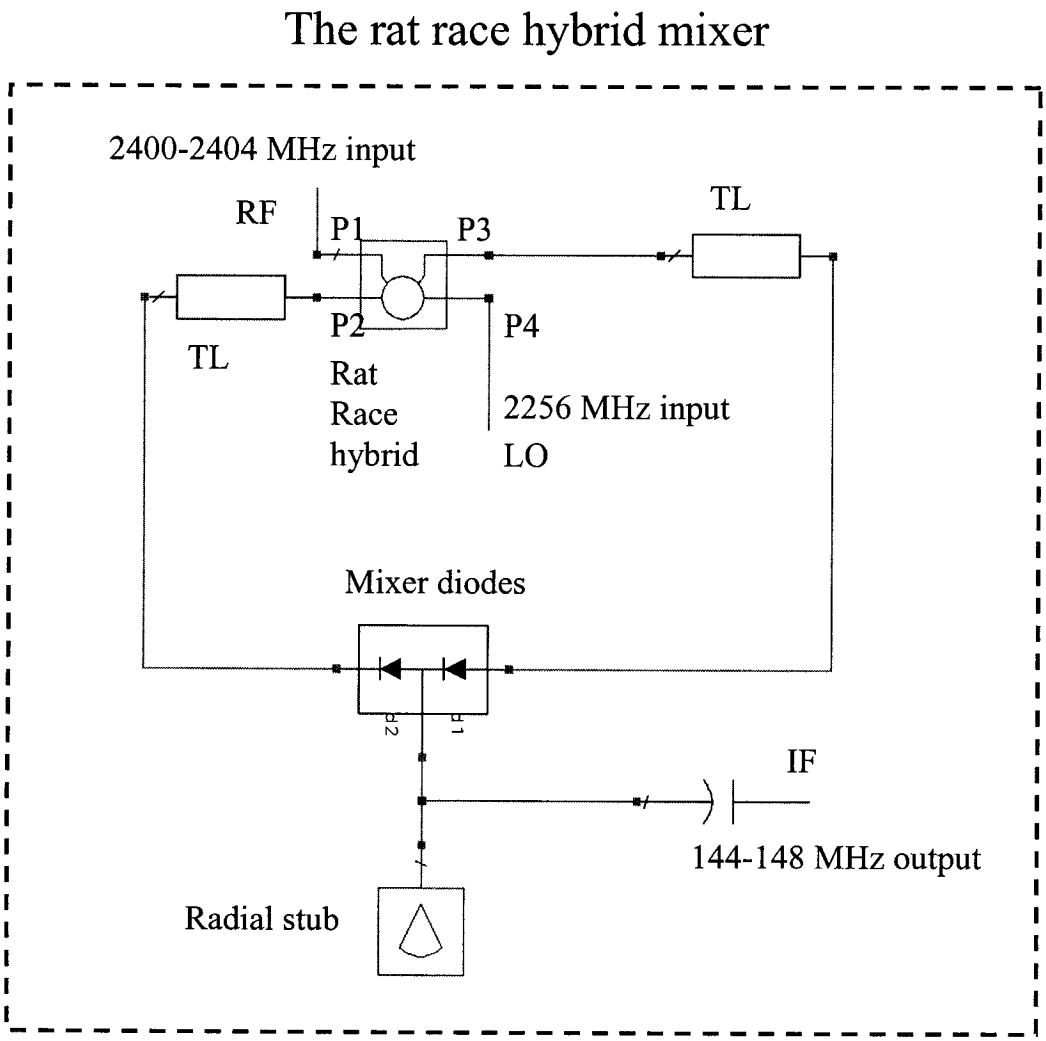

Figure 4.13: The schematic view of the rat race hybrid mixer.

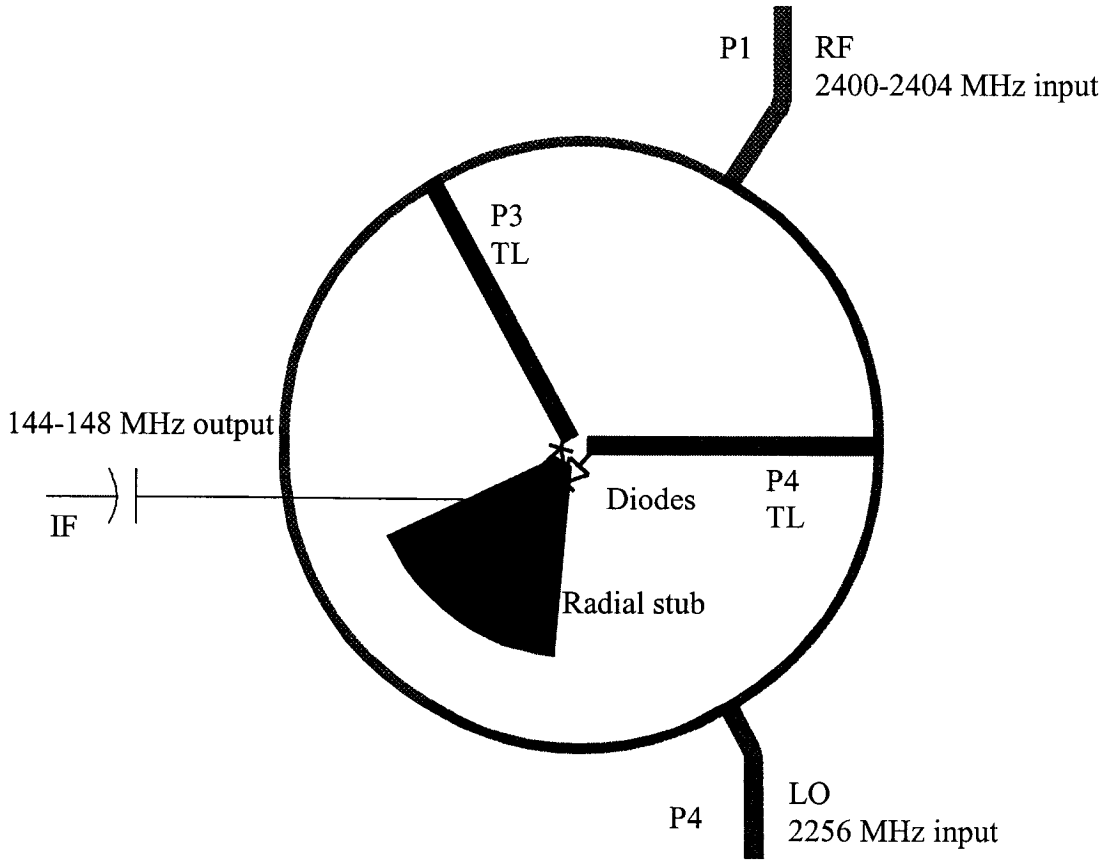

Figure 4.14: The layout view of the rat race hybrid mixer.

Although the mixer is complete, no mixing effects are being analyzed yet. That is, the S-parameters in Figure 4.15 are obtained, under the condition that the input and the output frequencies are the same. So, IF - IF and RF – LO isolation performance of the mixer is given in Figure 4.15.

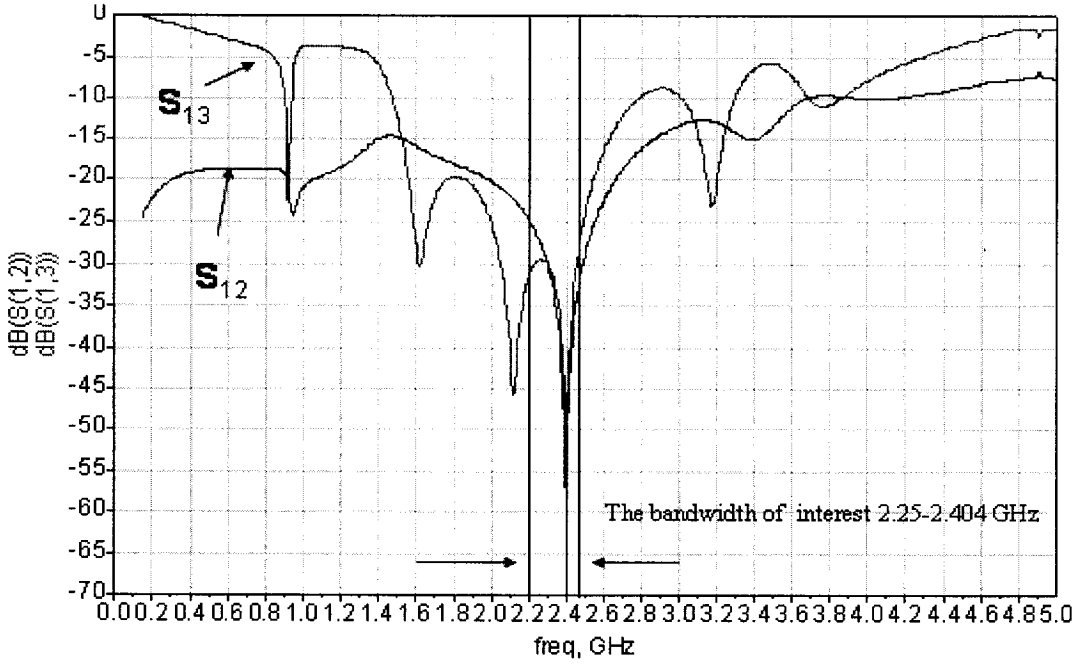

Figure 4.15: The isolation of the mixer.

S_{13} corresponds to the isolation between RF and LO, S_{12} corresponds to the isolation between RF and IF.

The frequency range of interest is between 2.25 - 2.41 GHz; it is seen that the RF – LO isolation (S_{13}) is better than 25 dB and the RF – IF isolation (S_{21}) is better than 30 dB.

4.4.3 Effect of the Radial Stub

It is common practice to use radial stubs instead of straight quarter wave transmission line stubs, because the radial stub has a better bandwidth, and it is not any harder to manufacture than an ordinary stub.

At the IF port of the mixer, a radial stub is placed just at the output end of the mixer for matching purposes. The radial stub designed at the centre frequency of 2400 MHz and in

order to increase the isolation between RF and LO and create a ground for the signals at 2256 - 2404 MHz which are reflected from the IF terminal.

4.4.4 Harmonic Balance Simulation of Mixer

For testing the system, the *Harmonic Balance Simulator* of ADS was used. Ordinary AC circuit analysis can not be used because more than one frequency and nonlinear effects are involved. The Harmonic Balance Simulation model uses a frequency-domain analysis technique for simulating the distortion in non linear circuits and systems. The Harmonic Balance Simulation enables the multitone simulation of circuits that exhibit intermodulation frequency conversion, which includes the conversion between harmonics.

As an illustration, if f_1 and f_2 are combined in a mixer using the Harmonic Balance Simulator, according to the selection of the order of harmonics considered the following results obtained.

If the maximum order is 0 or 1, no mixing products are simulated; the result will be f_1 and f_2.

Frequency	**Combination**
0 Hz	DC Term
f_1	Fundamental 1
f_2	Fundamental 2

$2f_1$	Second harmonic of Fund 1
$2f_2$	Second harmonic of Fund 2
$3f_1$	Third harmonic of Fund 1
$3f_2$	Third harmonic of Fund 2

Table 4.1: The harmonics of the signals

If the maximum order is specified as 2, the harmonics in Table 4.1 are obtained as well as the harmonics in Table 4.2.

Frequency	**Combination**
0 Hz	DC Term
$f_1 - f_2$	Fund 1 – Fund 2
$f_1 + f_2$	Fund 1 + Fund 2
$2f_1 - f_2$	Second harmonic of Fund 1 – Fund 2
$2f_2 - f_1$	Second harmonic of Fund 2 – Fund 1
$2f_1 + f_2$	Second harmonic of Fund 1 + Fund 2
$2f_2 + f_1$	Second harmonic of Fund 2 + Fund 1

Table 4.2: The higher harmonics of the signals.

Obtaining various harmonics by changing the order is possible.

The response of a mixer to the harmonics is crucial in determining its performance. The frequencies of the harmonics are known but the relative amplitudes of the harmonics have to be determined. So, a simulation was carried out using the harmonic balance simulator in order to find the mixer output spectra and conversion gain. The order of maximum harmonics considered was specified as eleven. Signals were applied to the RF and LO ports of the mixer in various amplitudes. The results will be given in Chapter 6 along with the experimental data.

4.5 RF AMP Simulations

The RF Amplifier circuit was designed using ADS and the schematic is given in Figure 4.16.

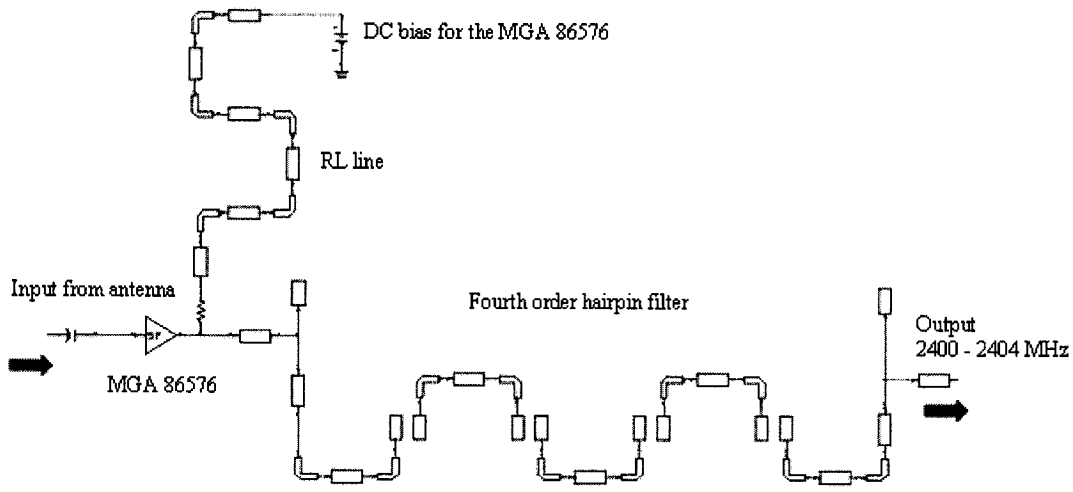

Figure 4.16: The RF AMP circuit schematic.

The input signal coming from the antenna is first amplified at MGA 86576 by the gain of 23 dB at 5 V DC. Afterwards the bandwidth of 2400 – 2404 MHz it is passed by using 5-pole hairpin filter. Finally at the output, the amplified and filtered signals at 2400 - 2404 MHz bandwidth become ready to enter the mixer as the RF.

4.5.1 The RF Power and Spur Rejection Simulations

A simulation was carried out in order to see the RF filtering and amplification performance of the RF AMP as well as the spur response. The Harmonic Balance Simulator was used in order to perform the analysis. In this simulation, signals in the frequency band of 2112 -2116 MHz to 2400 -2404 MHz were applied as RF input with a step of 1 MHz. In the output the following results were obtained.

Applied RF Signal Power at 2400-2404 MHz (dBm)	The Output Signal Power at 2400 - 2404 MHZ (dBm)	Applied Signal Power at 2112-2116 MHz (dBm)	The Output Signal Power at 2112-2116 MHZ (dBm)
-70	-47.253	-70	-122
-60	-37.253	-60	-112
-50	-27.253	-50	-102
-40	-17.253	-40	-92
-30	-7.253	-30	-82

Table 4.3: RF AMP power and spur rejection simulation results.

As seen from Table 4.3, the RF power amplification in 2400 - 2404 MHz band is around 22 dB, which is expected. The MGA 86576 has a flat gain of 22.9 dB under 5 V DC bias. The spur rejection is 52 dB and the relative amplitude difference between the signal at 2400 MHz and 2112 MHz at the output, assuming both have the same amplitude, is 74 dB. So, the spur rejection of the RF AMP is 74 dB.

4.5.2 The RL line

The "RL line" stands for the resistor-inductor line and it passes the DC bias to the amplifier, and blocks all AC signals. In the RF AMP, the RL line takes the duty of separating AC signal from DC bias circuitry in both the RF AMP and HG. The DC bias to the amplifier was supplied using a regulator, to be discussed in Chapter 6. In order to avoid the AC voltage in the signal from going to the regulator the RL line was introduced between the regulator and the AC trace. The RL line lets DC pass but rejects AC. The layout is shown in Figure 4.17.

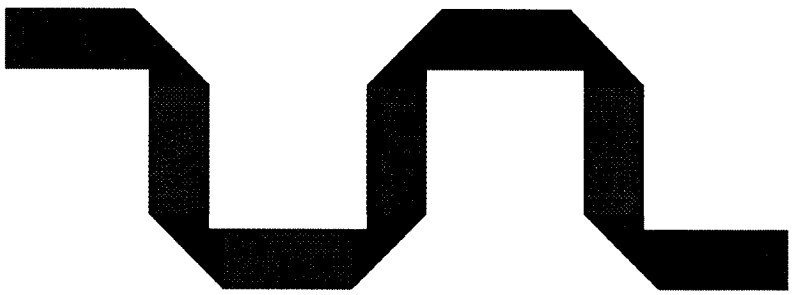

Figure 4.17: The layout for the RL line.

The S_{11} and the S_{21} of the RL line are shown in Figure 4.18.

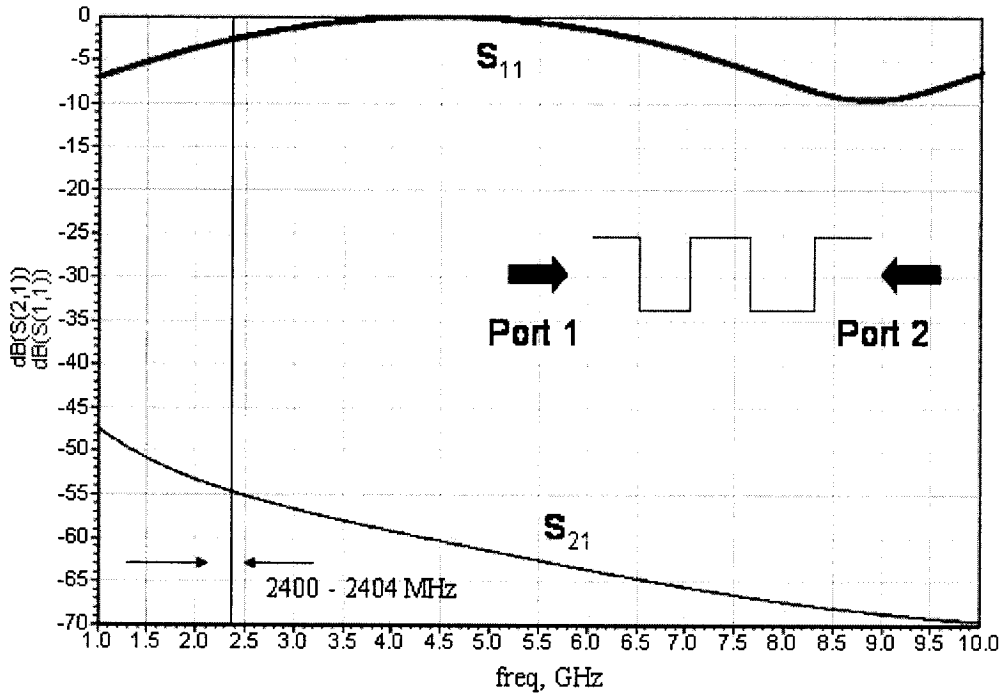

Figure 4.18: The S_{11} and the S_{21} of the RL line.

We see that at 2.4 GHz S_{21} value is less than -50 dB, which means that the AC signals are effectively looking into an open circuit. So, the RL line works as AC high impedance between regulator circuitry, while passing the DC. Since the amplitude of the applied signal will be in the range of 5 to 10 dBm, an isolation of 50 dB is a good result.

4.6 HG Simulations

The Harmonic Generator circuit was designed using ADS as shown in Figure 4.19.

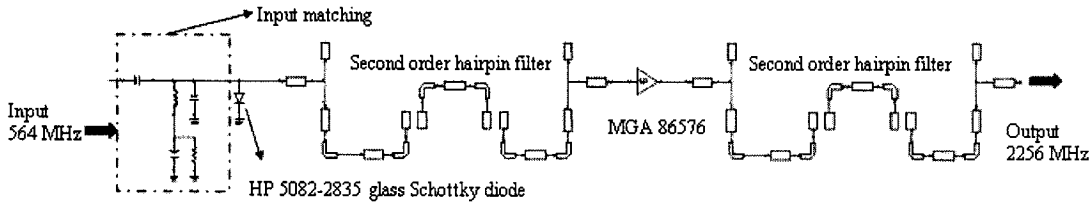

Figure 4.19: The harmonic generator circuit schematic.

The signal of interest is the fourth harmonic (2256 MHz) of the input signal 564 MHz. Since the diode generates all order harmonics of the input signal, filtering out the desired frequency is crucial. As only the discrete multiplies of the input signal generated as the harmonics, the output spectra have the following signals:

$$f(n) = 564n, \text{ n} = 1, 2, 3, 4\ldots$$

The signal being interested is 2256 MHz and it is the two close to the 3^{rd} and 5^{th} harmonics at 1692 MHz and 2820 MHz respectively. So, a filter that can suppress these two frequencies is required. The 3-pole hairpin filter simulated in the Chapter 4 has a rejection of more than 40 dB at both frequencies. Adding two stages of filtering enhances the rejection of the unwanted signals. As described in Chapter 3 obtaining an undistorted LO signal is very important.

The input signal coming from an output signal generator at 564 MHz first passes through a matching circuit, then the harmonics of the signal are generated by using a HP 5082-2835 glass Schottky diode. Then, the harmonic enter the 3-pole hairpin filter centered at 2256 MHz so that the other harmonics components generated at the diode are suppressed and the resulting signal enters the MGA 86576 amplifier, which has a gain of 23 dB at

5V DC. Afterwards, the amplified signal enters the 3-pole hairpin filter. Finally at the output of the filter, the signal at 2256 MHz (The fourth harmonic of 564 MHz) becomes ready to enter the mixer LO input.

Note that a matching network is used between the 564 MHz input and the Schottky diode, however no matching is used between the Schottky diode and the hairpin filter. The matching circuit is shown in Figure 4.20 and its response is shown in Figure 4.21.

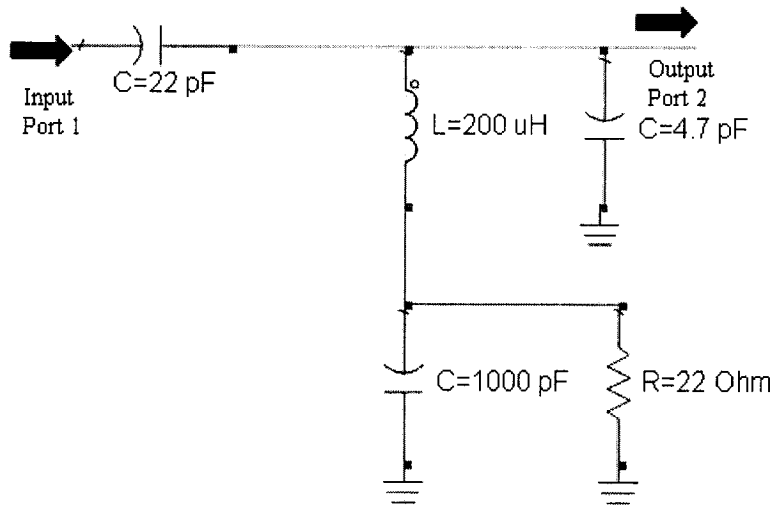

Figure 4.20: The matching circuit schematic.

The response is given in Figure 4.21.

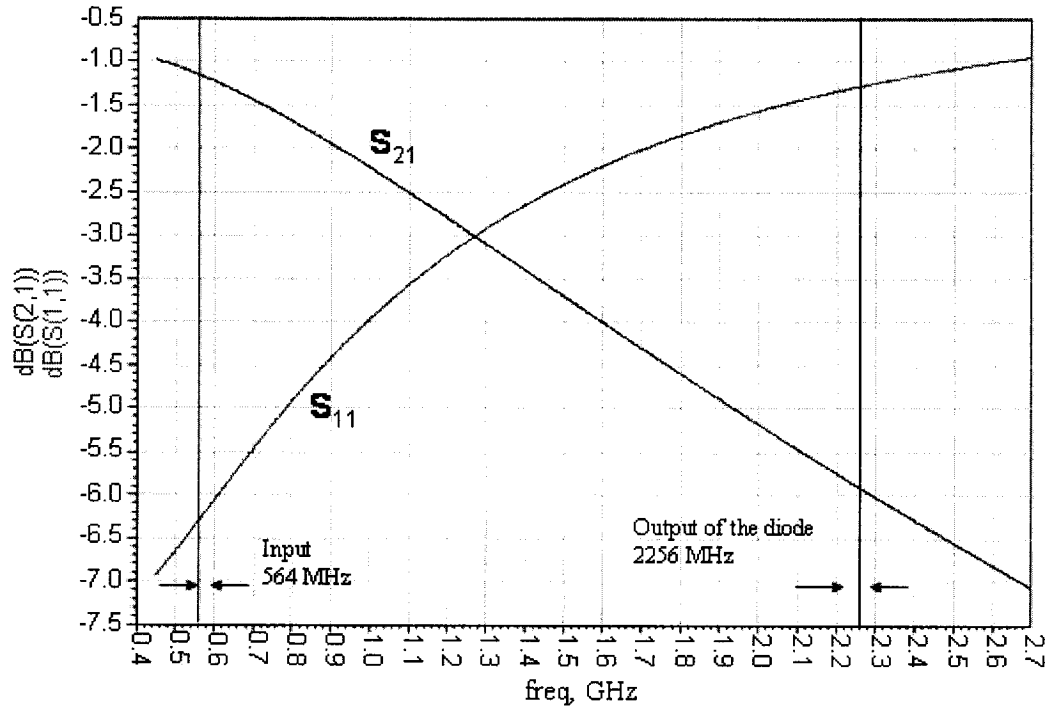

Figure 4.21: The response of the matching circuit in Figure 4.20.

As seen from Figure 4.21, the response of the matching circuit, it passes the input at 564 MHz with a loss of 1 dB but rejects the harmonics generated by diode. Especially, at the frequency of interest (the 4th harmonic of 564 MHz, 2256 MHz) the S_{21} is better than -6 dB.

4.6.1 The Output Spectra Simulations

The simulations to predict the performance of the HG were carried out using the Harmonic Balance Simulator of ADS. The simulations were similar to those for the RF AMP. The input signal at 564 MHz was applied at one end and the output spectrum is observed. The results obtained are in Table 4.4.

	The desired 4th harmonic	3rd harmonic	5th harmonic
Applied RF Signal Power at 564 MHz (dBm)	The Output Signal Power at 2256 MHZ, (dBm)	Applied Signal Power at 1692 MHz (dBm)	The Output Signal Power at 2820 MHZ (dBm)
12	13.3	-28	-32
10	12.1	-30	-35
8	11.0	-32	-38
7	10.3	-33	-39
6	9.5	-34	-40
5	8.2	-35	-41
4	7.0	-36	-41
3	5.9	-38	-42
2	5.0	-40	-44
0	3.2	-40	-45

Table 4.4: HG output power simulation results.

So, as seen, the HG has a gain around 1.5 dB. Actually the amplitude of the fourth harmonic is 23 dB lower than the seen output and the gain of the amplifier, which is 23 dB, increases the amplitude of the output. So, in the end, the HG has a gain of 1.5 dB and has a satisfactory rejection.

5 Fabrication

Since the goal of this thesis is to give the head to toe approach of design and implementation of a 2400 MHz input – 144 MHz output downconverter, the fabrication process of the circuit is a very important step and as complex as its design. In order to get a circuit board manufactured, the manufacturing company needs some files in specific formats. For the fabrication process of the design, a Canadian company called APCircuits was used [16]. APCircuits required Gerber files of both layers. The excellon drill data for the board uses formats specified on their website.

Basically, the Gerber files use ASCII text format in a specific way, named RS-274D, RS-274X so that photoplotting machines can read, understand and physically produce the desired board. There are various CAD programs on the market, which can produce Gerber files for a given design. The most common programs are Protel and Eagle but they require the board to be designed using their design engine. However, designing the complicated microwave circuits using those programs is not possible.

On the other hand, ADS has a built-in Gerber converter so that the circuit designed in ADS can easily be converted to a Gerber file in the desired format. The other important file is the excellon drill data which again uses an ASCII format to specify the drill locations on the board as well as their dimensions. Generating this file is also possible using ADS.

5.1 Creating the Gerber files

In order to convert a design into Gerber file, first create the layout of the circuit in the schematic window using "Layout" menu and "Generate/update layout..." option. ADS creates the layout in a new window. When the layout is created, go to the "file" menu and select the "export" option. Select "export to Gerber" for the file type. When "OK" is pressed, ADS opens a new dialogue box named "MSTools" which is the dialog box we need to use to create the Gerber files.

In that dialog menu, there are options named: "translation settings," "Gerber file options," "translate," "edit apertures," "view mask" and "view Gerber." The options enable us to specify the properties of the Gerber file to meet the requirements of the manufacturer company.

For instance APCircuits demands the files in RS-274X file type, format in 2.4, "trailing zero suspension" ON, data type ASCII.

If "Gerber file options" is clicked from the main dialog box, it opens a box and changing the format to 2.4, changing the status of "trailing zero suspension" is possible. When OK is clicked the program returns to the main dialog box. Then we click the "translation settings." Changing the file type to RS-274X is possible from that menu. We must make sure that the "Fill" box is clicked in "fill/outline" menu before clicking OK.

The board is ready for translation and this is done by clicking the "translate" box. When it is clicked, the program asks that the layers to translated. Select the layers except the "hole" layer, if and there are any holes in the design. If there are no holes in the design,

there won't be a "hole" option. Then click OK to continue. ADS creates the Gerber files at that moment under the names of the layer names, not the design name.

ADS names the top layer as "cond" and bottom layer as "cond2" in default, which is important to mention because after generation of Gerber files, they are the files that have the design parameters. The Gerber files associated with the design will be "cond.gbr" and "cond2.gbr."

The drill data obtained after the translation of the layers is completed. When translation finishes the main dialog box appears again. From that box, click the "aperture settings" and when the new box opens click "auto flash" and click "save." The main dialog box comes again, click "translate." Select only the "hole" layer this time and unselect the other layers, click OK.

From main dialog box, click "view Gerber" and it opens a new dialog box. From that box, click the "aperture." In the new dialog box the dimensions of the holes are given. Find the dcode type "Poex" and write numbers in to column named "tool #" starting from one. Also write the diameter of the each hole to the "drill dia." box. By doing that the dcode in the Gerber file are associated with the holes. Finally, go to Tools menu, click "Drill" then "Excellon." Select suppress leading zeroes and click OK. By doing that a new file named "hole.drl" will be created. The locations and the specifications of the holes are stored in that file.

The procedure above concludes the creation of Gerber files. Besides, in the "Gerber viewer" check if the actual design is converted to Gerber without any mistakes. If another Gerber translation is to be made, the mask file (a file with .msk extension) must be

deleted before starting a new one because ADS does not delete it by itself and the old information affects the new translation.

APCircuit asks for the Gerber files for the top and the bottom layers as well as the drill data. So, if a single layer design was made, three files needed to be sent to APCircuits and their names would we "cond.gbr," "cond2.gbr" and "hole.drl" if the default names were used for the layers.

After obtaining the Gerber file, different software named Viewmate [10] has used, which is free software to display Gerber files, to check if everything was fine. Besides, it is important to check the requirements and the restrictions of the producer company. For instance, the hairpin filters designed by ADS's internal design engine leave spaces, which are smaller then the minimum spacing restriction of APCircuits (7 mils) so that physical realization of those circuits is problematic. The accuracy of APCircuit designs are ± 7 mils of the original design.

APCircuits has a predefined board size of 10.25 inch by 8.25 inch which uses 20 inch Rogers 4350B as the substrate. Rogers 4350B has a dielectric constant of 3.48 ± 0.05, loss tangent of 0.0031 and costs around $300 CAD for two boards. Actually, in this thesis in order to experiment, each component was made separately. Only two downconverters were fit to a board but it is possible to fit six downconverters in two boards so that would make each one $50 CAD. The cost of parts for one downconverter is around $30 CAD, indeed there is a minimum order price for the parts if the amount exceeds some quantity, the price for each part drops. Since this downconverter is for experimental purposes, the cost of the parts became expensive. Moreover, three SMA connectors were needed,

which cost around $20 CAD in total. Hence, it is possible to produce a downconverter for $100 CAD.

A board of that size was prepared and sent to APCircuits. During the whole process of sending, the assistance of the ECE technician Robert Idsinga was very useful. The board sent is shown in Figure 5.1.

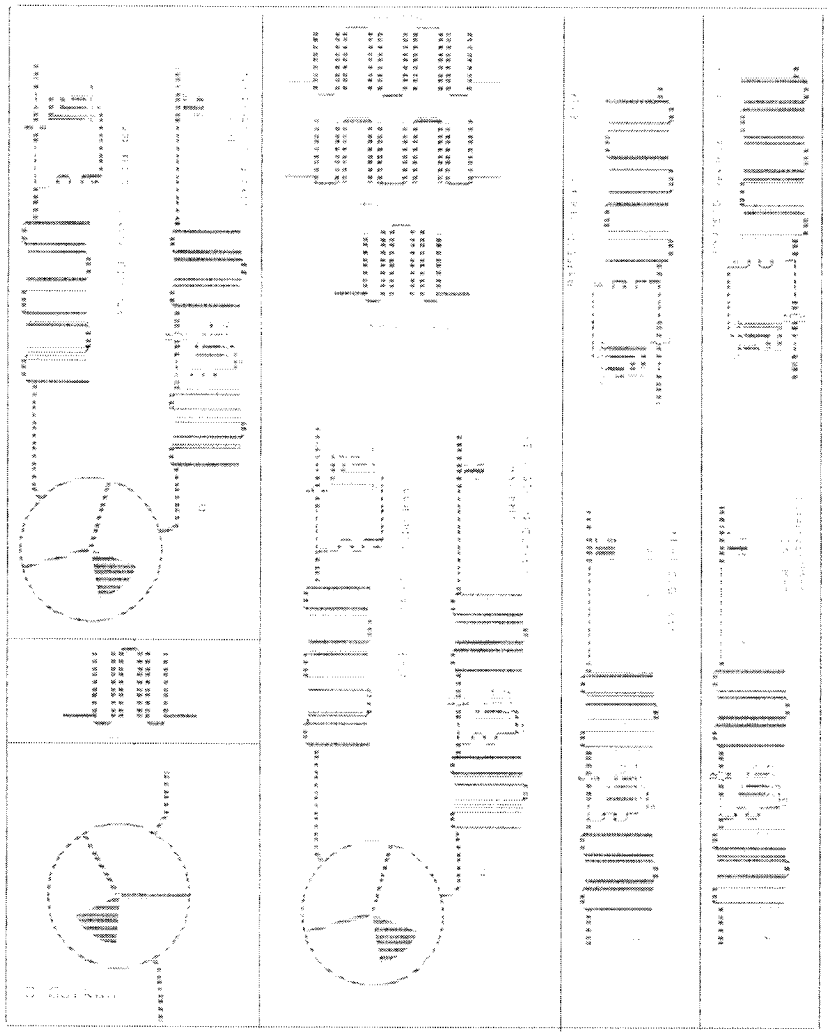

Figure 5.1: 8.25 by 10.25 inch board sent to APCircuits (Gerber file).

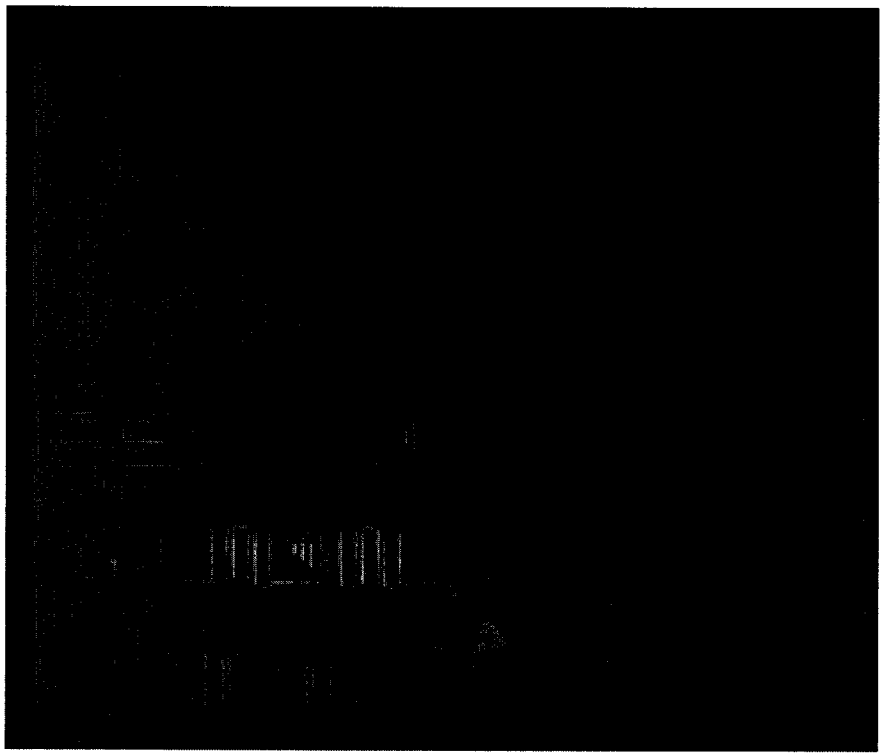

Figure 5.2: The real picture of the board.

Two copies of the board were produced and each has two 5-pole filters at 2400 MHz, a 3-pole filter at 2256 MHz, a rat race coupler mixer, two RF AMP modules, two HG modules and two downconverters.

5.2 Physical Construction of the Design and Mounting of the Parts

How the circuit should be realized in practice is an important issue in the theoretical design. The board is designed in such a way that chopping the components up is easy. There were straight clearings for cutting with a guillotine. Moreover, in realizing the

filters, 15 mm transmission lines added to both sides of the filter in order to solder SMA type connectors for experimental purposes. The gaps between microstrip transmission lines were designed just enough for the necessary part to fit in. The soldering of surface mount components was accomplished with the help of the technical staff of ECE and their expertise on using the surface mount equipment.

In the design stage of the downconverter, the layout was modified according to the exact dimensions of the parts. The layout generator of ADS does not automatically give the usable layout for the design. The grounding pads, the pads for surface mounts, the spacing and grounding for amplifiers were all designed manually. The grounding obtained was by via pads of 0.020 inch in diameter; basically they create a plated hole between the ground layer and top layer. The 0.020 inch diameter drill sizes were chosen due to fact that it is the minimum drill size offered by APCircuits. The size of the holes is important because using a large hole in diameter, causes it to behave like an inductor.

The amplifiers have four legs and two of them require grounding. The grounding was accomplished by inserting two grounding pads on both sides of the amplifier clearance. This is shown in Figure 5.3.

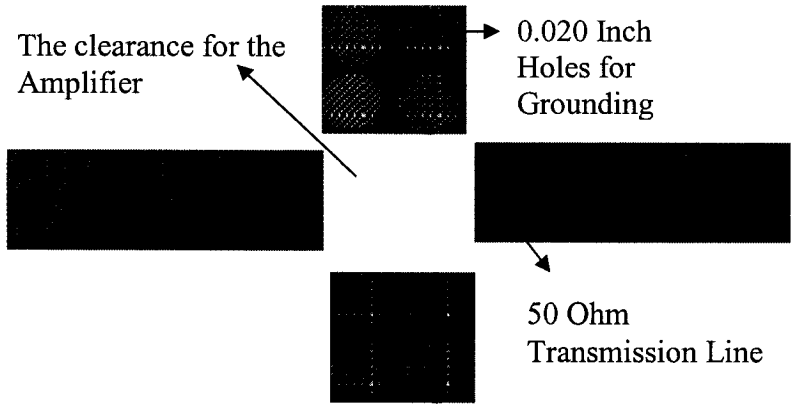

Figure 5.3: The clearance for the amplifier.

In a similar manner, the DC path for the LM317LZ regulator was designed in a way to leave enough clearance for the resistors and capacitors connected in shunt or in series. This is shown in Figure 5.4.

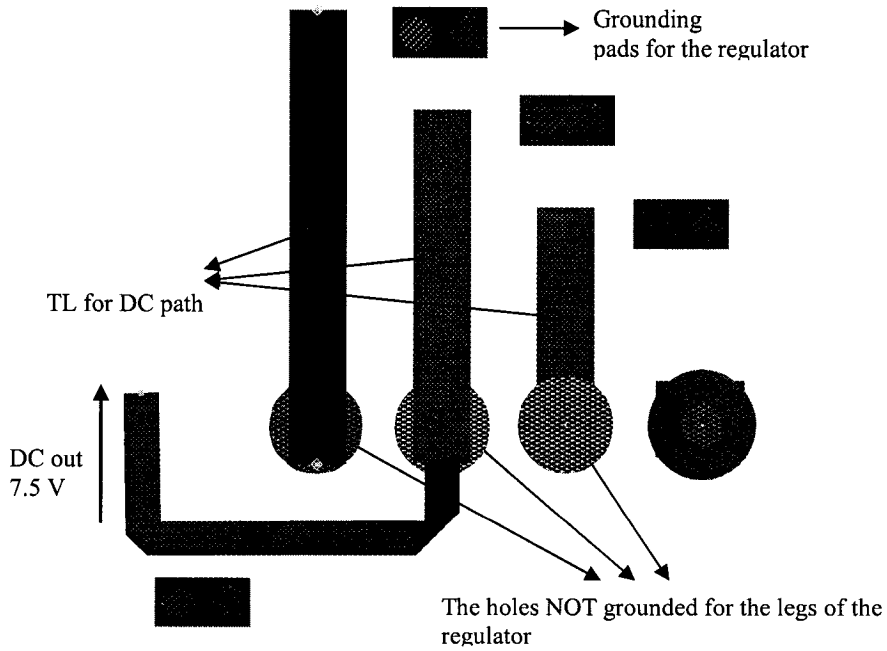

Figure 5.4: The DC bias circuit.

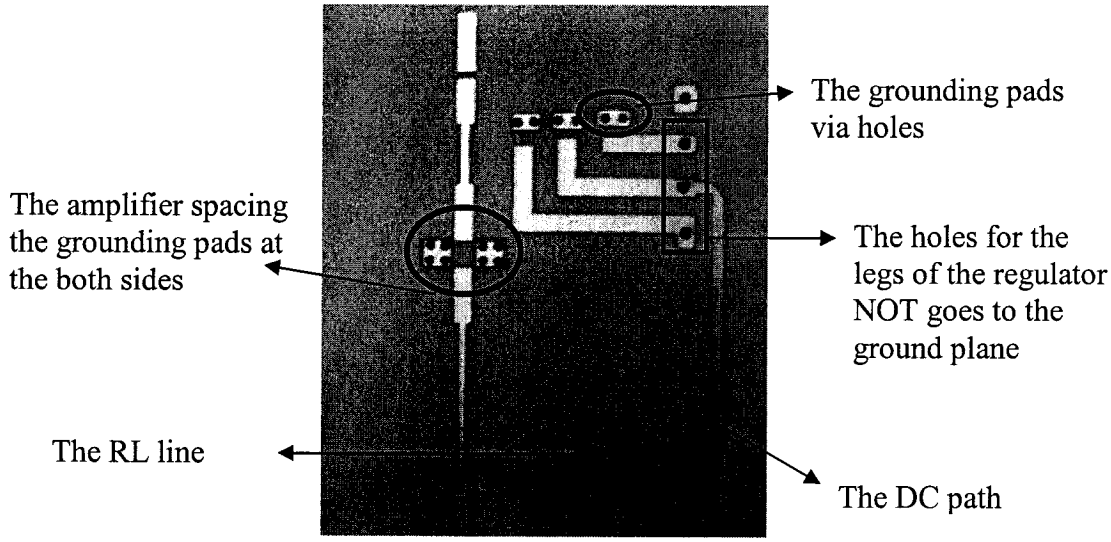

Figure 5.5: The orientation on the part of the actual board.

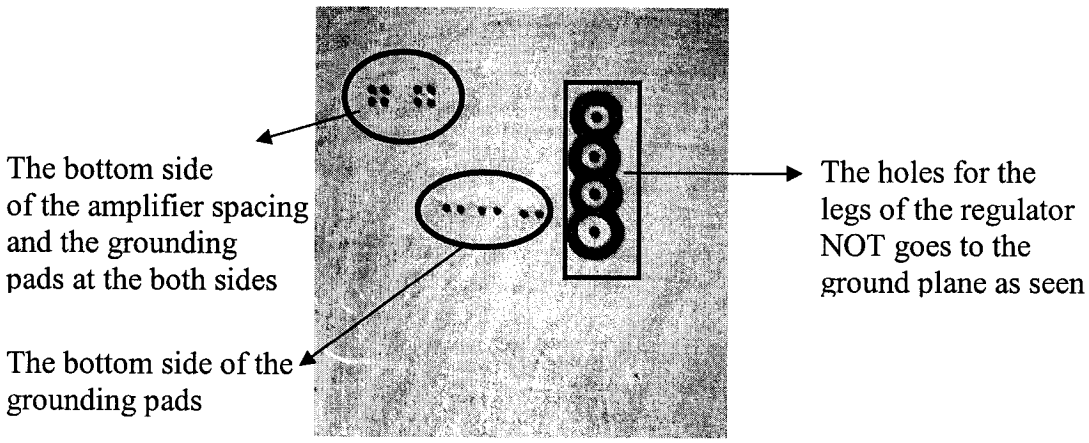

Figure 5.6: The bottom side of the board shown in Figure 5.5.

As seen from Figure 5.5 and Figure 5.6 there are pads at the other end of the regulator. The via holes in the bottom plane are not grounded. The pads provide a soldering pad for the legs of the regulator. By using this procedure, soldering the non-surface mount devices becomes easier because otherwise, the legs of the parts would be soldered to the

transmission line and if not made properly, could cause the copper line to peel off the substrate. Yet, this procedure is valid as long as DC path is considered because the microstrip line needs a grounding plane beneath it in order for electric and magnetic fields to propagate uniformly. Hole would disturb the field.

The holes left ungrounded for the legs of the regulator can be seen clearly. The parts mounted for the RF AMP is shown in Figure 5.7.

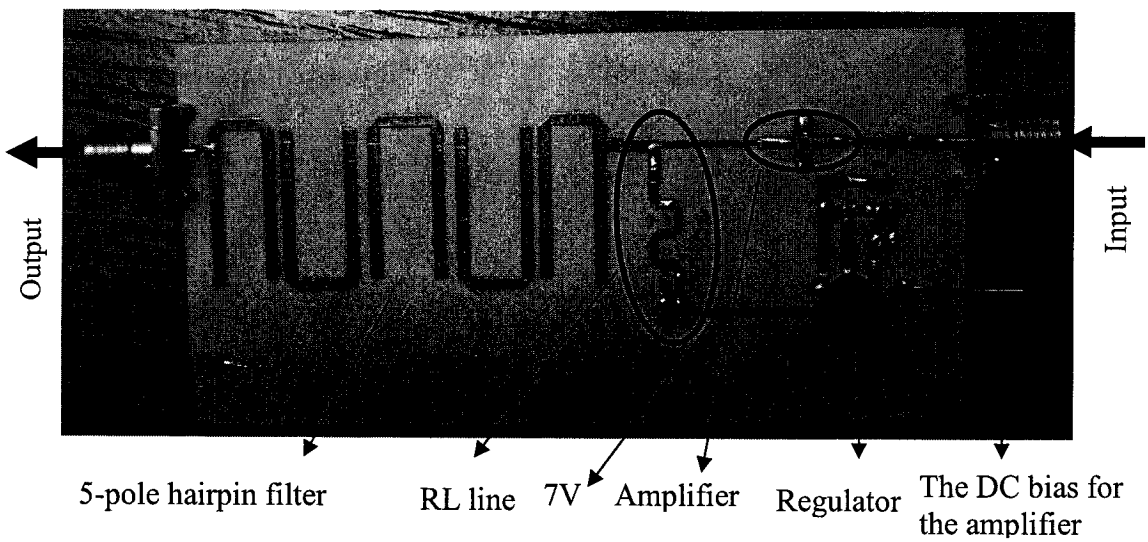

Figure 5.7: The RF AMP board.

As seen, the dimensions are very small and the parts that form the bias circuitry for the regulator can barely be seen. The soldering of surface mount parts was done by ECE technical staff with great care, in order to not damage the trace and the parts. The pins of the SMA connectors were shortened in order to suit the physical distance available on the circuit board. The manufactured modules are shown in Figure 5.8 to 5.13.

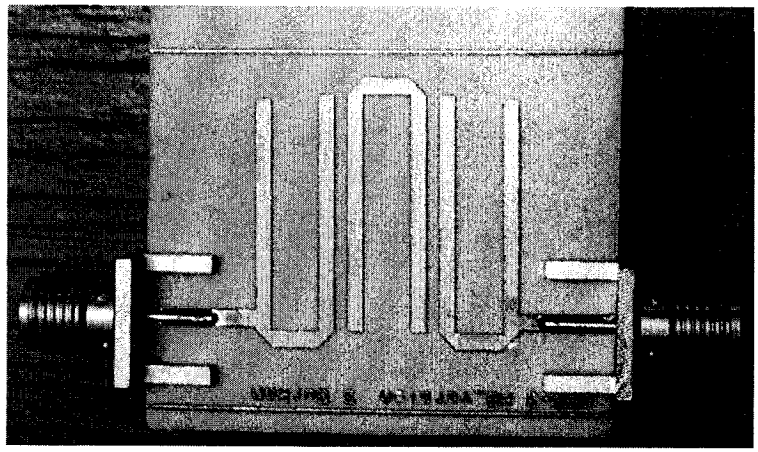

Figure 5.8: The 3-pole hairpin filter for the HG.

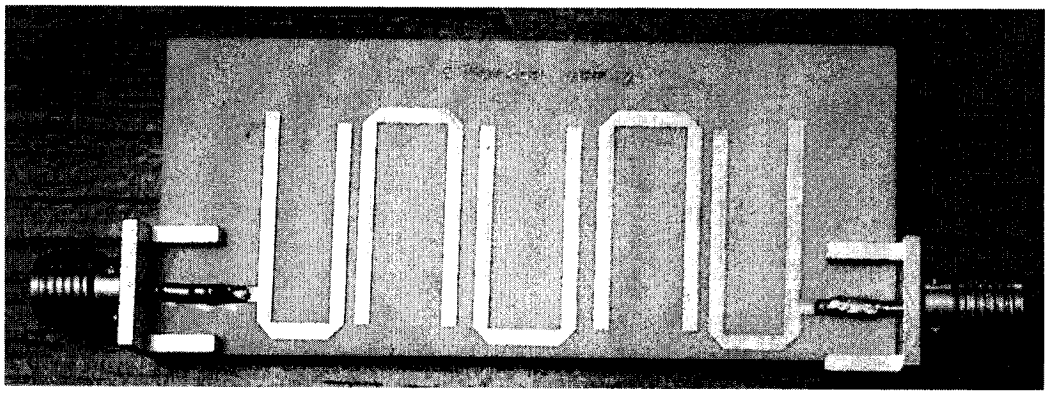

Figure 5.9: The 5-pole hairpin filter for the RF AMP.

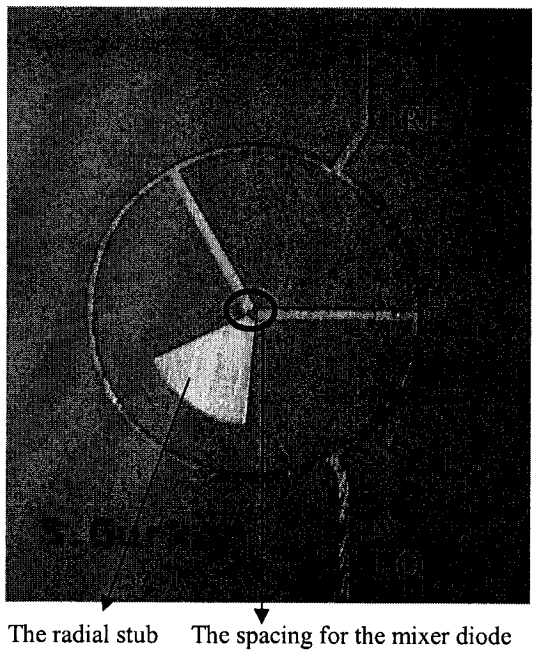

Figure 5.10: The rat race coupler.

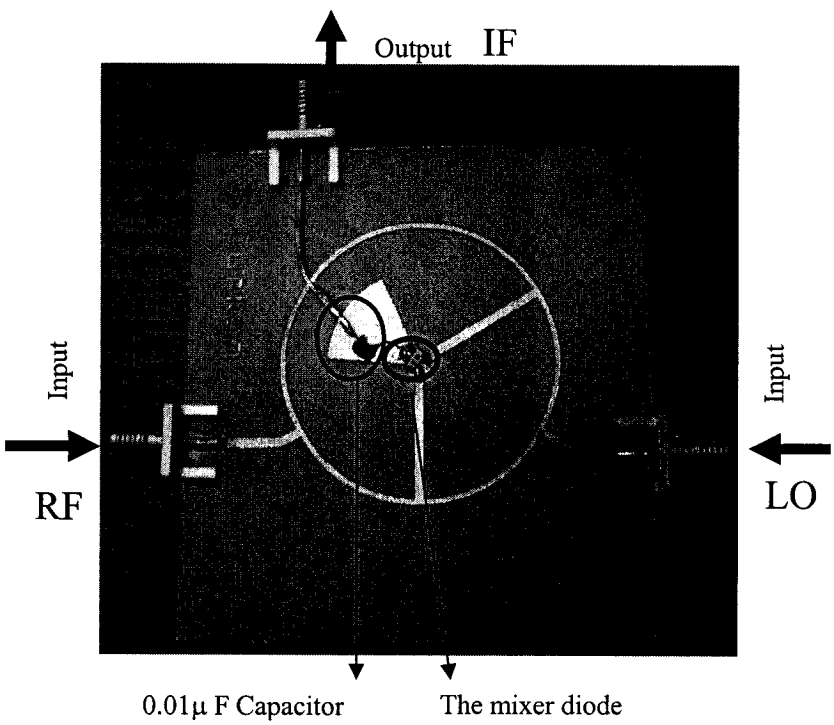

Figure 5.11: The rat race hybrid mixer.

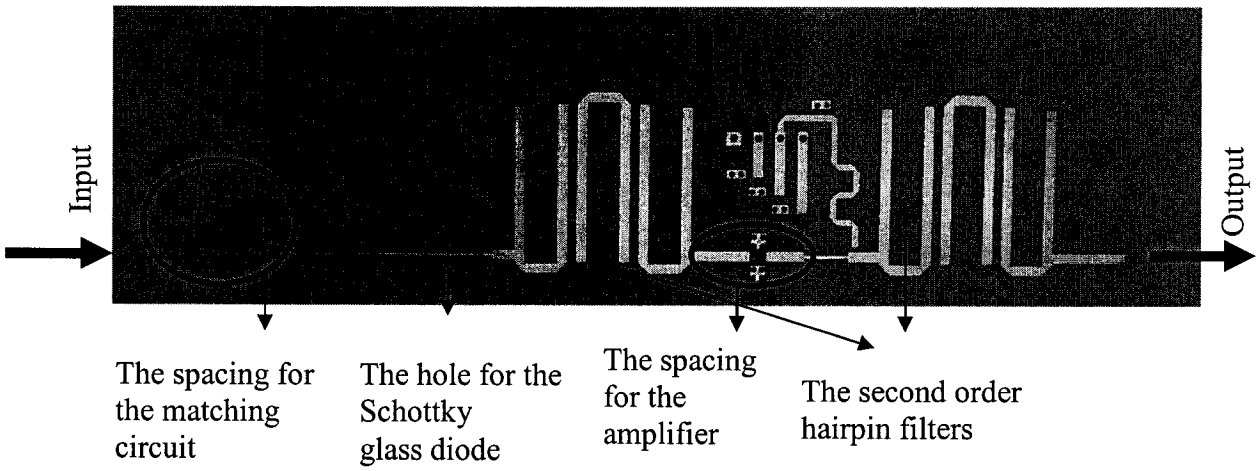

Figure 5.12: The board of the harmonics generator.

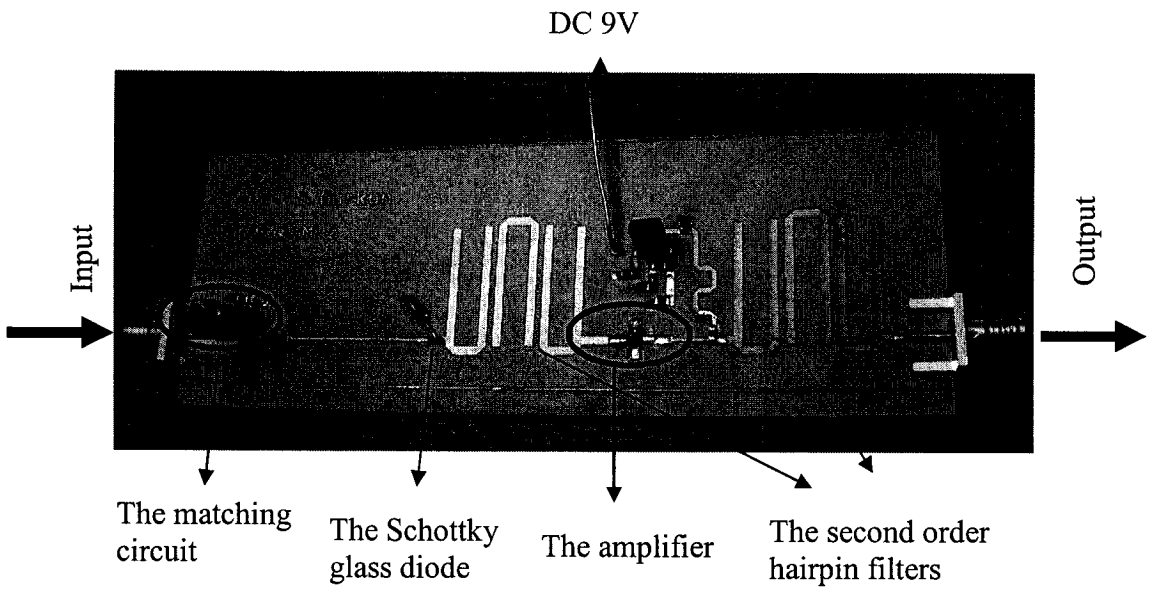

Figure 5.13: The harmonics generator.

5.3 The Effect of the Fabrication Errors

A simulation was carried out in order to see the effect of possible errors on the design. APCircuits manufactures the designs in an error range of ± 7 mils (0.1778 mm). In order

to see the influence of this possible error on the design a simple simulation was carried out. A half wave transmission line optimized for 2400 MHz designed and then simulated by adding and subtracting 7 mils from its length and width to see the effect. The circuit simulated is shown in Figure 5.14 and the results are given in Figure 5.15.

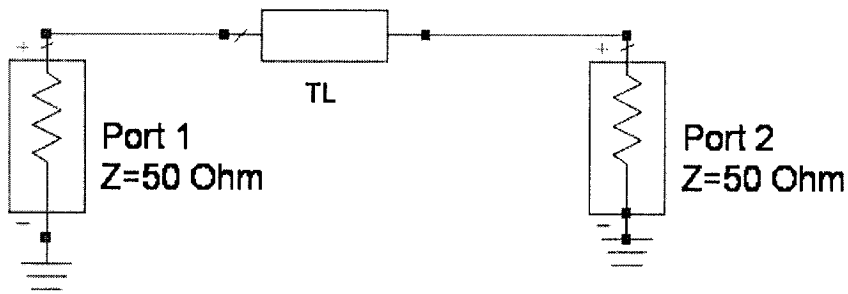

Figure 5.14: The schematic view of the circuit simulated.

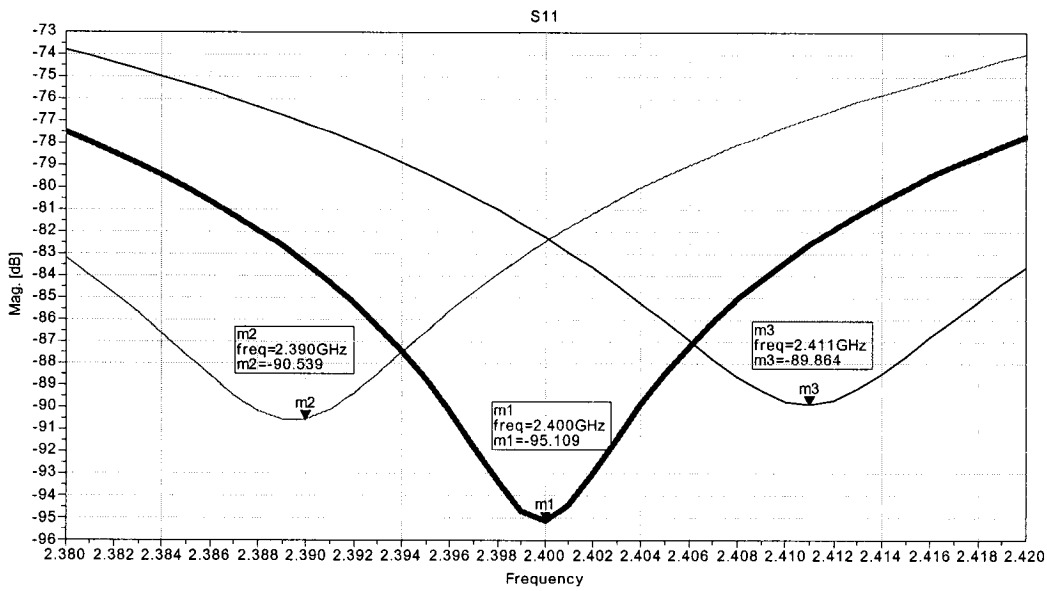

Figure 5.15: The original S_{11}, 7 mil added and subtracted from the length of the TL.

As seen from the full wave simulation results, a 7 mil change in the length of the transmission line causes 10 MHz of shift at the center frequency. The magnitude of the S_{11} also changes. If the error happens in the width of the transmission line, the changes in Figure 5.16 occur.

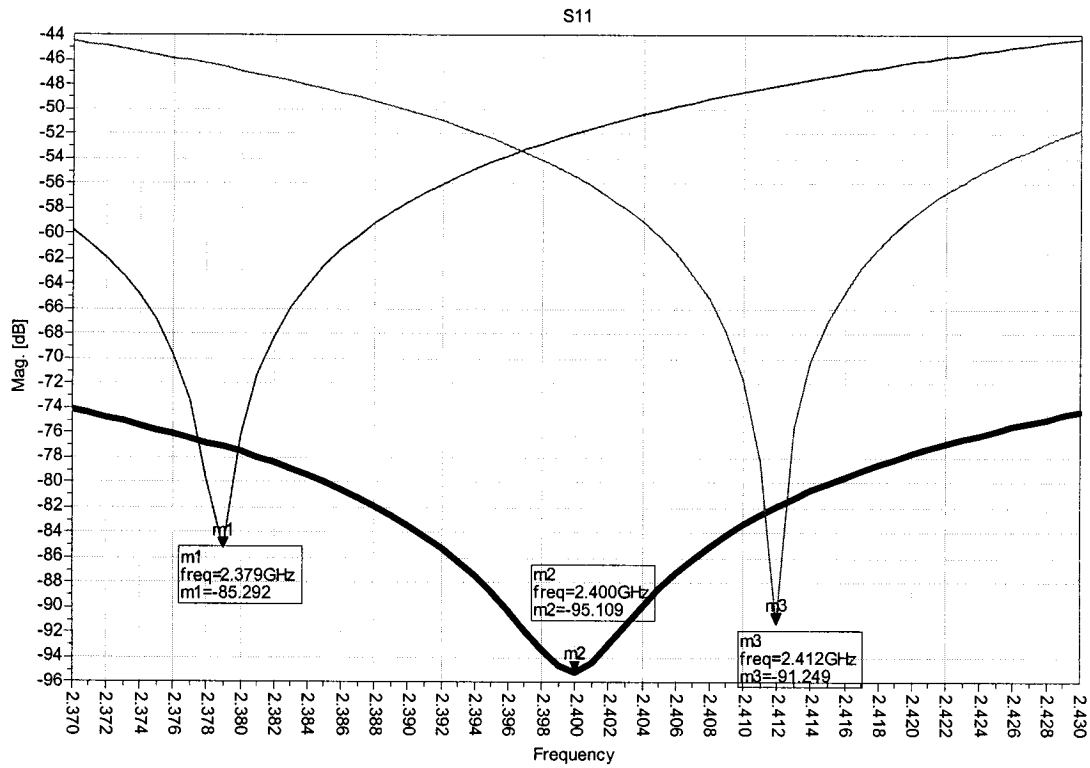

Figure 5.16: The original S_{11}, 7 mil added and subtracted from the width of the TL.

The change in the width of the transmission line causes a shift of 12 MHz and S_{11} reduces more sharply when its value changes. So, as seen from the simulation results, even a tiny change in either width or the length of the transmission line affects the whole response. In a complicated structure like hairpin filters or rat race couplers, a small change can cause bigger deviations from the expected results. The errors can happen any part of the

components and it is impossible to foresee them. An error in the range of 7 mils at the coupling structures of a filter can easily alter the whole response of a filter. So, before starting to experiment with the design in the lab, some deviations from the simulated results can be anticipated.

6 Testing and Results

6.1 Introduction

In this chapter, the testing of the circuits and the results of the experiments are discussed. The experiments were held at the Microwave Lab, H-853, using the available tools and test equipment. The obtained results were printed out using the Linux GPIB computer of the lab. In different applications, microwave coaxial connectors of various types were used such as APC-7 to N male adapter, N to SMA male adapter, female SMA adapter and SMA short circuit.

6.2 Hairpin Filters

The hairpin filters were tested using both HP 8720A and HP 8410 networks analyzers for cross check. In both cases some deviations from the simulated results were observed.

6.2.1 5-pole Filter Test and Results

The 5-pole filter designed for filtering of the 2400 - 2404 MHz bandwidth and specifically rejecting the 2112 -2116 MHz (spurious response) bandwidth has a response as shown in Figure 6.1.

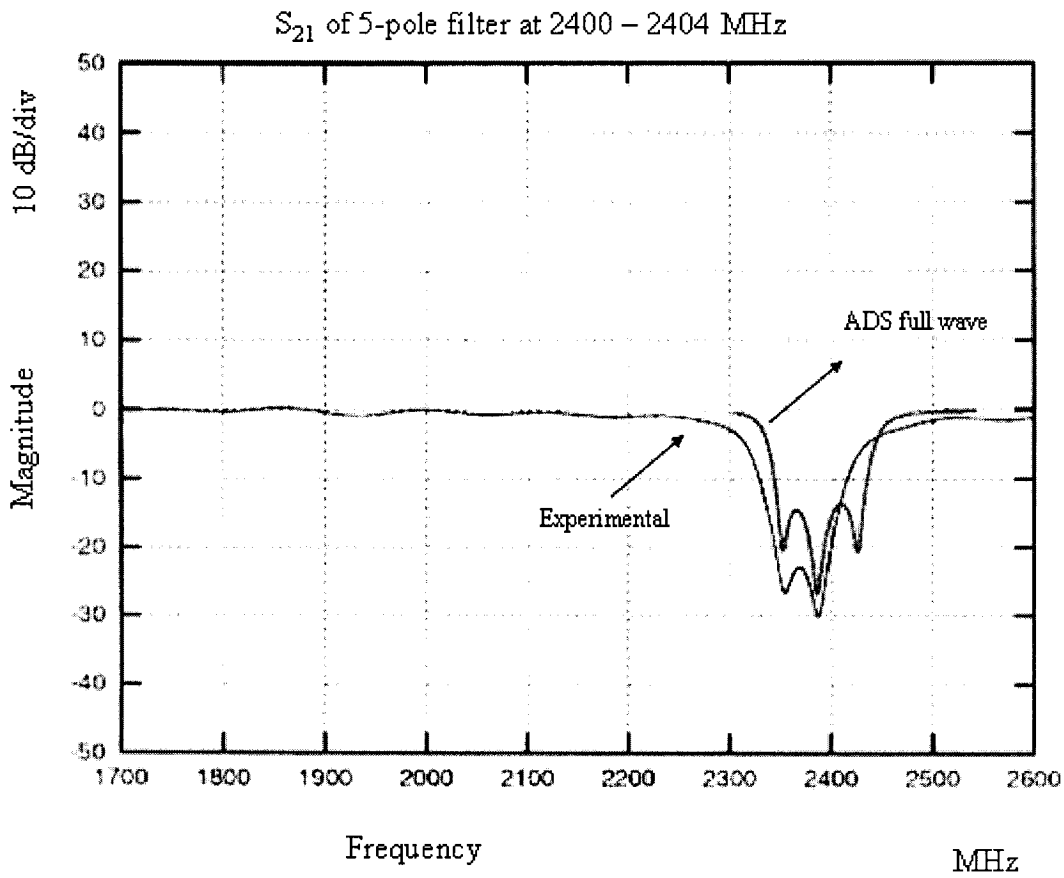

Figure 6.1: The S_{11} of the 5-pole filter at the RF AMP.

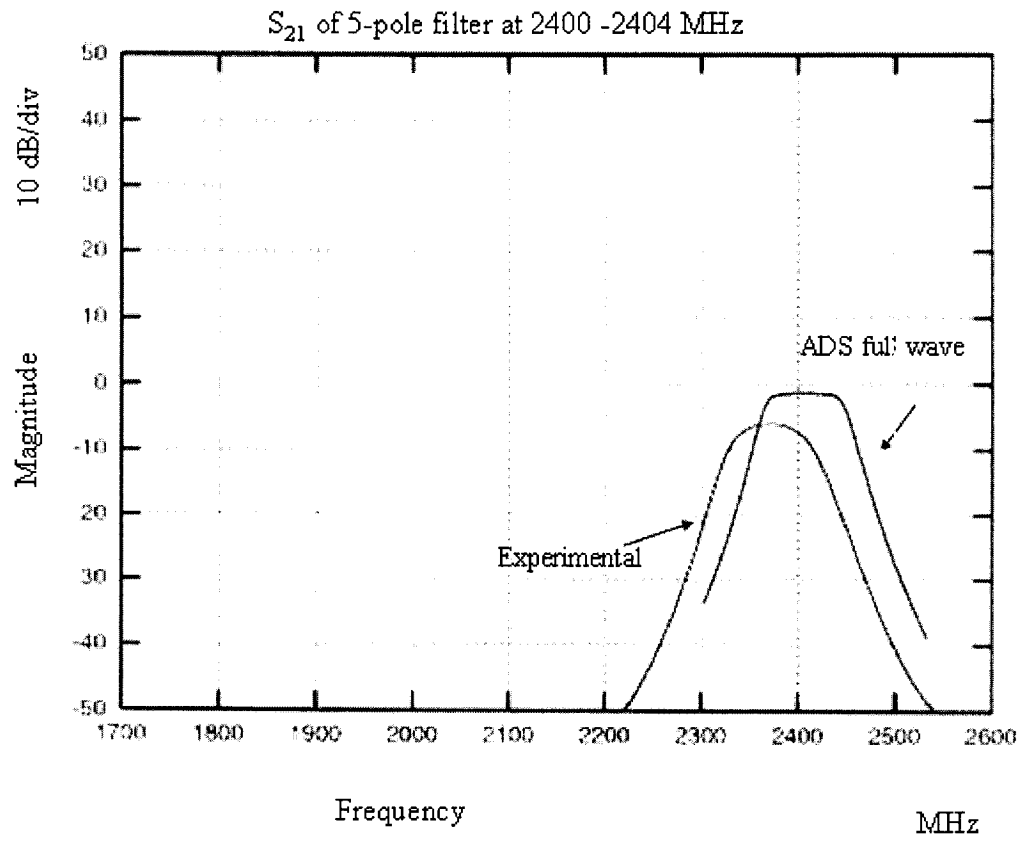

Figure 6.2: The S_{21} of the 5-pole filter at the RF AMP.

In order to remind us, the design specs were: 0.5 dB Chebyshev, center frequency 2400 MHz, bandwidth 105 MHz, spur rejection better than 30 dB.

The result has some differences than the expected result of ADS. The bottom peak of the S_{11} shifted 10 MHz, which caused S_{11} to be -30 dB at 3990 MHz instead of 2400 MHz. At 2400 MHz the S_{11} is -20 dB and the insertion loss of the filter is -7.27 dB which is around 5 dB more than the expected. However, the spur rejection of the filter is still as satisfactory as expected which is around -55 dB. So, the relative rejection is around 48 dB is still a satisfactory result.

In the Figure 6.1 the theoretical result suggests that there are three poles but the experimental response shows only two. As mentioned earlier, the resonators must be very well tuned in order to get the desired pole from it but they are very fragile that even a small error in the dimensions of the resonators can change its response. The dimension error in the fabrication process could be the reason for that change in the respone.

Indeed, there is a shift in the response of the filter. The response shifted down and the possible reason would be the fact that the dielectric constant of the substrate was slightly different (higher) than the anticipated value of 3.48. The tolerance of the board is 0.05 but the value of the dielectric constant is so fragile that even any change in the temperature can cause the dielectric constant to vary.

6.2.2 3-pole Filter Test and Results

The 3-pole filter passes the 2256 MHz LO signal. It forms part of the HG and the S-parameter results are given in Figure 6.3 and Figure 6.4.

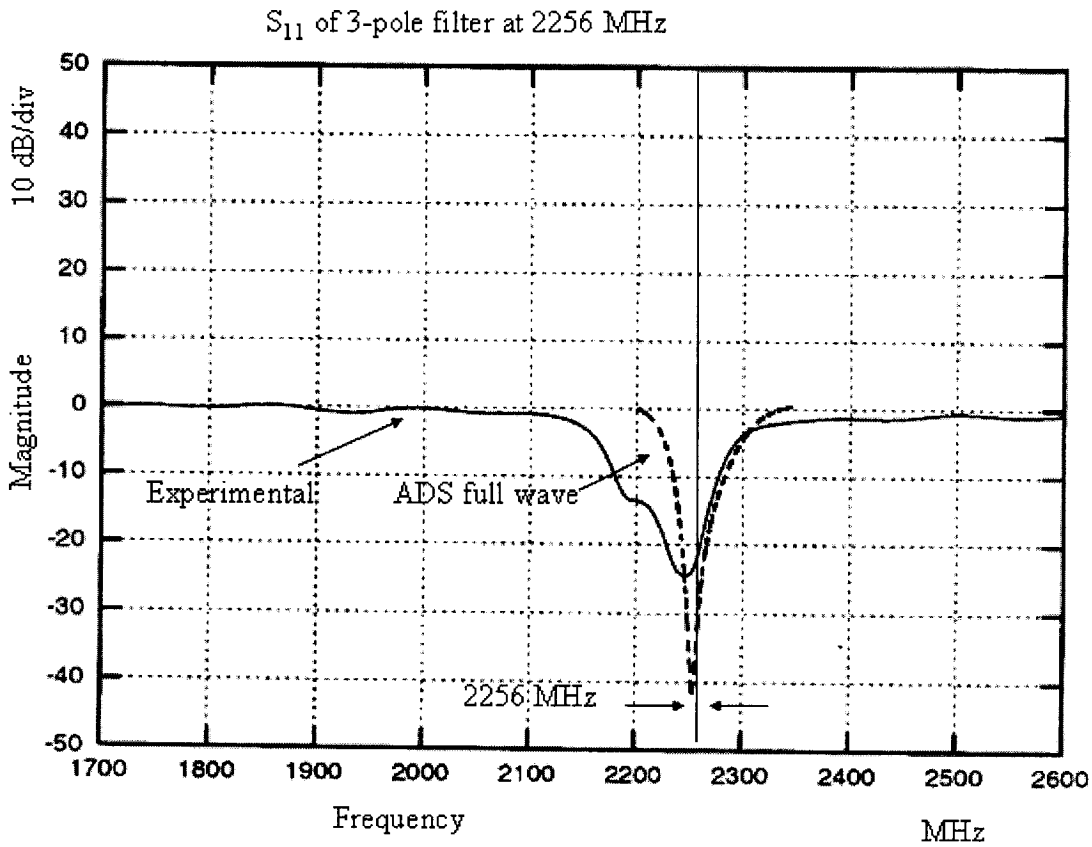

Figure 6.3: The S_{11} of the 3-pole filter used in the HG.

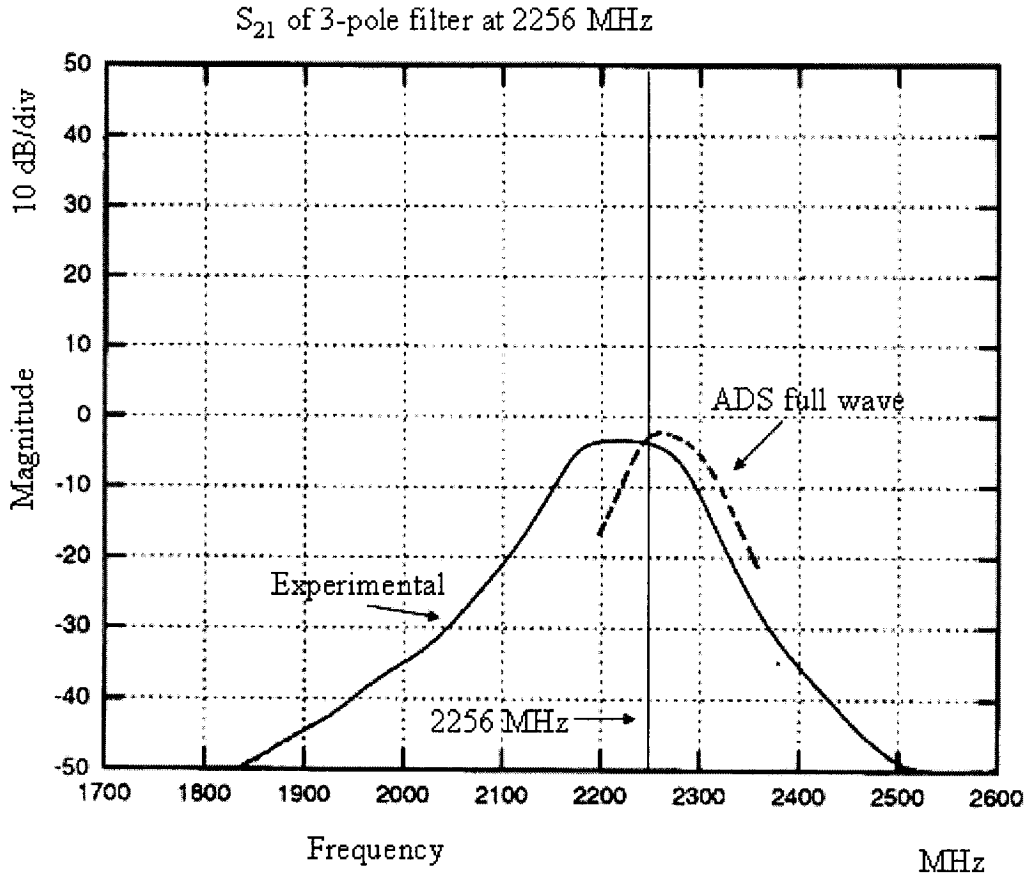

Figure 6.4: The S_{21} of the 3-pole filter used in the HG.

In order to remind us, the design specs were: 0.5 dB Chebyshev, center frequency 2256 MHz, bandwidth 115 MHz, spur rejection (3^{rd} and the 5^{th} harmonics) better than 30 dB.

The result of this filter is, as expected, different from the simulation results. The expected result of S_{11} at 2256 MHz was -22 dB, while in here it is -20 dB. This filter is designed to pass the fourth harmonic of 564 MHz so its rejection of third and fifth harmonics ($2256MHz \pm 564MHz$) is important. The response is satisfactory as seen from Figure 6.4.

The response of the filter is shifted down and it is possibly because the small change in the dielectric constant as it was the case in the 5-pole filter. Also, only one pole is seen in the experimental response of the filter whereas there should be three.

Besides, there observed some differences between the simulated and the experimented results and they could be due to the difference in the dielectric constant that the board has a tolerance 0.05. The reason why some poles disappeared in the responses could be due to the fabrication errors and the tolerance in the dielectric constant.

Finally, as shown in Chapter 5, some filters, which chopped up from the board have sharp ends and this sharp ends could interfere the distribution of the electromagnetic waves. In order to test that we put our finger to the sharp end of the filter and it affected the response. This shows that the difference in the experimental response could also been happened due to the sharp corner effect.

6.3 Rat Race Coupler Mixer

6.3.1 Isolation Experiments

The mixer was simulated using Agilent HSMS 2822 diodes, however in the real design MA4E2054B-287T diodes of the AMP Corp. were used. This happened due to the fact that, the AMP diodes of interest were not available in simulator diode library. The MA4E2054B-287T diode is similar to the HMMS 2822.

The measurements were accomplished using the HP 8720 Network Analyzer to test the isolation properties of the mixer. The results in Figure 6.5 and Figure 6.6 were obtained.

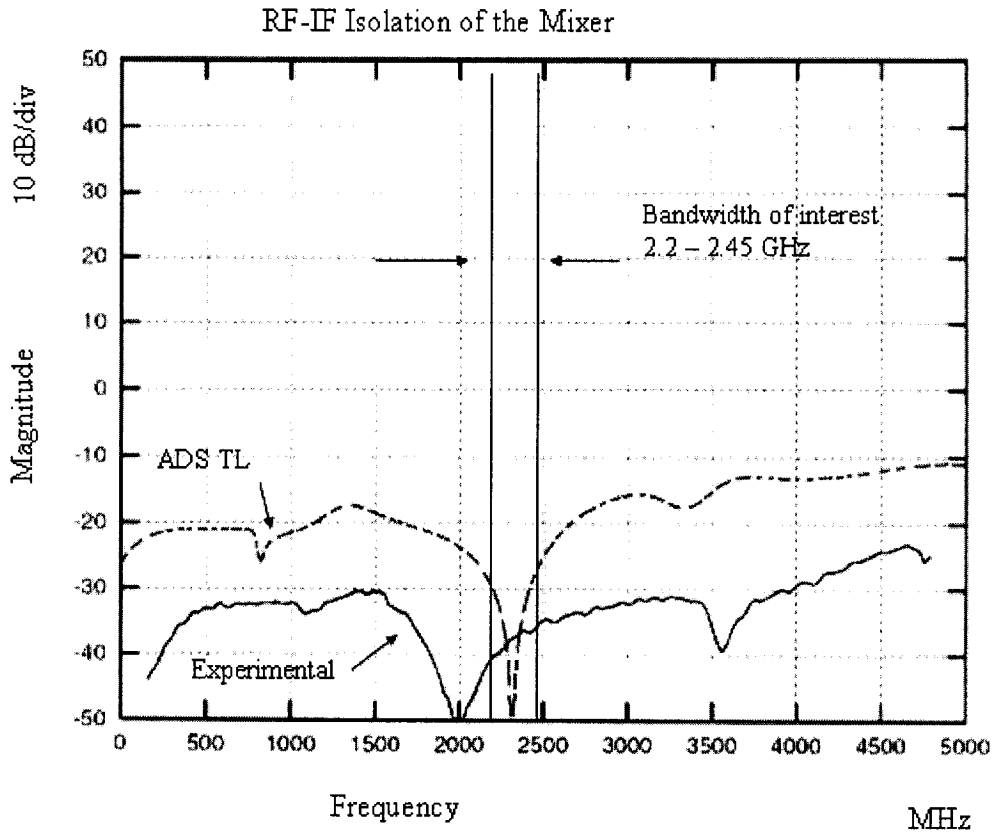

Figure 6.5: The RF-IF isolation experiment of the rat race hybrid mixer.

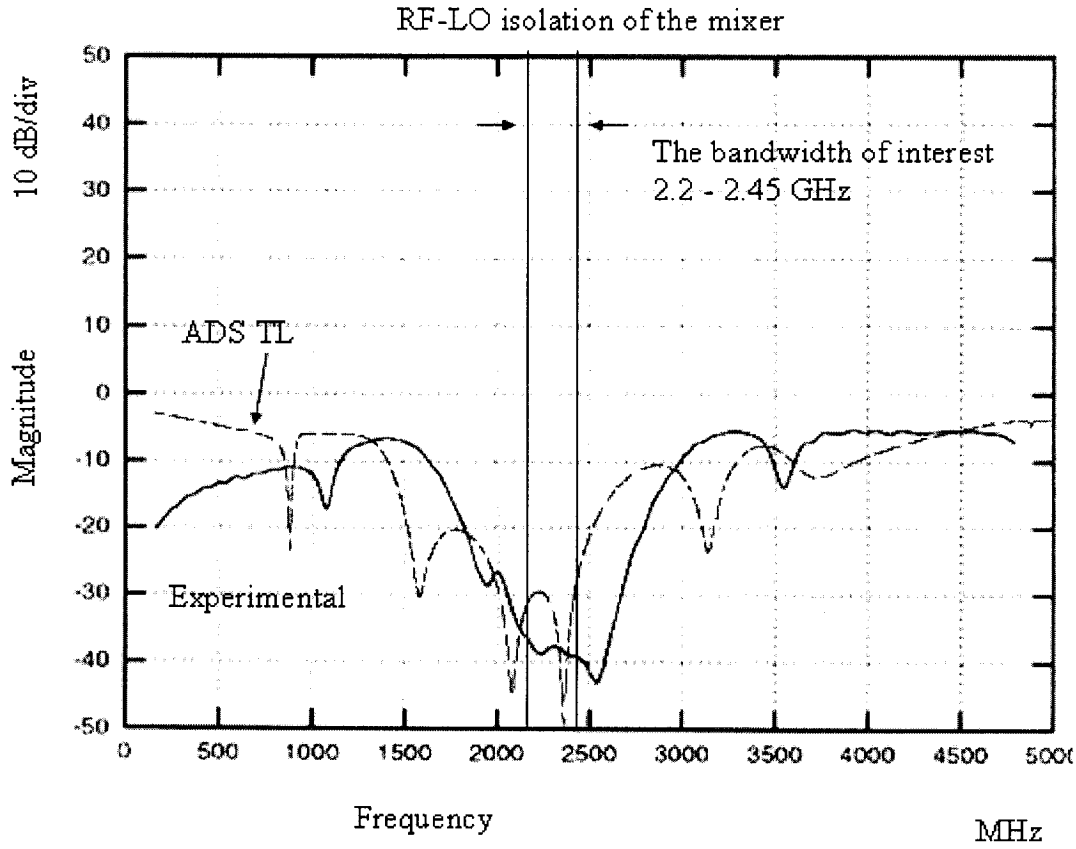

Figure 6.6: The RF-LO isolation experiment of the rat race hybrid mixer.

The results are satisfactory moreover; they are pretty consistent with the ADS simulation results. The peak of the isolation is at RF-LO is at 2500 MHz, it has a 100 MHz shift from the expected result. Also, the RF-IF isolation is close to the expected even though the peak of the isolation shifted around 400 MHz. The overall isolation in the band is close to the simulated results.

6.3.2 Harmonics Experiments with the Mixer

The most important feature of a mixer, which mostly determines its performance, is its harmonics response along with its conversion loss and the magnitudes of the harmonics

relative to the expected fundamental frequency. The experiments in order to test its harmonics response were carried out using a HP 8569 spectrum analyzer. Generally, the expected frequency responses read with an error of 6 MHz. However, the frequencies of the harmonics are known using from ADS so, the error of the spectrum analyzer can be compensated. When it comes to the reading of the amplitudes, since the relative (relative to 144 MHz) positions of the harmonics are important, any error in reading the absolute value of the signal is not vital.

The experiments were carried out by applying the two frequencies (2400 MHz and 2256 MHz) from two synthesized signal generators, the Agilent E4438C and HP 8672A and the output observed using the HP 8569 spectrum analyzer. The response of the mixer is shown in Figure 6.7.

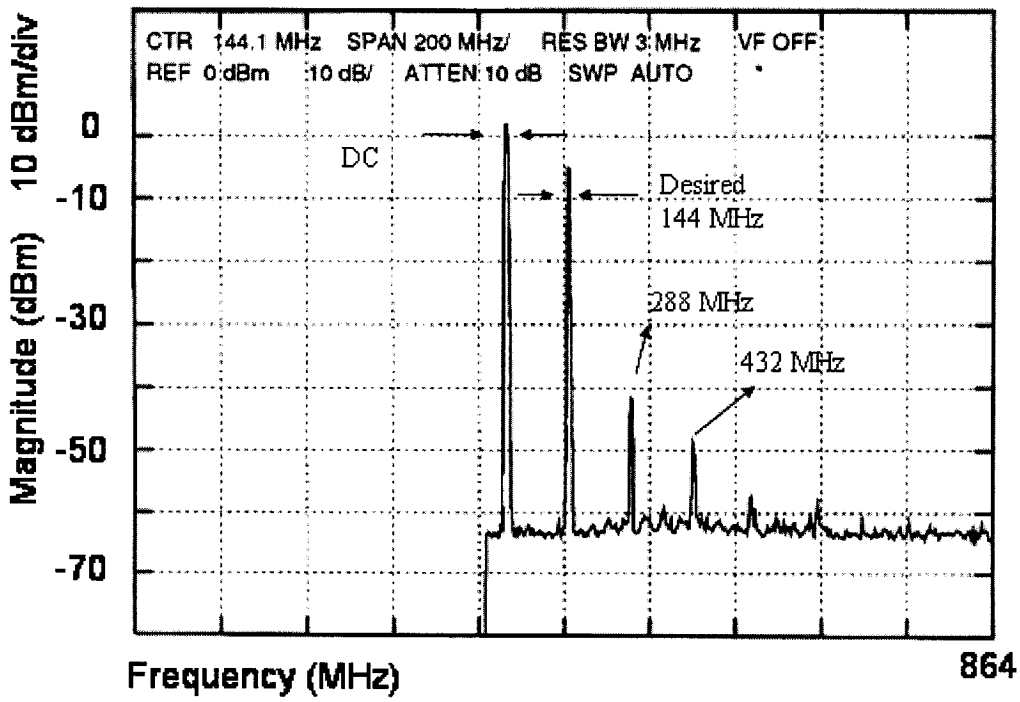

Figure 6.7: The band spectrum response of the mixer between 0 - 864 MHz.

The results in Figure 6.7 were obtained when the RF (2400 MHz) is 0 dBm and the LO (2256 MHz) is 7 dBm. As seen, the fundamental output of 144 MHz is at -6 dBm, which indicates a conversion loss 6 dB. Besides, the second harmonic $[2(RF-LO)]$ at 288 MHz is the closest harmonic to the desired 144 MHz output and it is around 35 dB down. The third harmonics seen in Figure 6.7 is at 432MHz $[3(RF-LO)]$ and around 40 dB down.

The results are almost consistent with the ADS simulation results. ADS predicts that 144 MHz output is -9 dBm, 288 MHz output is 36 dB down and 432 output is 34 dB down. The conversion loss that ADS simulates is 5.3 dB, which is close to the experimental 6 dB.

Indeed, another mixer simulation was carried out with a different diode pair, HSMS 8200, in order to see the difference. The HSMS 8200 series are designed for frequencies higher than 4 GHz and the conversion loss become 7.8 dB. This shows that the conversion efficiency is very dependent on to the diode used and the difference between simulated and experimented results are due to the fact that simulated and used diodes are different but the choice of the simulated diodes is accurate that the results are close.

During the experiments, some signals were observed mostly below 144 MHz in the spectrum analyzer. It has been realized that theses signals belong to the FM radio stations that broadcast in Montreal area and they contribute as ambient noise to the mixer experiment. It has been observed that they are more than 80 dB down from the desired 144 MHz signal. In order to get rid of the ambient noise for the measurement, the circuit

was covered with a horn antenna and the antenna was touched to the ground plane of the mixer so that a Faraday cage effect was created.

6.4 RF Amplifier (RF AMP)

The RF AMP measurements were carried out using the HP 8672A synthesized signal generator and the HP 8569 spectrum analyzer. The input signal applied is from the signal generator and the output is observed on the HP 8569. The biggest difference between the RF AMP and the modules tested earlier (filters and the mixer) is that the RF AMP is an active circuit and the MGA 86576 amplifier requires a DC bias voltage to operate.

According to the specs of the MGA 86576, it gives 23 dB gain at 2.5 GHz when 5 V DC is applied to the RF OUTPUT leg. However, in the original design of the "No-Tune Transverter for 3456 MHz" by Jim Davey [2], 7.5 V was applied to the MGA 86576 in order to achieve more gain from it. In the specification of the amplifier, it has been indicated that applying a DC bias voltage up to 9 V does not harm the device. So, the design of the DC bias circuitry for the amplifier was designed in order to supply 7.5 V to the amplifier. In fact, if the voltage to the device increased from 5 V to 7.5 V, the gain increases too. However, at 7.5 V the amplifier saturates and the gain stays the same after that. In the experiments, the DC bias voltage was applied to an upper limit of 8 V in order not to harm the device.

For the DC bias circuit to the amplifier, a National LM317LZ regulator was used. The LM317LZ regulator is an adjustable three terminal regulator, which supplies up to 100 mA between 1.2 to 37 V. The bias circuitry in the design of Jim Davey [2] used in order

to supply 7.5 V to the amplifier. The regulator needs at least 9 V to give 7.5 V and up to 25 V input, the output stays at 7.5 V. The schematic of the circuit is shown in Figure 6.8 [21].

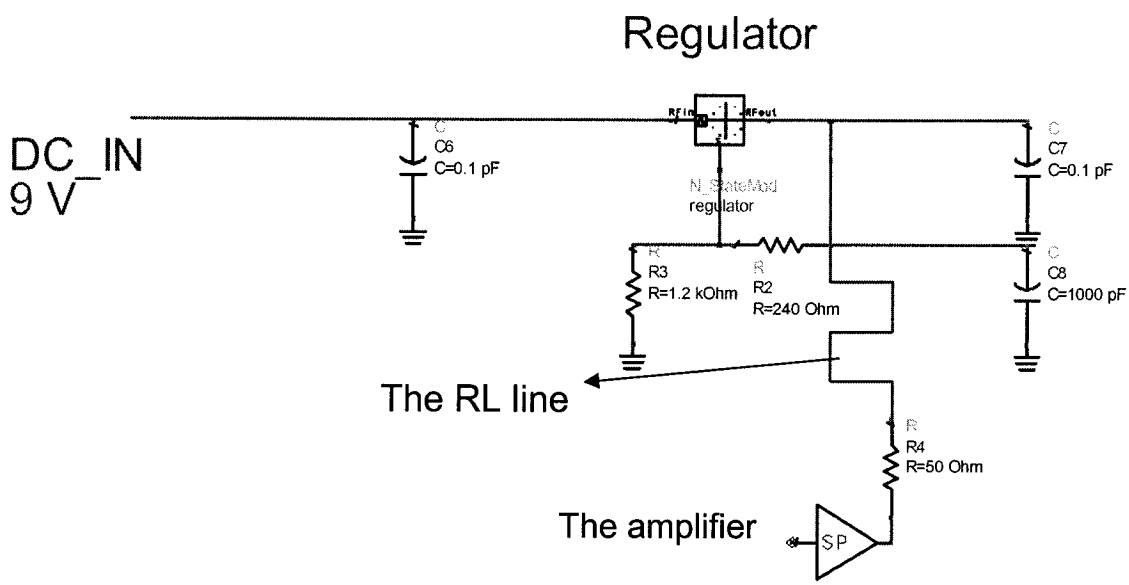

Figure 6.8: The schematic of the regulator circuitry.

The regulator circuit was designed in order to supply 7.5 V to the amplifier, but in reality only 6.83 V was obtained from it. This 0.67 V difference occurred because there are small differences between the theoretical values of the parts and the parts actually used. For instance, instead of the 270 ohm resistor, a 240 ohm resistor was used, similarly, the 52 ohm resistor was substituted by a 49.9 ohm resistor. Besides, the values of the capacitors and the resistors are not exact and both have tolerances. This 0.67 V difference causes 0.5 dB gain reduction at the amplifier. Finally, the RF line does its job well of creating a buffer between AC and DC bias circuitry.

6.4.1 RF AMP Experimental Results

In the measurements of the RF AMP, the input signal was obtained from an Agilent E4438C signal generator and the output observed on the HP 8569 spectrum analyzer. The results are shown in Table 6.1.

Applied RF Signal Power at 2400 MHz (dBm)	Experiment Results (dBm)	Simulated Results (dBm)	The Difference (dB)
-70	-50	-45	5
-60	-40	-35	5
-50	-30	-25	5
-40	-20	-15	5
-30	-10	-5	5

Table 6.1: The RF AMP experiment results.

As seen from the results, the RF AMP has 20 dB gain, which is 5 dB lower than the simulated result. This difference probably comes from the loss in the circuit and the insertion loss of the filter. However, the response of the RF AMP is very satisfactory.

If 2112 MHz (the spur frequency) was applied as an input to the RF AMP at the level of 15 dBm, the output was observed as -30 dBm which means the RF AMP has 45 dB spur rejection. If the amplification of 2400 MHz is taken into account, the relative rejection becomes 45 + 20 = 65 dB.

6.5 Harmonic Generator (HG) Experimental Results

In the harmonic generator, the MGA 86576 amplifier was used as the amplifier and the LM317LZ regulator was used to supply DC bias to the amplifier. The same regulator

circuit was used as for the RF AMP. The DC voltage at the output leg of the regulator was measured as 6.24 V.

The measurement of the HG was carried out by using the same procedure, as explained in the RF AMP part. Only, this time 564 MHz was applied as input of the HG. In the output spectrum the other harmonics might have been observed (1st harmonic 564 MHz, 2nd harmonic 1182 MHz etc.) However, the output spectrum of the HG has only 2256 MHz an undistorted signal, as seen in Figure 6.9.

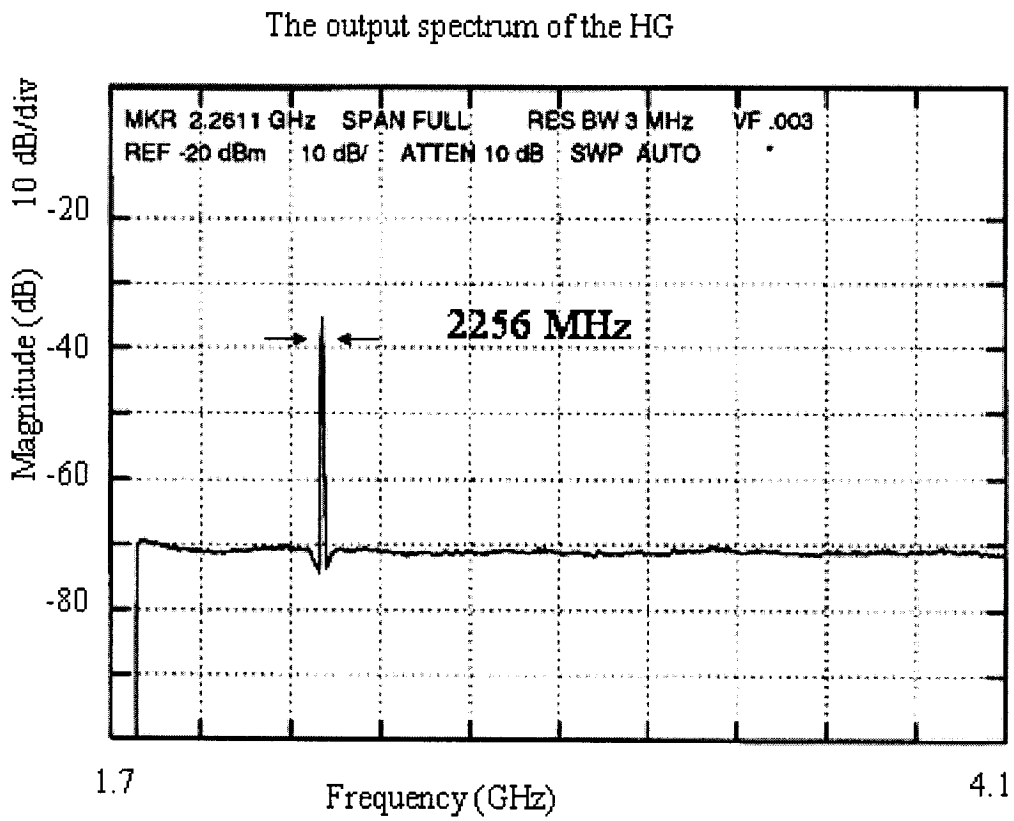

Figure 6.9: HG spectrum output between 1.7 - 4.1 GHz.

The measured values are shown in Table 6.2.

Applied Signal Power at 564 MHz (dBm)	Experiment Results (dBm)	Simulated Results (dBm)
0	2	3
3	6	6
5	8	8
7	10	10
10	12	12
12	14	13

Table 6.2: The HG experimental results.

The gain of the system is around 3 dB, which was expected. Actually, since the frequency of interest is the fourth harmonic of the input signal and it is down about 20 dB, the gain of the amplifier gives just the right amount of power.

Note that in the matching circuit of the HG, a 200 μH inductor with a ferrite dielectric material in the core was used. The low frequency behavior of the inductor is 200μH but its high frequency behavior is not very well known. However, the value of the inductor is not critical in the matching circuit that if it was substituted with a capacitor less than 1 pF, the response would stay almost the same. So, the inductor of 200μH was used in the HG and the expected performance was achieved.

6.6 Overall System Experiments

All the circuit boards were connected together by using male to male SMA connectors. The RF signal at 2400 MHz was applied to the RF AMP as the RF input with amplitude

of -50 dBm from the HP 8672A. The 564 MHz signal was applied to the HG from an Agilent E4438C at 7 dBm. The output of 144 MHz was observed at the HP 8569 as -42 dBm. The closest unwanted harmonic generated by the mixer was observed at 576 MHz at a level of 35 dB down of the 144 MHz. The output spectrum is given in Figure 6.10.

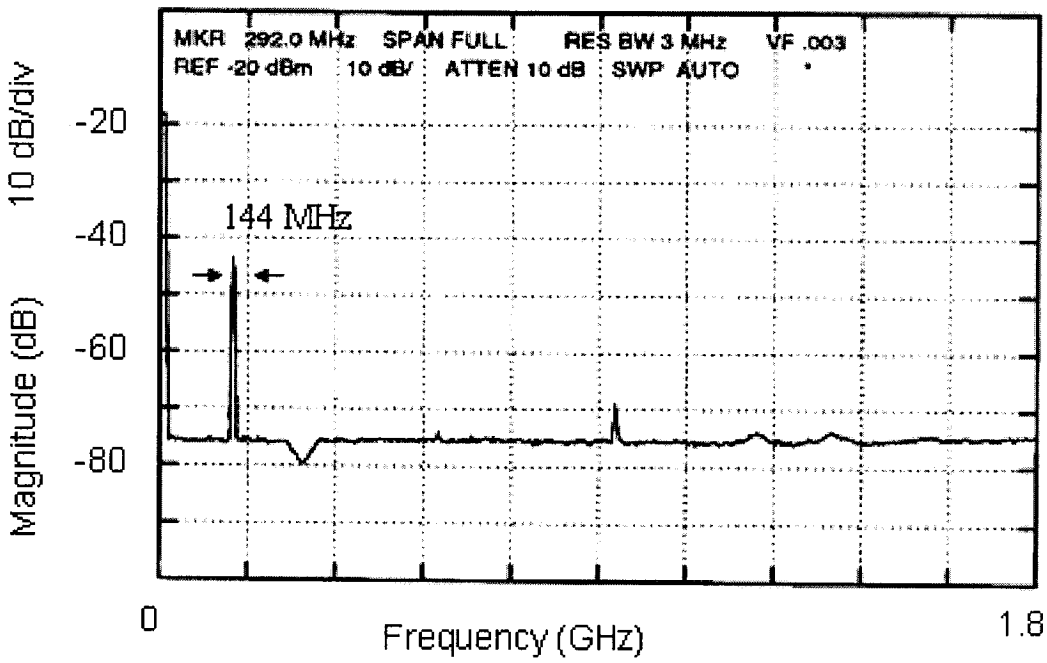

Figure 6.10: The output spectrum of downconverter 0 – 1.8 GHz.

As seen, from Figure 6.10, the output spectrum is very clean. This shows that all the modules work well together. Some experiments carried out to observe the dependence of the output signal to the LO and the results are given in Table 6.5.

RF signal at 2400 MHz at -50 dBm	
Applied Signal Power at 564 MHz (dBm)	**Experiment Output at 144 MHz (dBm)**
0	**-54**
3	**-44**
5	**-40**
7	**-35**
9	**-34**

Table 6.5: The overall system experiment results.

Getting the desired output of 144 MHz from the 2400 MHz signal concludes the design of the downconverter.

7 Conclusions and Discussions

7.1 Summary

In this thesis, the theory, design and the implementation of a 2400 - 2404 MHz input, 144 -148 MHz output downconverter was discussed. The theory of coupling structures between folded resonators was discussed and the coupling coefficients were calculated. The full theoretical approach to the hairpin filter, rat race coupler mixer, amplifier and frequency multiplier were discussed. The design and the full wave microwave simulations of the coupling structures, hairpin filters and the rat race coupler mixer were carried out using ADS. Several simulations (conversion loss, gain, S-parameter, harmonic balance) were carried out in order to analyze the behavior of the hairpin filters, rat race hybrid mixer, harmonic generator and the RF amplifier. The full wave simulation results were compared with the TL simulation mode of the ADS; the differences between the results were discussed.

The implementation of the designed and simulated components was accomplished. The creation of Gerber files, drill files, buying the parts and having the board manufactured were completed and each step explained in detail. The whole design of one prototype cost about $500 CAD.

The chopping of the board to free the components and the mounting of the parts were done carefully by ECE technicians. The experiments were carried out using the available equipment in the ECE Microwave Lab and all the results obtained were discussed in the

thesis. The differences between the theoretical design, the ADS simulations and the experiments presented and the possible reasons were discussed.

7.2 Discussions and Observations

Even though there were differences between the simulations and the experiments, in the end the 2400 – 2404 MHz input, 144-148 MHz output downconverter worked successfully. The spur rejection, and the gain performance of downconverter is satisfactory, as well as the isolation, distortion and the conversion gain of the rat race hybrid mixer. Even though the poles are missing in the S-parameter characteristics of the hairpin filters the results were satisfactory. Indeed the differences between the simulated and the experimented results could be due to the difference in the dielectric constant that it has a tolerance of five percent. Also, there is a problem with edge effects, because the circuit board was cut, very close to the edges of the hairpin resonators.

The design of the 2400 MHz downconverter can be applied to any frequency only with some modification in the design. The design used in this thesis was adopted from Lau's 2456 MHz design [14] and Davey's 3456 MHz design [2]. Our results showed that this system topology works very satisfactory at 2400 MHz.

As explained in the Chapter 3, due to their complexity, the approximate design equations were introduced for hairpin filters. Even though the design equations used for the hairpin filters are not precise, the results were very promising. However, it has to be mentioned that some poles of the filters were different than the anticipated.

The rat race coupler mixer worked just as planned. The most important task of getting a clean LO for the mixer from the HG was achieved. The gain of the RF AMP and HG are just enough for system to work properly.

It has been realized that in the process of design, simulation and implementation a great deal of planning was required before going from one stage to the next. The design has to be very accurate because otherwise the simulation results do not match the measurements. Indeed, the most important of all was going from simulation stage to implementation stage. Changing the design or the simulation part was easy thanks to the CAD environment. On the other hand, any mistake in the implementation part was either irreversible or very costly to reverse. Before sending the circuit board design to have it manufactured, the physical dimensions of the circuit had to be laid out in the Gerber file format.

The contributions of this thesis consisted of three parts. Firstly, we started with a well-known design by Davey [2]. His design, however, was for 3456 MHz. We rescaled the design for use in our 2400 MHz application. Second, detailed simulations of the harmonics generator, RF amplifier and mixer were done using the Agilent Advanced Design System (ADS) [15]. Third, ADS was used to write Gerber files, which were then sent to a circuit board manufacturing company, APCircuits in Alberta [16]. Hence, we have gained experience in these three areas. In the end, some conclusions were reached and discussed. In this thesis a head to toe approach of design and implementation of a 2400 MHz input – 144 MHz output downconverter was presented.

To sum up, a great deal of time was spent before going to the last stage in order to have problem free implementation and experimental stage. Thanks to the comprehensive planning at the design and the simulation stages, the aim of problem free implementation was achieved.

8 References

1. Down East Microwave Inc. 954 Rt. Frenchtown, NJ 08825. [Online] Available: http://www.downeastmicrowave.com

2. J. Davey "A no-tune transverter for 3456 MHz." in: *The ARRL UHF/Microwave Projects Manual--Volume 1.* Newington CT: American Radio Relay League 1996, p 3.28-3.34

3. AMSAT 850 Sligo Ave. Suite 600 Silver Spring, MD 20910. [Online] Available: http://www.amsat.org

4. E. Cristal and S. Frankel, "Hairpin-line and hybrid hairpin-line/half-wave parallel-coupled-line filters," IEEE Trans. Microwave Theory and Tech., vol. MTT-20, pp.719-728, Nov 1972.

5. J.-S. G. Hong, M. J. Lancaster, *Microstrip Filters for RF/Microwave Applications.* Wiley-Interscience, 2001.

6. D. M. Pozar, *Microwave Engineering*, Wiley, 1997.

7. J.-S. G. Hong, M. J. Lancaster, "Couplings of microstrip square open-loop resonators for cross-coupled planar microwave filters." *IEEE Trans. Microwave Theory and Tech.*, vol. 44, pp.2099-2109, Dec. 1996.

8. J.S. Wong, "Microstrip Tapped-Line Filter Design." *IEEE Trans. Microwave Theory and Tech.* vol. 27, pp.44-50, Jan 1979.

9. E.G. Cristal, S. Frankel, "Design of hairpin-line and hybrid hairpin-parallel-coupled-line filters." GMTT International, Microwave Symposium Digest. Vol. 71, pp 12-13, May 1971.

10. Viewmate™, Pentalogix Corp. [Online] Available: http://www.pentalogix.com

11. C. D. Salamat, M. A. Lorenzo, and E. J. B.Roxas, Jr., "Design of a Narrowband Hairpin Filter on PTFE Laminate," in *Philippine Engineering Journal*, Philippines, 2002.

12. H. Shuch, "Rat-race Balanced Mixer for 1296 MHz." *Ham Radio*, pp 33-39, July 1977.

13. D. M. Pozar, *Microwave and RF Design of Wireless Systems.* Wiley, 2000.

14. R. F. Graf, W. Sheets, "3456-MHz Transverter by Zack Lau, W1VT."

in: The ARRL UHF/Microwave Projects Manual, Vol. 2. Newington CT: American Radio Relay League, 2001.

15. Agilent Advanced Design System User Manual. Version 2003 A, Agilent Technologies. [Online] available: http://eesof.tm.agilent.com

16. APCircuits, Unit 3, 1112-40th Ave. N.E. Calgary, AB Canada T2E 5T8. [Online] Available: www.apcircuits.com

17. B.A. Syrett, "A Broad-Band Element for Microstrip Bias or Tuning Circuits (Short Papers)." *IEEE Trans on Microwave Theory and Tech.* pp. 925-927, Vol. 28, Aug. 1980.

18. F. Giannini, R. Sorrentino, J. Vrba, "Planar Circuit Analysis of Microstrip Radial Stub (Short Paper)." *IEEE Trans. on Microwave Theory and Tech.* Vol. 32, pp. 1652-1655, Dec. 1984.

19. R. K. Hoffmann, *Handbook of microwave integrated circuits.* Norwood, MA: Artech House, c1987

20. T. Marek, J. C. Faber, E. Miroslaw E. Adamski, *Microwave and millimeter-wave diode frequency multipliers.* Artech House Publishers, 1995.

21. LM317LZ voltage regulator data sheet, National Semiconductor Corporation. [Online] Available: http://www.national.com